STUDY OF LOW GLOBAL WARMING POTENTIAL REFRIGERANTS IN HEAT PUMP SYSTEMS FOR STATIONARY APPLICATIONS

By

ATHARVA BARVE

Bachelor of Science in Mechanical Engineering

Oklahoma State University

Stillwater, OK

2010

Submitted to the Faculty of the
Graduate College of the
Oklahoma State University
in partial fulfillment of
the requirements for
the Degree of
MASTER OF SCIENCE
December, 2012

STUDY OF LOW GLOBAL WARMING POTENTIAL REFRIGERANTS IN HEAT PUMP SYSTEMS FOR STATIONARY APPLICATIONS

Thesis Approved:

Dr. Lorenzo Cremaschi

Thesis Adviser

Dr. Daniel Fisher

Dr. Afshin Ghajar

Dr. Sheryl A. Tucker

Dean of the Graduate College

TABLE OF CONTENTS

Chapter Page

LIST OF TABLES

Table Page

LIST OF FIGURES

Figure Page

Figure Page

CHAPTER I

INTRODUCTION

Refrigeration and the components that work on its principle have indeed made human life easy and have made habitation possible in the worst climatic conditions. We work, sleep and enjoy comfortable environment at our work places and houses because the air-conditioning systems work round the clock to deliver conditioned air. In order to achieve the required cooling or heating in a refrigeration cycle, a fluid is circulated round the loop which absorbs and rejects heat along its run. This fluid is called a refrigerant, coolant or working fluid. Today, we have many refrigerants in our library, but the question which is of utmost importance is which refrigerant works the best. This study focuses on an experimental comparison of the drop-in energy performance and capacities of two new candidates of refrigerants in a R410A heat pump split system for ducted HVAC in residential applications.

Phase out of CFCs and HFCs

'Global warming' is a serious issue and the whole world is trying to come up with the measures to curb it (Karber et al., 2012). In my opinion high Global Warming Potential (GWP) refrigerants which have been used in commercial and residential applications are alleged to pose a threat to the environmental security.Efforts are being made all around the world to find the alternatives for high GWP refrigerants in order to secure a green and better future. In 1987, the Montreal protocol (UNEP, 1987) established that CFCs (chlorofluorocarbons) which have a very high GWP were the cause of ozone depletion and proposed its phase out (Reasor et al, 2010). The Kyoto Protocol in 1997, regarded hydrofluorocarbons (HFCs) as potential threat to the ozone and asked to regulate its emission. Another stepping stone towards environmental safety was laid when European Union (EU) directed the phase out of R-134a in automobile air conditioning by 2017. Thus it is evident that the world is alarmed by the possible outcomes of the global warming and more research is carried out to find the alternative refrigerants which will not only perform efficiently but also maintain the integrity of the environment.

Assessment Parameters: GWP, TEWI, LCCP

The contribution of working group I to the fourth assessment report of the Intergovernmental Panel on Climate Change (IPCC) (Forster et al., 2007) explains in detail the changes in atmospheric constituents and the concept of radiative forcing. In order to understand the concept of GWP it is important to define radiative forcing. Radiative forcing (RF) is a concept used for quantitative comparisons of the strength of different human and natural agents in causing climate change. "The Third Assessment Report (TAR) also represents RF as the stratospherically adjusted radiative flux change evaluated at the tropopause. Positive RFs lead to a global mean surface warming. Radiative forcing can be understood as a measure of the influence on energy balance of the Earth-atmosphere system with alteration in the factors that affect the climate. The

radiative balance controls the Earth's surface temperature and the term of RF is used to indicate how far the Earth's radiative balance is being pushed away from its normal state. RF is quantified as the 'rate of energy change per unit area of the globe' and thus is expressed in 'Watts per meter square'" (Forster et al., 2007). The results from the climate model studies since the Working Group I Third Assessment Report of IPCC state that the combined (human and natural responses) anthropogenic RF is estimated to be +1.6 W m^{-2}. Figure 1 which was originally proposed by Foster et al. (2007), illustrates a flowchart of how RF is linked to other aspects climate change assessed by the IPCC. Human activities and natural processes are responsible for either direct or indirect changes in climate changes.

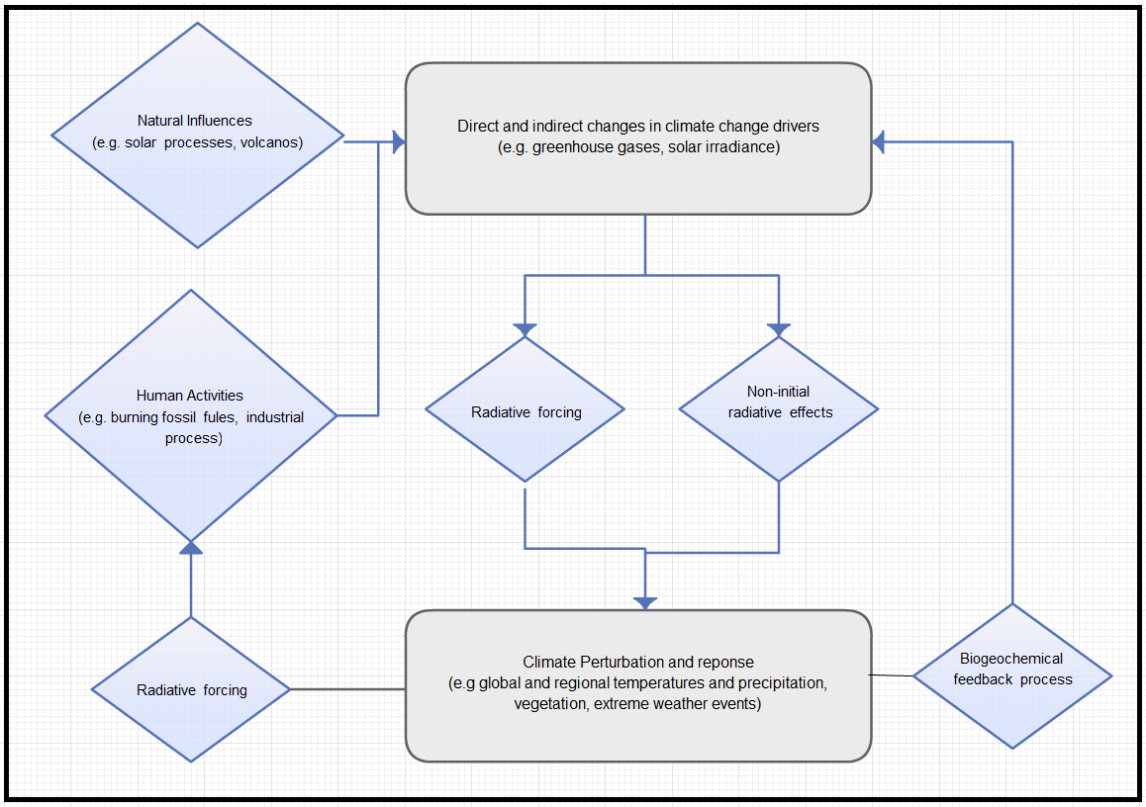

Figure 1: Diagram illustrating how RF is linked to other aspects of climate change evaluated by the IPCC (adapted from Forster et al., 2007).

The results indicate that since 1750 humans have exerted a substantial warming influence on climate. This RF approximation is predicted to be at least five times greater than that due to solar irradiance changes. Increasing concentrations of the long-lived greenhouse gasses also called as LLGHGs (such as carbon dioxide CO_2, methane CH_4, nitrous oxide N_2, halocarbons and sulphur hexafluoride SF_6) have led to a release of high levels of RF. The Montreal Protocol gases (chlorofluorocarbons (CFCs) hydrochlorofluorocarbons (HCFCs) and chlorocarbons) as a group contributed +0.32 W m^{-2} to the RF in 2005. Concentrations of many of the fluorine laden Kyoto Protocol gases (hydrofluorocarbons (HFCs) perfluorocarbons SF_6) have increased by factors ranging between 4.3 to 1.3 between the years 1998 and 2005. Their RF is rapidly increasing by roughly 10 % $year^{-1}$ (Forster et al., 2007).

It is necessary to have a framework and numerical values in order to develop mitigation strategies of anthropogenic climate change. Global Warming Potential (GWP) provides a tool that can be used to implement comprehensive and cost effective policies so that industries and nations that emit the greenhouse gasses contributing to the RF can form mitigation measures. GWP is a physical index of the total radiative forcing due to an emission of a particular greenhouse gas. It gives guidelines to attain specified emission constraint by allowing for substitution between different climate agents (Eckaus, 1990). GWP is based on the time-integrated global mean radiative forcing of a pulse emission of 1 kg of some compound (i) relative to that of 1 kg of the reference gas CO_2 over the span of 100 years (IPCC, 1990). The formulation of GWP was adopted for use in Kyoto Protocol. The GWP value of a gas (i) is defined as

$$GWP_i \equiv \frac{\int_0^{TH} RF_i(t)dt}{\int_0^{TH} RF_r(t)dt} = \frac{\int_0^{TH} a_i*[C_i(t)]dt}{\int_0^{TH} a_r*[C_r(t)]dt} \quad (1.1)$$

TH is the time span and RF_i is the global mean radiative forcing of the gas under consideration. a_i is the instantaneous radiative forcing due to a unit increase in the concentration of gas (i) and $C_i(t)$ is the fraction of gas (i) remaining at time t. The corresponding of reference gas (r) [a_r, $C_r(t)$] are

in the denominator. The reference gas (r) is carbon dioxide CO_2. Table 1 provides a list of the natural and synthetic refrigerants with their chemical formula and GWP values. As per the definition the GWP of carbon dioxide CO_2 is 1. It can be seen that the GWP value of the substances controlled by Montreal Protocol is indeed very high. This table has been adopted from the work presented in the Working Group I to the Fourth Assessment Report of the Intergovernmental Panel on Climate Change (IPCC) (Forster et al., 2007).

Table 1: GWP values of refrigerants and blends (adapted from Forster et al., 2007).

Industrial Designation or Name of substance	**Chemical formula**	**GWP (100-yr)**
Carbon dioxide	CO_2	1
Methane	CH_4	25
Nitrous oxide	N_2O	298
Sunstances controlled by the Montreal Protocol		
CFC-11	CCl_3F	4750
CFC-12	CCl_2F_2	10900
CFC-13	$CClF_3$	144000
Carbon tetrachloride	CCl_4	1400
Methyl bromide	CH_3Br	5
HCFC-22	$CHClF_2$	1810
General refrigerants		
HFC-23	CHF_3	14800
HFC-32	CH_2F_2	675
HFC-134a	CH_2FCF_3	1430
HFC-407c	blend	1774
R-410a	blend	2088
HFO-1234yf		4

The refrigerant in an air-conditioning system is prone to leaks. Heating and cooling equipment typically run at a pressure above the atmospheric pressure favoring the leaks. The leakage may also occur due to improper brazing of pipelines and insufficient support. When the refrigerant leaks, its exposure to the surrounding contributes to the greenhouse effect. Thus it is essential to contain the refrigerant leakage in order to safeguard the environment.

Another parameter used to estimate the environmental impact is the Total Equivalent Warming Impact (TEWI). The aim of this parameter is to create an index and compare different refrigeration systems from a point of view of their impact on the environment. TEWI regards the Global Warming potential (GWP) of carbon dioxide as a reference. The GWP of carbon dioxide is 1 irrespective of the time period. This way, while computing the GWP of the refrigerant, the contribution of carbon dioxide emissions from the fossil fuel power plants in the production of energy to operate the system in which the refrigerant is contained can be incorporated. Thus TEWI is the sum of two parts: namely the 'direct part' being the release of the refrigerant to the atmosphere and the 'indirect part' which is due to the release of the carbon dioxide from the power plant in order to operate the refrigeration system (Kruse, 1998).

A third parameter in assessment of impact on environment is the Life cycle climate performance (LCCP) which has been used vastly in the mobile air conditioning industry. It has evolved to be a useful parameter to understand total product environmental impact beyond the direct global warming potential (GWP) of the refrigerant. This parameter is a "start-to-end analysis" of the environmental impact at all points in the life cycle chain which includes manufacture of components, system operation and end-of life disposal (Minor and Spatz, 2008). In the model provided by the Global Refrigerants Energy and Environmental Mobile Air Conditioning (GREEN-MAC) to calculate the LCCP, all the direct and indirect effects are accounted for (Papasavva, Hill, & Andersen, 2010)

$$
\begin{aligned}
&LCCP \\
&= GWP(direct\ from\ MACs\ leaks) \\
&+ GWP\big(direct\ from\ additional\ sources{:}\ (atmospheric\ reaction\ products\ of\ refrigerants) \\
&+ (manufacturing, transport\ and\ service\ leakage) + (EOL\ refrigerant\ emmisions)\big) \\
&+ GWP(indirect\ from\ MACs\ leaks) \\
&+ GWP\big(indirect\ from\ additional\ sources{:}\ (production\ of\ refrigerant\ and\ transport) \\
&+ (MACs\ manufacturing\ and\ vehicle\ assembly) + (EOL\ recycling\ process)\big)
\end{aligned}
$$

In this formula EOL refers to end of life period of the refrigerant.

Thus the GWP accounts for just direct impacts on the environment while TEWI incorporates both direct and indirect impacts. The concept of LCCP, which is popular in small scale refrigeration systems like Mobile air conditioning, is a "start-to-end" analysis of the environmental impact which includes the processes right from manufacturing of the refrigerant to the end of life disposal. LCCP is highly modeling oriented, while the present thesis focuses more on experimental results. LCCP and TEWI account for cost of manufacturing for which the data are not readily available. Also we were not able to measure the indirect effects of the system on the environment. The assumption for the work in this thesis is the life of the system in consideration remains the same. This assumption is reasonable only if same system is used or with only minor adjustments, throughout the experimental campaign. In such case the scope of the work is reduced to measuring the parameter of GWP, power consumption and performance of the system under design and off-design operating conditions. The parameter of GWP is considered as a way of comparing the theoretical environmental impact among the three refrigerants namely, R410A, R32 and HFO 1234yf.

The Future of Refrigerants

A new generation of refrigerants seems to be driven by scientific findings, regulatory requirements and market pressure. One major selection criteria for the new generation of refrigerants might be the GWP. There are different refrigerating fluids that are presently known to mankind which are used in a specific thermodynamic cycles. The new generation of refrigerants must offer high energy efficiency in addition to low GWP. Currently the regulatory pressures are with respect to the mobile air conditioning, future extension to other stationary applications is most likely. The refrigerants which are currently being viewed as alternatives like R410A soon could become old rejects (Calm, 2008). Choice of the refrigerant solely depends on the nature and size of the refrigeration cycle. A particular refrigerant which performs efficiently on one thermodynamic cycle might not be the best candidate for a drop-in replacement for other cycle. From an engineering perspective, each element of added complexity increases costs, refrigerant charge, the threat of potential leaks and thermodynamic irreversibility's. Each addition also reduces the system reliability (Calm & Didion, 1998). Thus extensive amount of research is being done in these areas to see if there exists a refrigerant with a low GWP value, which will serve as a drop-in replacement for the high GWP refrigerants which are presently used in residential air-conditioners and heat pumps. If such refrigerants were discovered, it will be convenient for the users and the industry to transit to the new refrigerants. The components which already exist will also be able to function by a mere replacement of the working fluids. On the other hand, there might be a possibility to modify one of the components in the refrigeration cycle so that the new alternative refrigerant performs more efficiently than simple drop-in replacement. In that case, the modification needs to be inexpensive and less laborious so that even the units that are presently working will be able to run with the new refrigerants.

CHAPTER II

REVIEW OF LITERATURE

Since this study presents the candidacy of two refrigerants with low GWP, it is essential to have some knowledge of the physical properties of these refrigerants. R410A has a considerably high volumetric capacity and thus is the most popular refrigerant used in residential air conditioners and heat pumps. Due to the regulations on GWP value of the refrigerants, it is desirable to find alternative refrigerants with reduced GWP and capacity and thermodynamic properties comparable to R410A. R1234yf is foreseen to be a replacement for R134a in automobile air conditioning systems after the European Commission directed a phase out for R134a. R32 is another pure refrigerant with a GWP of 675 and is thought of a suitable replacement in Asian countries. In this section, the physical properties of the refrigerants R1234yf and R32 and the conventional refrigerant R410A will be discussed in detail. Since some similarities will be observed for the experimental campaign conducted in this thesis, although for different system characteristics and capacities the most relevant experimental and modeling results from sources from literature are also highlighted in more detail in this chapter.

Properties of R410A

Refrigerant R410A is a near-azeotropic blend of R32 and R125, with a critical temperature of 161.83 °F and a critical pressure of 714.5 psia. It does not contribute to the ozone depletion and it has been adopted in air conditioning and heat pump systems for residential and light commercial applications. R410A has a high volumetric cooling capacity, which means that this refrigerant can absorb significant amount of heat from the air in direct expansion evaporators for a unit volume of refrigerant. R410A operates at higher pressures than R22 and its GWP is 2,088, which is higher to that of R22 (Forster et al., 2007). In case of leakage or improper refrigerant charge management, the direct contribution of R410A to the greenhouse effect might be assessed by considering its GWP. The system coefficient of performance (COP), and system reliability and life cycle time must be also considered in order to evaluate the refrigerant indirect contributions to the greenhouse effects. The indirect contributions are linked to the carbon emissions due to the power consumption of the unit during service and due to the energy and materials required for building the system (Minor and Spatz, 2008).

Properties of HFO1234-yf

Refrigerant R1234yf is a hydrofluoroolefin 2,3,3,3-tetrafluoroprop-1-ene that falls in the category of partially fluorinated olefins (Minor and Spatz, 2008). R1234yf has a GWP of 4 and is low in toxicity. It is classified as a low flammable (2L) refrigerant and has been proposed to replace R134a in automobile air conditioning systems. Its critical temperature is 202.5 °F and the critical pressure is 490.3 psia. While its vapor pressure is similar to that for R134a, its thermodynamic properties do not quite match those for R410A (Reasor et al, 2010). The ratio of operating pressure when compared to R410A is 40% lower (Endoh et al., 2010). The tests results for the compatibility of R1234yf and lubricant at typical operating conditions seems to suggest that the lubricating properties are unhampered by the use of R1234yf. The GWP analysis for HFO-1234yf

suggested that molecules of Hydro-Fluoro-Olefins (HFO) have a very short atmospheric life span of about 11 to 18 days (Yana Motta et al., 2010). Some modeling work in the literature showed that when R1234yf was retrofitted in R410A AC systems, the COP was similar to that for R410A but the cooling capacity generally decreased by as much as 50% (Leck, 2010).

Properties of R32

Refrigerant R32 is a difluoromethane and it is a pure fluid with a GWP of 675. The critical temperature for R32 is 173.1 °F and its critical pressure is 780.3 psia, which are close to that for R410A. R32 belongs to low flammable refrigerants class 2L but might pose a greater fire hazard than R1234yf as a result of its faster flame propagation speed. R32 has a higher volumetric capacity than R410A and thus it has the potential of higher COPs. However, R32 yields to generally higher compressor discharge temperatures. This characteristic seems to adversely impact the system reliability because of metal fatigue of the valves and thermal stress of the lubricant (Leck, 2010). Taira et al. (2011) observed that since R32 has a larger volumetric capacity than R410A the amount of R32 charge can be reduced by 50% of that of R410A for same system performance. Lower refrigerant inventory might decrease the direct impact to the greenhouse gases effects in case of refrigerant leakage. R32 has been proposed as possible replacement for R410A in various countries, especially in Asia, but its flammability characteristics still pose some serious concerns when it is considered for residential applications. To mitigate the negative traits of R32 Leck (Leck, 2010) suggested using R32 in refrigerant blends.

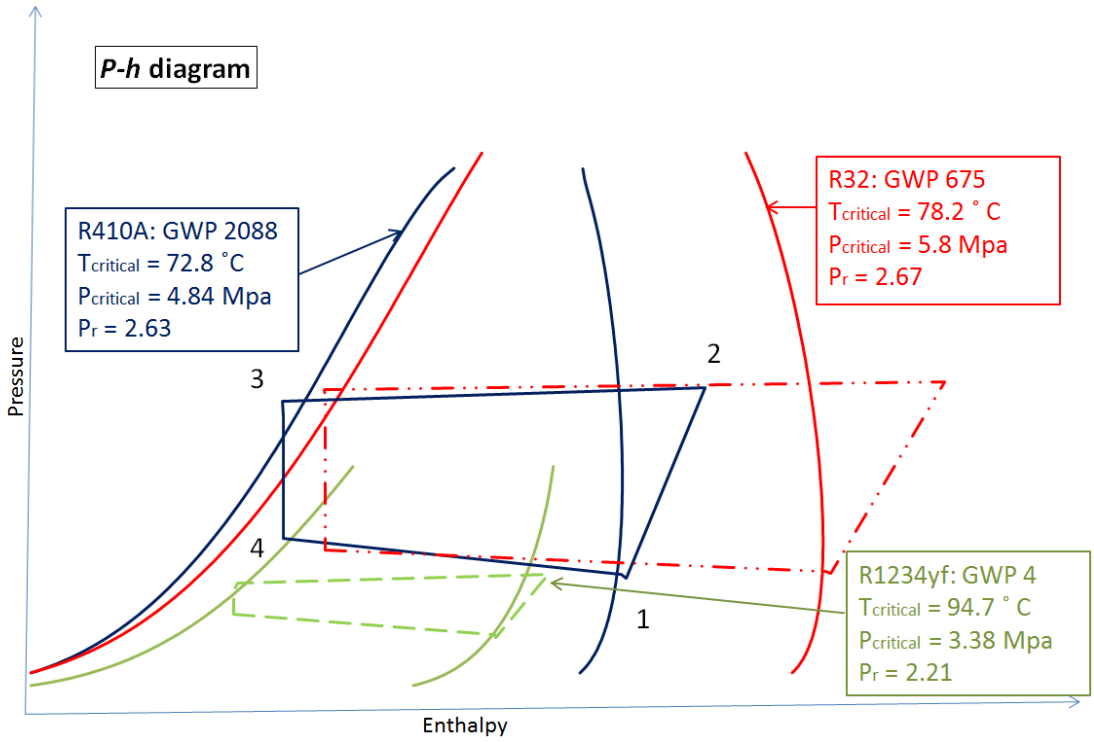

Figure 2: Measured state points (from present work) in a thermodynamic refrigeration cycle comparison for R410A, R32 and R1234yf at AHRI standard 210 A cooling test condition.

Figure 2 shows the p-h diagram for the three refrigerants. The state points were measured from one test in this thesis at AHRI standard A cooling test condition. Details regarding the test condition can be found in test procedure section of this thesis. It is evident that the R32 operates at similar pressures as that of R410A. The compressor ratio was 2.67 for R32 which was largest among all the 3 refrigerants. This means that in case of R32 the discharge pressure is 2.67 times that of the suction pressure. This term is also referred as 'pressure lift' in the refrigeration industry. R1234yf on the other hand operated at very lower pressure. The pressure lift was also smaller as compared to R32 and R410A. It can also be noted that R32 operates at higher temperatures between points 1 and 2 on the refrigeration cycle. Points 1 and 2 represent compression process in the refrigeration cycle and thus the compressor has to work under high

temperature conditions. Conversely, for R1234yf the compressor discharge and suction temperatures was fairly low.

Literature on experimental and modeling test results for R32 and R1234yf

Wang, Amrane and Johnson (2012) provided an overview of the AREP program started by AHRI describing its scope and procedure. In response to the alleged environmental issues by high global warming potential refrigerants, the Air-Conditioning, Heating and Refrigeration Institute (ARHI) initiated an industry-wide cooperative research program called AHRI Low-GWP Alternative Refrigerants Evaluation Program (Low-GWP AREP). The aim of this program is to identify and evaluate likely alternative refrigerants for heat pumps, chillers, water heaters, ice makers and refrigeration equipment. It has been observed that the hydrofluorocarbons (e.g., R410A, R134a) which have served as replacements for hydrochlorofluorocarbons (HCFCs) have come under scrutiny due to global warming issues. In order to tackle these issues, chemical producers and equipment manufacturers have accelerated efforts to develop low global warming potential (GWP) refrigerants and more efficient products. Low-GWP AREP program was launched by AHRI in March 2011. The AREP program shows urgency in performance evaluation of air conditioning and refrigeration systems using these candidates to ensure acceptable system capacity and efficiency. Along with the notion of identifying and evaluating promising refrigerant, the program also intends to provide common sets of quality data for industry use so that duplicative work will be avoided and also the technical challenges could be understood by identifying the research needed for the use of these refrigerants. The AREP program mainly consists of a series of laboratory testing for compressor calorimeter tests, drop-in tests and soft optimization test. Forty low-GWP refrigerants were identified as potential alternatives by this program out of which thirty-eight have been selected for testing. AREP regards R32 a possible replacement for R410A and R123yf for R134a. The program does not set upper or lower limit on either GWP values or the safety classifications, as long as a candidate refrigerant has a significant

reduction in its GWP relative to the refrigerant it is intended to replace. The program describes guidelines for testing procedures. The drop-in tests are to be conducted with the alternative refrigerants placed in representative existing systems using baseline refrigerants with only minor modifications, if any made to the equipment. The testing procedure need to follow the latest industry-wide accepted standards specified by AHRI. The program lists AHRI standard 210/240 and ASHRAE standard 37 for testing unitary air-conditioners and heat pumps. During the soft optimization tests, the system can be modified using standard production line component. The heat transfer area of the evaporator and condenser for the new system can be changed provided that the sum of the total area remains the same as the baseline system. Thus the AREP program is a continuing effort to recognize alternative refrigerant for high-GWP refrigerants.

Leck (2010) provided modeling results for drop in tests for R32 and HFO-1234yf. The model was developed for AC cooling cycle performance at evaporator temperature of 44.6 °F and condenser temperature of 116.6 °F. Liquid sub cooling of 12 °F and suction superheat of 3 K was also maintained over the model. It was observed that the compressor efficiency was 70%. The model predicted that for the given evaporator and condenser temperature, R32 would have a discharge pressure of 426.3 psi and discharge temperature of the order of 215.6 °F. the modeling results also state that R32 had 9.7 % more cooling capacity than that of R410A. The COP was 0.3 % more than the baseline R410A. HFO-1234yf gives a cooling capacity that is about 57% lower than that of R410A with a COP of 6 % more than the baseline. To get a feel of comparison between R134a and HFO-1234yf, the results for R134a versus R410A are also provided. R134a gives a cooling capacity about 55% less and a COP 8% higher than R410A. Thus it can be seen that as far as capacity is concerned R134a and HFO-1234yf fare about equal with respect to R410A. The model covers three ranges of temperature variations. These results are explained the table provided below.

Table 2: Simulated cooling performance and comparison (adapted from Leck, 2010)

AC cooling performance					
Evaporator temperature		44.6 F	**Evaporator temperature**		116.6 F
Refrigerant	**GWP**	**Discharge pressure**	**Discharge temperature**	**Capacity wrt. R410A**	**Capacity wrt. R410A**
		psi	F	%	%
R410A	2088	410.7	177.8	0	0
R32	675	426.3	215.6	9.7	0.3
HFO-1234yf	4	175.3	131	-57	6
R134a	1430	177.2	147.2	-55	8

Heat pump performance data for the same candidates are provided in the following table. The evaporator temperature of 32 °F and condenser temperature of 113 °F was set as input for this model.

Table 3: Simulated heating cycle performance and comparison of candidate refrigerants (adapted from Leck, 2010)

Heating cycle perfoemance					
Evaporator temperature		32 F	**Evaporator temperature**		113 F
Refrigerant	**GWP**	**Discharge pressure**	**Discharge temperature**	**Capacity wrt. R410A**	**Capacity wrt. R410A**
		psi	F	%	%
R410A	2088	310.9	183.2	0	0
R32	675	406.5	228.3	10	0.25
HFO-1234yf	4	175.3	131	-55	8
R134a	1430	177.2	147.2	-57	6

A similar form of trend was predicted by the model for heating tests. R32 shows a gain of 0.3% in capacity while the HFO-1234yf performs almost the same way as the cooling tests.

Validation of the theoretical cycle modeling results for air conditioning was done by performing cooling and heating tests in a mini-split heat pump unit. The unit used for the experiment was a commercial Toshiba model RAS-281BDR, with a rated capacity of 0.8 tons for cooling and 0.9 tons for heating. For the first series of tests (drop-in tests), R410A was run first to establish a

baseline which was then replaced with HFO-1234yf. For these tests, the COP cooling were 52% less and COP heating was 38% less than that of R410A.In the second round of testing the unit was modified by replacing the compressor with a different one having 211% of the capacity of the original. In addition to this, heat exchangers were modified with more passes and larger diameter pipes in order to reduce pressure drop losses. Improvements were observed on COP values after the modifications. For this series, the COP cooling was 14% and COP heating was 12% less than that of R410A. A third test was made with a unit of larger capacity. The nominal rated capacity on this unit was 1.14 tons. Cooling COP of 29% and heating COP of 19% less than the baseline was observed. Thus to summarize the experimental results from Leck (2010), decrease in COP performance was observed for heating and cooling for HFO-1234yf in a R410A system. With the compressor size increased in order to increase the capacity, the pressure drop and higher energy consumption resulted in COP fairly less than model prediction. With the modifications to the system, the COP performance with HFO-1234yf was improved, but still did not match the R410A baseline.

Endoh, Matsushima and Takaku (2010) also evaluated the cycle performance of HFO-1234yf as a refrigerant for room air conditioning. They used a similar approach of validating theoretical cycle performance with experimental data and later on modifying the system to look for possible improvements.

Table 4: Conditions for HFO-1234yf theoretical cycle performance (adapted from Endoh et al., 2010)

Model inputs		
	Cooling	Heating
Condensing temperature (F)	113	100.4
Evaporating temperature (F)	50	33.5
Subcooled temperature (F)	5	15
Superheated temperature (F)	5	3

The inputs to the model are provided in table 4. The model simulated cooling and heating conditions for a room air conditioner at the rated capacity of 1.14 tons for cooling and 1.42 tons for heating. The results are provided as a ratio of the parameter (HFO-1234yf divided by R410A). The ratios of HFO-1234yf operating pressures to R410A were 40% suggesting that HFO-1234yf is a low operating refrigerant. The discharge temperature for HFO-1234yf was about 18 °F lower than R410A. The capacity per unit mass of the refrigerant was 30% lower for HFO-1234yf than R410A.

Table 5: Results for theoretical cycle performance of HFO-1234yf relative to R410A (adapted from Endoh et al., 2010)

Model results		
	Cooling	Heating
Condensing pressure ratio (%)	42	42
Evaporating pressure ratio (%)	40	40
Discharge temperature difference (F)	-17	-18
Capacity per unit mass ratio (%)	73	72
Suction specific volume ratio (%)	170	171
Adiabatic compression work ratio (%)	70	69
COP ratio (%)	105	104

Thus the compressor suction volume of HFO-1234yf needs to be around 2.3 times that of R410A to get the same capacity. Owing to the capacities and the adiabatic compression work, the COP of HFO 1234yf was 5% more than R410A. The theoretical cycle analysis also showed that the increase in pressure loss for HFO-1234yf is expected. The specific volume and mass flow rate of HFO-1234yf is larger than that of R410A while the capacity per unit mass is smaller. As a result, the flow velocity of HFO-1234yf in the pipe becomes larger. The flow velocity of HFO-1234yf is predicted to be 2.3 times and the pressure loss 3 times as that of R410A at compressor suction. Experimental data was collected by abiding by the standards of JIS B 8615-1. These conditions are provided in the table 6.

Table 6: Test conditions according to standard JIS B 8615-1(adapted from Endoh et al., 2010)

		Cooling	Heating
Indoor conditions	Dry Bulb (F)	80.6	68
	Wet Bulb (F)	66.2	59
Outdoor conditions	Dry Bulb (F)	95	44.6
	Wet Bulb (F)	75.2	42.8
Indoor fan rotational speed		constant volume	constant volume
Outdoor fan rotational speed		constant volume	constant volume

The drop-in test was the first series of test for performance evaluation. To increase the compressor suction volume and decrease the pressure loss, following modifications were done on the system; compressor displacement was increased 1.9 times the original and an oil separator was installed. The number of paths on indoor and outdoor heat exchanger was doubled and the pipes with larger cross sectional diameter were used. The amount of charge for R410A was adjusted to get maximum COP at the rated capacity. For HFO-1234yf the charge was adjusted to get the sub cooling and superheated temperatures. The compressor suction volume of HFO-1234yf was about 2.4 times that of R410A in both drop-in and modification tests. The COP of HFO-1234yf decreases with increase in capacity for drop-in tests. The COP ratios were 97% for medium capacity and 87% for rated capacity. The improvement tests COP ratios were 98% at medium capacity and 93% at the rated capacity.HFO-1234yf could only deliver only 65% of the rated cooling capacity at the maximum rotational speed of the compressor. The results from this set of data conclude that the air conditioner had to be modified to meet the properties of HFO-1234yf. The prime modifications were doubling the number of paths of the heat exchangers, tripling the inner-diameter cross-sectional area of gas-side pipeline and installing oil separator. The refrigerant accumulates in some paths of the distributor coil of the outdoor heat exchanger and thus a decrease in the COP at medium cooling capacity is observed.

R32 was also studied by Yana Motta, Vera Becerra and Spatz (2010) as an alternative refrigerant for stationary air conditioning applications. The experiments were carried on a 3 ton R410A unit

with 13 SEER equipped with a scroll compressor. Tests were performed using standard AHRI 210 operating conditions. Along with the prescribed moderate ambient temperatures the test campaign also included off design conditions off 115 °F and 120 °F at outdoor conditions.

Table 7: Summary of cooling mode tests (adapted from Yana Motta et al., 2010)

AHRI Std. Test	Ambient temperature	Capacity	Efficiency	Mass flow	Issentropic efficiency	Volumetric efficiency
	F	%	%	%	%	%
A	95	107	101	67	102	95
B	82	104	100	68	102	95
C	82	106	102	71	100	96
MOC 1	115	108	100	67	103	93
MOC 2	120	-	-	-	-	-

Table 8: Coil performance for cooling mode tests (adapted from Yana Motta et al., 2010)

AHRI Std. Test	Ambient temperature	Cond. Temp	Evap. Temp	Pressure ratio
	F	%	%	%
A	95	101	97	102
B	82	101	97	102
C	82	101	100	100
MOC 1	115	101	97	103
MOC 2	120	-	-	-

All the results were compared to R410A which was chosen to be the baseline. For A test standard conditions, R32 had 7% more capacity and 1% more efficiency with respect to R410A. The mass flow rate was 33% less with comparable isentropic and volumetric efficiencies. The condensing and evaporating temperatures were also within 3% of R410A suggesting that the operating refrigeration cycle would almost coincide with the one for R410A. The pressure ratio or the ratio of discharge pressure to suction pressure was 2 % more than R410A this means that the compressor undergoes similar operating conditions as far as pressure lift is concerned. It can be generalized for all the tests that R32 matches R410A efficiency with a higher capacity at about 4% to 8%.

Table 9: Compressor discharge temperatures in cooling mode (adapted from Yana Motta et al., 2010)

AHRI Std. Test	Ambient temperature	Discharge Temperature		
		R410A	R32	Difference
	F	F	F	F
A	95	170	209	39
B	82	153	181	28
C	82	159	186	27
MOC 1	115	201	247	46
MOC 2	120	-	266	-

Table 9 depicts the measured discharge temperatures for R32 and R410A in the work of Yana Motta et al. R32 presented higher discharge temperature. It can be observed that the discharge temperature rises significantly with increasing ambient temperatures. The discharge temperature reached the limit of 266 °F which was the maximum upper limit recommended by the manufacturer. The tests had to be terminated in order to protect the compressor from damaging. Yana Motta et al. were not able to test R32 at 120 °F ambient conditions. The authors conclude that R32 delivers comparable efficiency with higher capacities than R410A but the higher discharge temperature is a concern.

In the study of Pham and Rajendran (2012), R32 and HFO blends were analyzed as a low-GWP refrigerant replacement for R410A in air conditioning and heat pump application. The focus of the study was more on R32 as the data available in such area of research is limited. The work done by the authors included test results from drop-in tests with different heat exchangers and scroll compressors. R32 was closely looked upon as a possible alternative refrigerant by China primarily due to its lower cost than R410A. R32 is not a new refrigerant, in fact it was studied during 1900s in search for zero ozone depleting potential (ODP) candidate but it failed to qualify due to regulations on flammability then. Although R32 is regarded as mildly flammable, the

requirements for low-GWP, lower costs and high efficiency could make R32 a promising candidate.

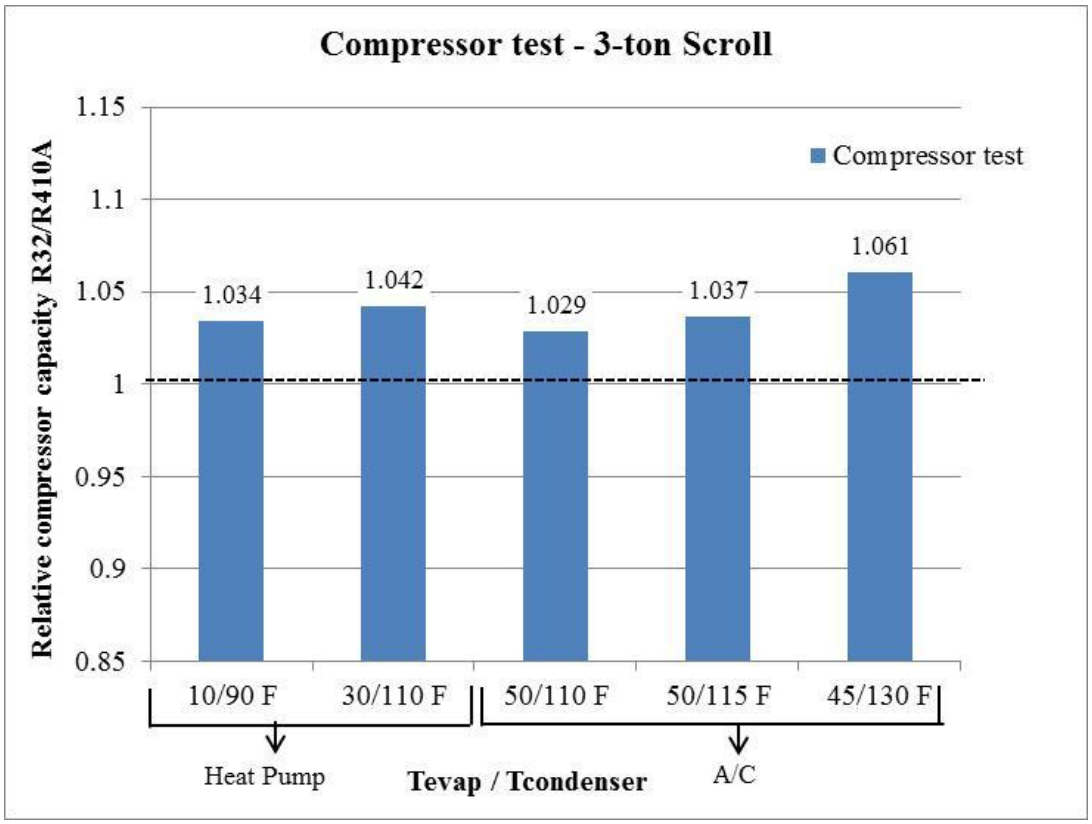

Figure 3: Ratio of compressor capacity of R32 with R410A (adapted from Pham & Rajendran, 2010)

The compressor performance depends on volumetric and isentropic efficiencies. Figures 3 and 4 show the relative capacity and EER for a 3-ton scroll compressor at three A/C and two heat pump, $T_{evaporator}/T_{condenser}$ conditions. The results obtained from the actual compressor tests by Pham and Rajendran, were compared with the theoretical model. Same test conditions were set as inputs to the model with an addition of 20 °F of superheat and 15 °F of liquid sub cooling. The authors observed that the actual compressor capacity was 3-4% lower and the actual compressor EER was 2-3% lower than the theoretical values.

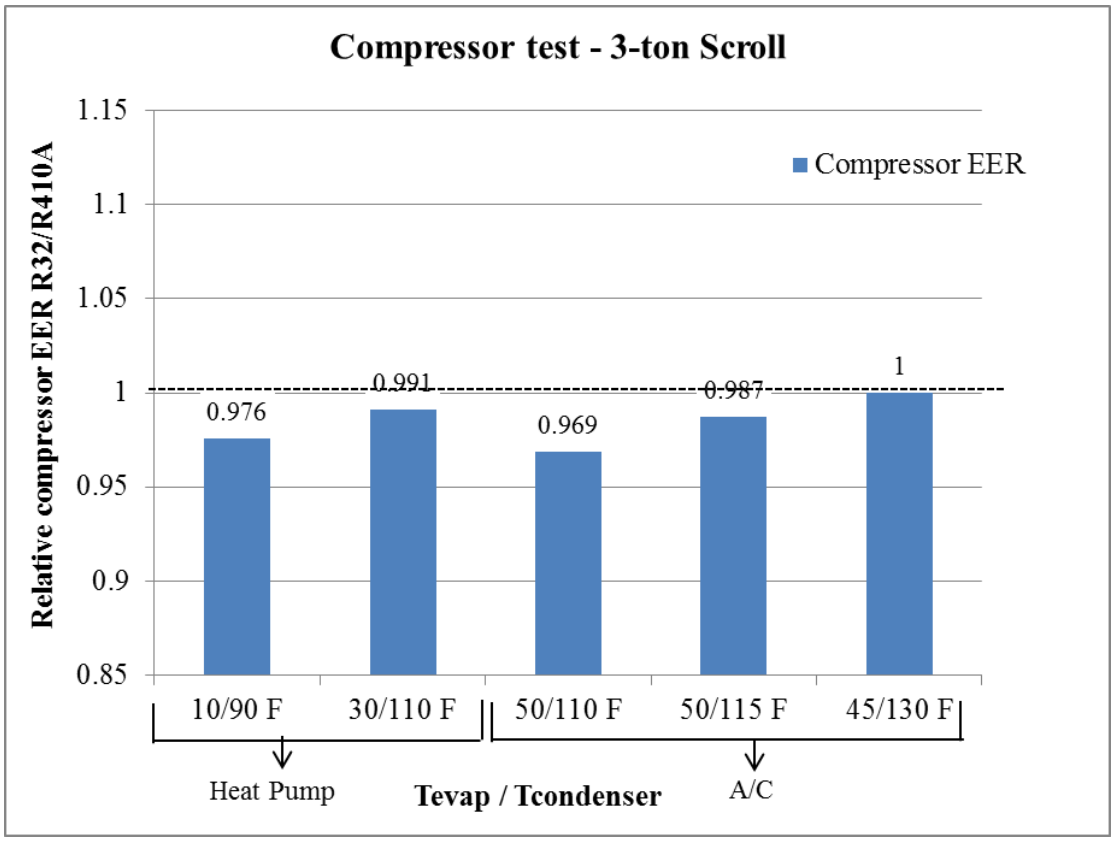

Figure 4: Ratio of compressor EER of R32 with R410A (adapted from Pham & Rajendran, 2010)

The work done by Pham & Rajendran also observes that the discharge temperature was generally 22% higher for R32 than R410A. Their work also suggests options for reducing the impacts of compression heat which include, 1) reduction of entering suction superheat by better system flow control like Electronic Expansion Valve (EXV), 2) optimization of compressor internal design, 3) employing compressor Vapor Injection (VI) and 4) improvement of oil in order to enable higher discharge temperatures. These changes to the system can be still cost effective owing to the savings from lower cost for R32. The next series of tests were the drop-in system performance comparison of R32 versus R410A.

A summary of advantages and disadvantages of R32 over R410A from this literature are summarized in the table below.

Table 10: Summary of advantages and disadvantages of R32 over R410A (reproduced from Pham & Rajendran, 2010)

Advantages	Disadvantages
Considerably lower cost than R410A.	Mildly flamable refrigerant.
Available in high volumes as it is 50% of R410A composition.	Higher compressor discharge temperature.
8% higher critical temperature.	Polyolester (POE) oil not miscible.
Better performance at higher ambient temperatures.	New oil may be required.
Similar presure ratios.	
Close drop-in replaement for R410A without major redesign.	
9% lower liquid density thus lower system charge required.	
28% lower system flow rate.	
Higher volumetric capacity due to 43-50% higher latent heat.	
Higher heat transfer coefficient at same mass flux.	

Thus as far as the efficiency and cost is concerned R32 is a possible solution for A/C and heat pump applications with performance comparable to R410A. The study by Pham & Rajendran believes that R32 can serve as the initial candidate for refrigeration applications to replace HFC which are foreseen to phase out in near future.

Summary from Literature Review and relevance to present work

From the literate review I observed that R1234yf was tested for low capacity (small scale) refrigeration system such as automobile and domestic refrigerators. R32 was tested in medium size AC systems mainly in research community in China and Japan. However the data available on performance of R32 in AC and heat pump system for residential applications are very limited. The present thesis expands the study in the literature for assessing the performance of R32 and R1234yf for a 5-ton nominal capacity split system.

Part of the present work overlaps with the studies conducted in the literature. While the performance evaluation of the system with R32 and R1234yf as working fluids is common method of assessment the unique aspect of the unique contribution of the present thesis are highlighted next.

System evaluation at off design conditions:

In order to evaluate the performance of the system with different refrigerants as working fluids, AHRI standard 210 was applied similar to most of the testing carried out in the literature. AHRI standard provides a guideline for testing a system at low, extreme low and moderately hot ambient temperatures. The present work takes a step further and assesses the system performance at extreme high ambient conditions. Such conditions are witnessed in Midwest America and many parts of the Middle East and south Asia. The results from the extreme ambient or off design conditions reveal some important observations which would not have been encountered only if AHRI standards were to be implemented.

System charge management:

The experimental campaign also takes special care in observing the effect of refrigerant charge on changing ambient conditions. Since the new refrigerants were tested in a system which was originally designed for R410A, the optimal charge that would provide maximum performance was not known a priori. Once the optimal charge was experimentally determined with using basically a trial and error approach at one outdoor temperature, I noted the same charge could not maintain superior performance at other outdoor temperature or when changing from cooling to heating mode. A detailed charge management procedure was investigated in the present thesis to address the issue of optimal charge in the system.

Assessment of indoor coil performance:

The behavior of indoor coil for varying ambient conditions for different refrigerants was monitored by assessing quantities such as refrigerant flow rates and pressure drop across the coil. Other important quantities such as indoor coil sub cooling and degree of coil superheat were investigated in order to get an insight of the behavior for the heat transfer capacity.

Optimization of working refrigeration cycle:

Based on the guidelines provided by the AREP, for the evaluation of alternative refrigerants, two series of testing is recommended. One being the drop-in test and the other is 'system soft optimization' or minor modifications to the system using standard production line. I have followed a similar trend for this work. Initially drop-in tests were carried out, followed by system optimization tests. Owing to the fact that the split system was originally designed for R410A, the TXV or the thermal expansion valve provided by the manufacturer would work best for R410A. As a part of soft optimization, TXV was modified and optimization of the refrigeration cycle was achieved. Optimization process involved fine tuning the low pressure side in order to achieve maximum capacity and COP.

There were some limitations associated with this work such as inability to check the effect of varying compressor speed on the refrigerant evaluation. A variable capacity compressor was not used for the present work and thus the compressor speed was kept constant throughout the experiments. In addition the present thesis does not cover the indirect effects of the refrigerant performance in the system to the environment. By using the same system for all refrigerants the assumption made was that the indirect effects from the production and manufacturing of the system were the same. The indirect effects from the refrigerant leakage to the environmental pollution were also not investigated in the present thesis.

CHAPTER III

OBJECTIVES

The purpose of the work presented in this thesis was to evaluate the energy performance and capacity of the two refrigerants R32 and R1234yf. It was concluded in the literature review that there is limited data available for these refrigerants for residential applications. Even though R32 is being tested as a replacement for R410A in Asia, there is no data for the 5 ton AC and heat pump system. R1234yf proved to be successful for low capacity refrigeration such as automobile applications, but it was never investigated for residential heat pumps. Thus this work presents energy performance for R32 and R1234yf for a 5 ton residential heat pump with a detailed analysis of the refrigerant based vapor compression cycle.

Specific Objectives

The specific objectives of this thesis are

- Study the thermodynamic cycle characteristics of R32 and R1234yf when they are used in heat pump split systems.
- Asses the energy performance and capacity for R32 and R1234yf with respect to R410A for 5 ton residential heat pump units commercially available in the US.
- Investigate minor adjustments on the system that can yield equal or comparable performance as R410A.
- Identify the potentials and shortcomings of these two low GWP refrigerants.

Along with these specific objectives following evaluation criteria were also assessed; system performance at off design conditions, system refrigerant charge characteristics and assessment of indoor coil performance.

Technical Approach

In order to achieve the evaluation of the energy performance and capacities, the experimental campaign was divided in two parts. The first phase of testing was evaluating the drop-in performance followed by TXV soft optimization.

Drop-in performance

In this series of tests, the proposed refrigerants were examined for direct drop in or retrofit for the split system heat pump which was originally designed for R410A. R32 and R1234yf were introduced in the system without any alterations to the system and the comparison was sought. Later on the charge in the system was varied to attain the maximum COP and capacity with a respectable degree of superheat at the compressor inlet. The drop-in performance was important to see if proposed refrigerants would work for the AC and heat pump system which exist on the

field and in the market. Positive results from these tests would mean that the existing units could be used without any modifications but mere change of the refrigerants. This will save money, material and energy and the transition to the new refrigerant will be rather smooth. The drop-in test would also be helpful in investigating the performance of each component in the refrigeration cycle and possibly provide suggestions to improve the performance of the overall system.

TXV soft optimization

The main objective of this phase of testing was to look for minor adjustments on the system that will yield equal or comparable performance as R410A. One can design a new refrigeration system for the proposed refrigerants to be able to deal with the load. But the question was what changes in the existing system would allow the system to work with the same load. Modification of the compressor, evaporator or condenser coils would be a possible option. TXV can be considered as the brain of the refrigeration system. This thesis suggests the modification of the TXV on the refrigeration cycle in order to optimize the cycle pressure. The word ‘soft’ indicates very basic changes. In this series of tests, the optimal charge or the charge that delivered a maximum COP and capacity was chosen and kept constant. Later on, the cycle pressure was optimized keeping the refrigerant charge same.

CHAPTER IV

EXPERIMENTAL SETUP

This section will provide a detailed overview of the equipment used for the study of low GWP refrigerants. The specifications and the assembly are explained in fair amount of detail so that this series of experiments can be replicated in any lab. The experimental campaign was carried out in a large-scale psychrometric chamber at Oklahoma State University (OSU). A psychrometric chamber is a highly insulated confined space where in the conditions inside the volume of the room is controlled to a very high level of accuracy. The facility was fairly large with respect to the equipment tested in this work in order to guarantee uniform temperatures and humidity around the equipment and to minimize thermal and fluid-dynamic interferences between the air streams to/from the unit with the walls and ceiling of the rooms. Figure 5 shows the layout of the heat pump split system ducted inside the psychrometric facility during the laboratory measurements.

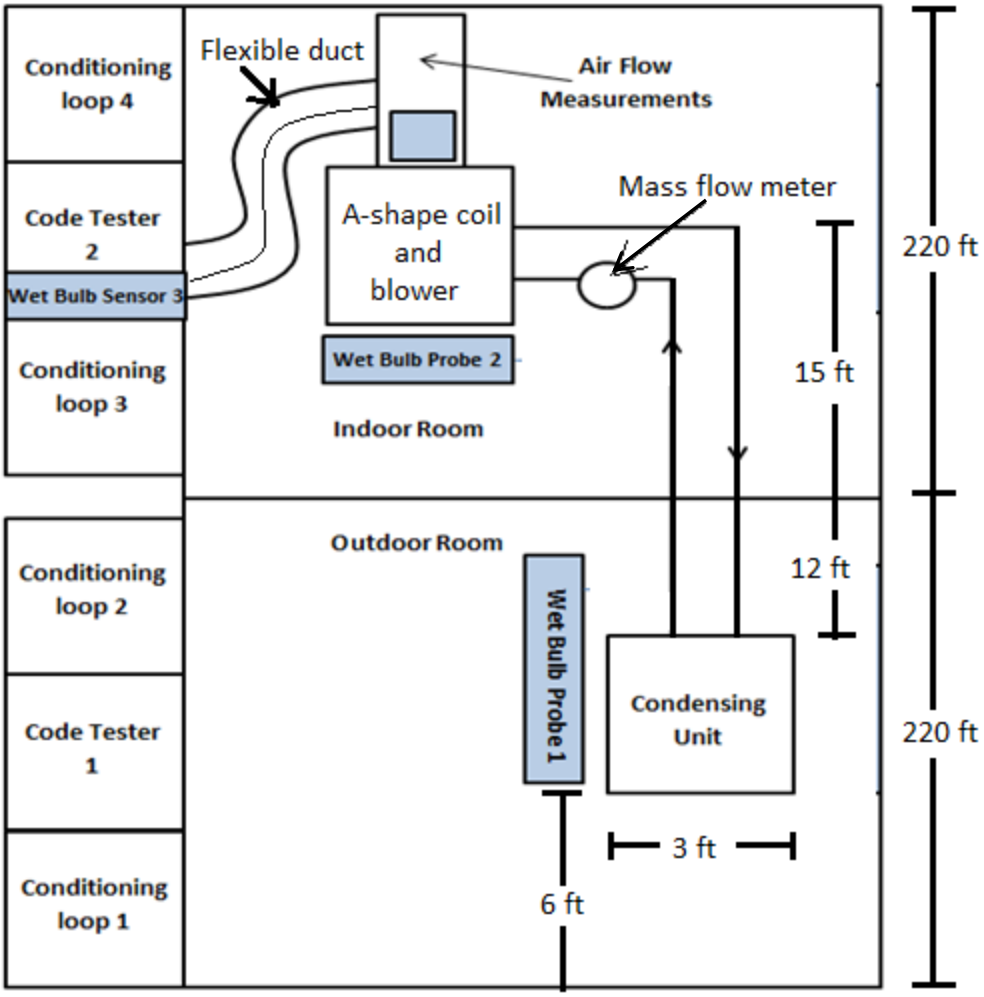

Figure 5: Floor plan of heat pump split system inside OSU large-scale climate control psychrometric chamber

Psychrometric chamber

The psychrometric facility shown in Figure 5 consists of two adjacent air conditioned rooms that are controlled over a wide range of conditions with and without a live load in it; one room artificially reproduced the outdoor climate conditions while the other room is employed to simulate the indoor environments and replicate indoor comfort conditions with thermal loads up to 20 tons of refrigeration It is possible to achieve a temperature range of -40°F to 135°F and

50°F to 135°F for the outdoor and indoor rooms respectively and a relative humidity from 10% up to 95% in both rooms. Stable and uniform conditions are achieved in the rooms by initially conditioning the air to the desired psychrometric states and later the circulating it inside the rooms. The dimension of each room is about 19ft x 21ft of floor and 16ft to the ceiling. Cremaschi and Lee (2008) provided details about the facility design, construction, and specifications for the psychrometric chamber used in this work. Specifications for the chamber in-house instrumentation and controls can be found in Worthington et al (2011).

Heat Pump Setup

A split system consists of two units namely a condensing unit and an indoor coil-blower assembly. The condensing unit consists of an outdoor coil, fan and a compressor. The heat pump used for the experiments was a R410A heat pump split system commercially available off-the-shelf and with a rated capacity of 5 ton. The unit was powered on 208VAC, 3-phase, and 60 Hz current in typical ducted HVAC residential applications in U.S. The unit had an A-shape fin-and-tube direct expansion evaporator with constant speed blower and a tube-and-fin condenser with constant speed fan. The indoor blower and coil were assembled and installed inside the indoor room as shown in figure 6 and figure 8. A scroll refrigeration compressor was in the condensing unit and it had 2.885 in^3/rev displacement volume and run at 3450 RPM at 60 Hz. The compressor was pre-charged by the manufacturer with 53 oz. of POE lubricant, which had a viscosity of 30 cSt at 104°F. A suction accumulator was installed by the manufacturer. The unit had two TXVs and a 4-way reversing valve: one TXV was installed at the inlet of the indoor coil for cooling mode operation while the second TXV was at the outdoor coil for heat pump operation. The unit did not have a discharge oil separator and additional 22 oz. of POE lubricant were charged into the compressor suction port to compensate for the oil that could be retained along the suction line during the unit operation.

Figure 6: Indoor blower/coil assembly (left side) and outdoor condensing unit (right side)

Condensing unit was installed in the outdoor room of the psychrometric chamber as shown in figure 7 and in the left photo of figure 6. The indoor coil-blower assembly sat in the indoor room where indoor comfort conditions were created in the room. The two units were located in the respective rooms in such a way that the uniform air flow from the chamber was not obstructed. The copper piping was used to connect the two units together. The copper pipe which transported the liquid refrigerant from the condenser to the evaporator in the indoor room via a TXV is called the 'liquid line' while the pipe which carried the superheated refrigerant from the evaporator to the compressor located in the outdoor room is called as the 'vapor line'. The liquid line is the high pressure side and the vapor line is the low pressure side on the refrigeration loop. The vapor line is larger in cross sectional length as it needs to accommodate larger volume of refrigerant

than the liquid line. Thus a 3/8” O.D. pipe was used for the liquid line while a 7/8” O.D. pipe served as the vapor line. The length of the liquid and vapor line each was about 40 feet. Once the pipelines were laid they were insulated with special care to avoid heat losses to the ambient air.

Table 11: Summary table of heat pump setup

Component	Description
Heat pump split system	R410A refrigerant 5 ton capacity
Unit power	208 VAC, 3-phase 60 Hz
Scroll refrigerant compressor	2.885 in^3/rev displacement volume
	3450 RPM at 60 Hz
POE oil	Viscosity of 30 cSt at 104°F
Liquid line	3/8" O.D. copper pipe
Vapor line	7/8" O.D. copper pipe.
Pipe insulation	3/8" thick ultra-flexible foam

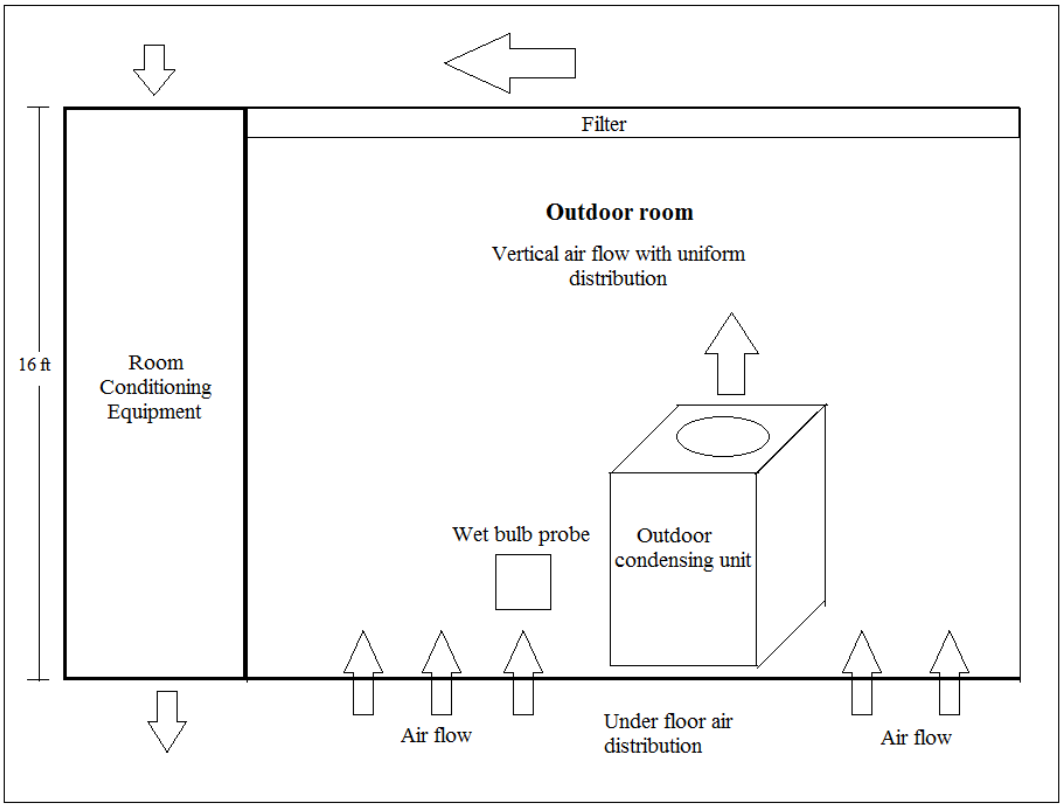

Figure 7: Schematic of outdoor room (side view)

The insulation used for the pipelines was 3/8" thick ultra-flexible foam rubber pipe insulation. The heat flow factor (k-factor) for this insulating material was 0.25 Btu-in/hr-ft^2-°F at 75°F with an operation temperature range of -295 to 220 °F. Once the pipes were insulated, the construction for the air ducts to measure the air flow was undertaken.

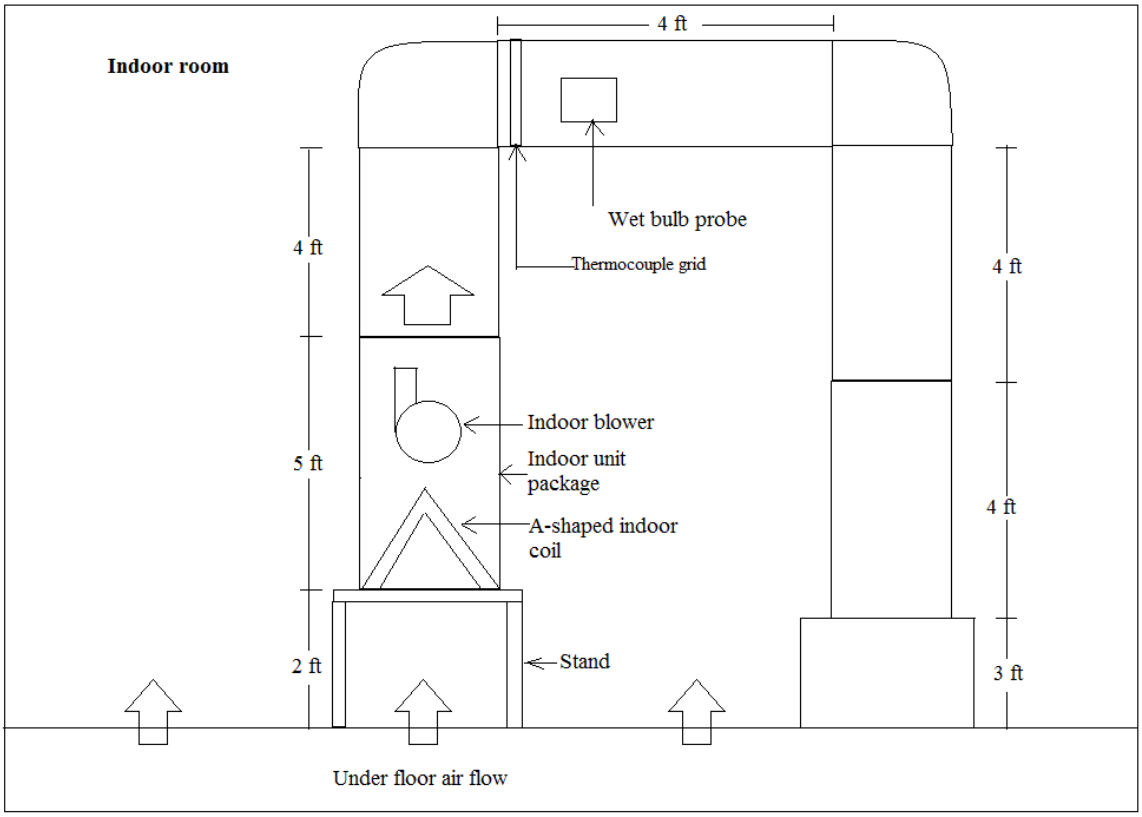

Figure 8: Schematic of indoor room (side view)

Air flow measurements

The construction of air ducts and instrumentation and specifications for air flow measurements will be covered in this sub-section. The conditioned air leaving from the indoor unit on the split system had to be channelized and measured. Flow nozzles were used to measure the air flow rate. The nozzle bank is located in code tester 2 in the indoor room of the psychrometric chamber. Air

flow rate with nozzles was calculated from the pressure differential measured across the nozzle bank. The junction with the chamber walls and all the connections back to the test-procedure outlet were properly sealed and the air leaks were within 1% of the air flow rate being measured. Cremaschi and Lee (2008) give more details on the specifications of the nozzle bank. The pressure differential across a flow nozzle was measured with a pitot tube. A specific number of nozzles were left open while the others were left closed in order to have a measurable pressure drop across the nozzle bank.

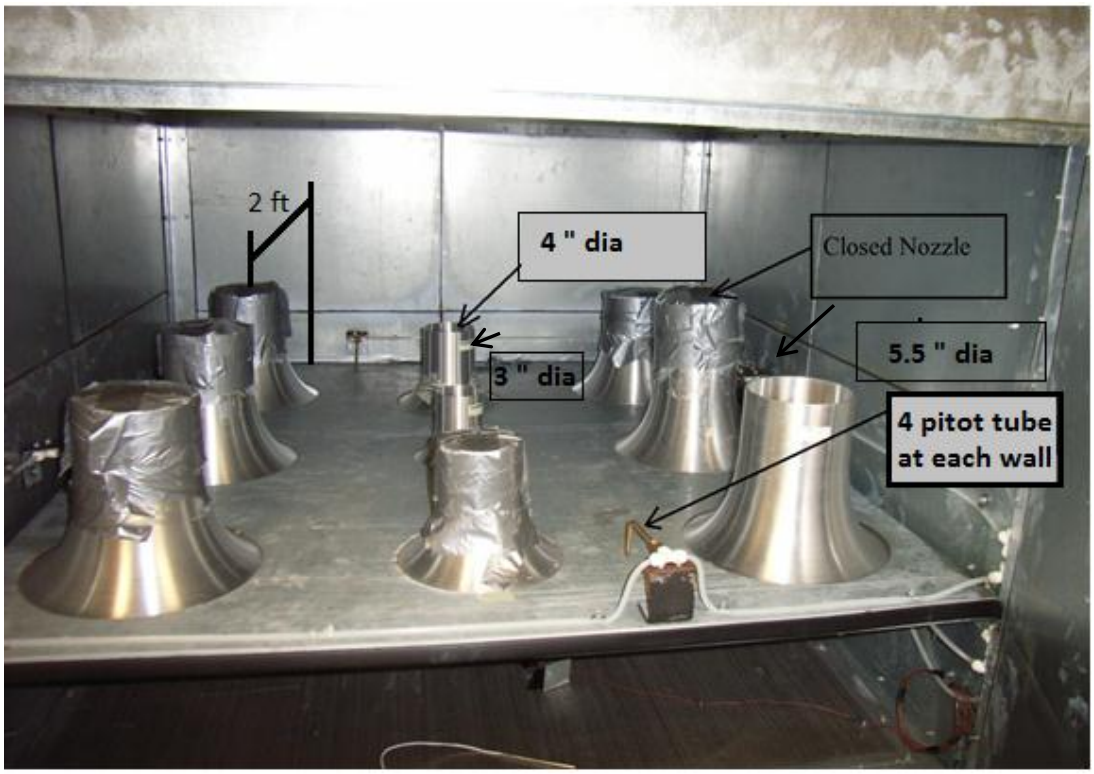

Figure 9: Nozzle bank inside code tester of indoor room

Figure 9 demonstrates the nozzle bank configuration to measure the air flow rate. There are 4 pitot tubes at each wall and static pressure is calculated by averaging the four readings. 3", 4" and a 5.5" diameter nozzle are kept open while all others are sealed.

AHRAE standard 41.2 was employed for measuring the air flow rate with nozzle bank. The pressure drop across the nozzle was used in the Reynolds number calculation which later was useful in determining the nozzle discharge coefficient. The air flow rate was then calculated with the knowledge of the nozzle discharge coefficient and the open area of the nozzles. Two sets of dry bulb and wet bulb probes (ASHRAE standard 116) were installed in front of the condensing unit and of the indoor coil.

Dry bulb and wet bulb probes against the condensing unit (labeled as 1 in figure 5) determined the air quality of the outdoor room while the ones located against the indoor unit (labeled as 2 in figure 5) determined the air quality of the return air in the indoor room. A third probe (labeled as 3 in figure 5) was installed downstream of the coil to measure the humidity ratio of the air stream leaving the indoor coil or the supplied air conditions. Each probe consisted of a RTD to measure wet bulb temperature, another RTD to measure the dry bulb temperature and a relative humidity sensor.

The major task was to connect the indoor coil-blower assembly to the nozzle bank in accordance with the standards. It is important to know the pressure drop across the indoor coil. The ASHRAE standard 41.2 dictates certain minimum distance for measuring the outlet pressure from the blower. According to this standard, minimum distance of 4 feet is required from the indoor coil/blower before the supplied air could be sampled. Hence a 4' tall duct work is constructed from the indoor coil after which the outlet pressure and temperature is measured. Figure 8 illustrates the ductwork and the exact location of sensors. 12" X 24" X 48" aluminum ducts were used for the ductwork. At the base of the duct a metal box was constructed to connect the rectangular metal duct to a 24" round flexible duct. It is via this flexible duct that the supplied air is the channelized in to the indoor code tester. Details of the ductwork and metal box construction are provided in figure 8. The duct and the metal box were then insulated with R-5 (1" thick) insulation to avoid heat losses. 8 feet tall ductwork was supported with metal strut channels.

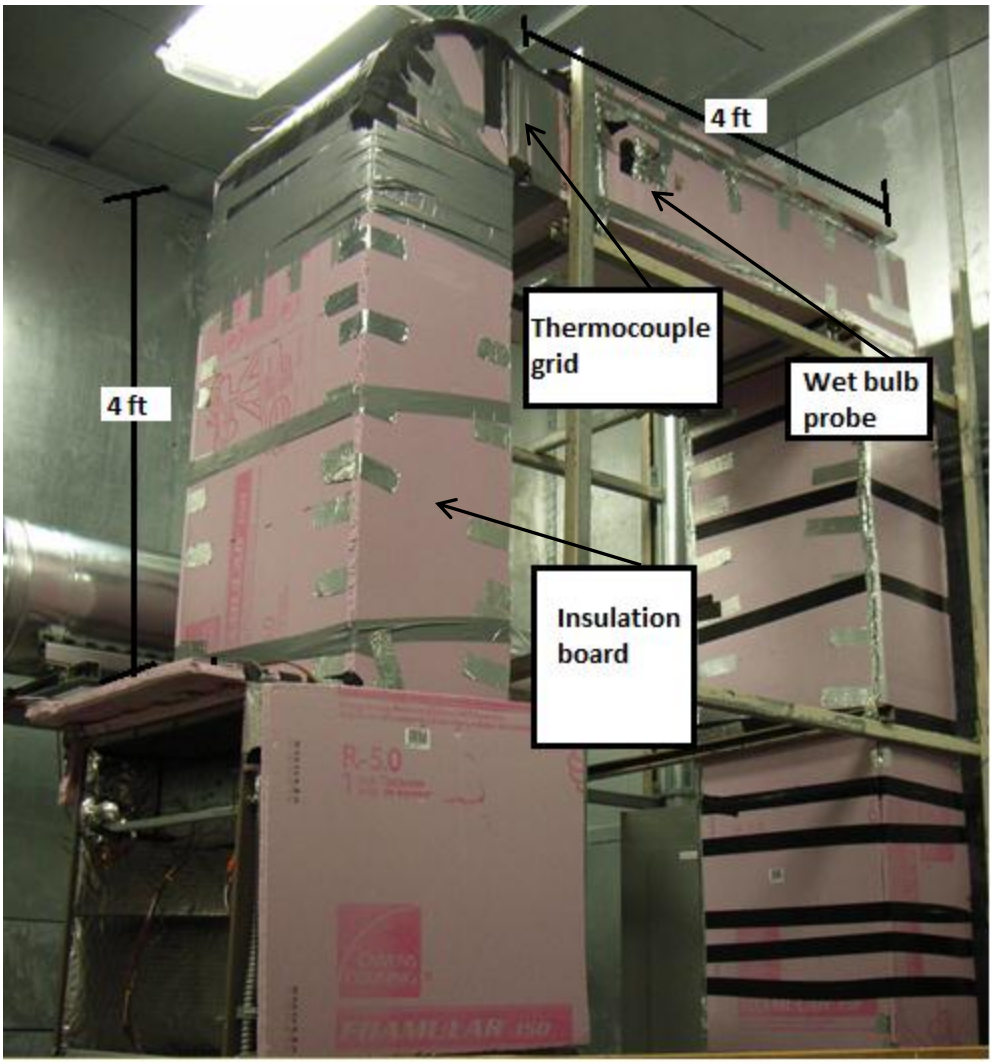

Figure 10: Air duct connecting indoor coil and psychrometric code tester and location of the thermocouple grid and wet bulb probe inside the duct.

A grid of five thermocouples was installed at the cross section of the duct right where it bends after the blower as shown in figure 10. The sampling tree to measure the moisture quality of the supplied air was also located after the bend next to the thermocouple grid. In order to direct the air from the sampling tree to the wet bulb sensor 3, a 4" duct was installed concentric with the 24" flexible duct as shown in figure 10. Once the air was received via the small duct at the wet

bulb sensor 3 inside the code tester 2, the wet bulb temperature and the relative humidity was read.

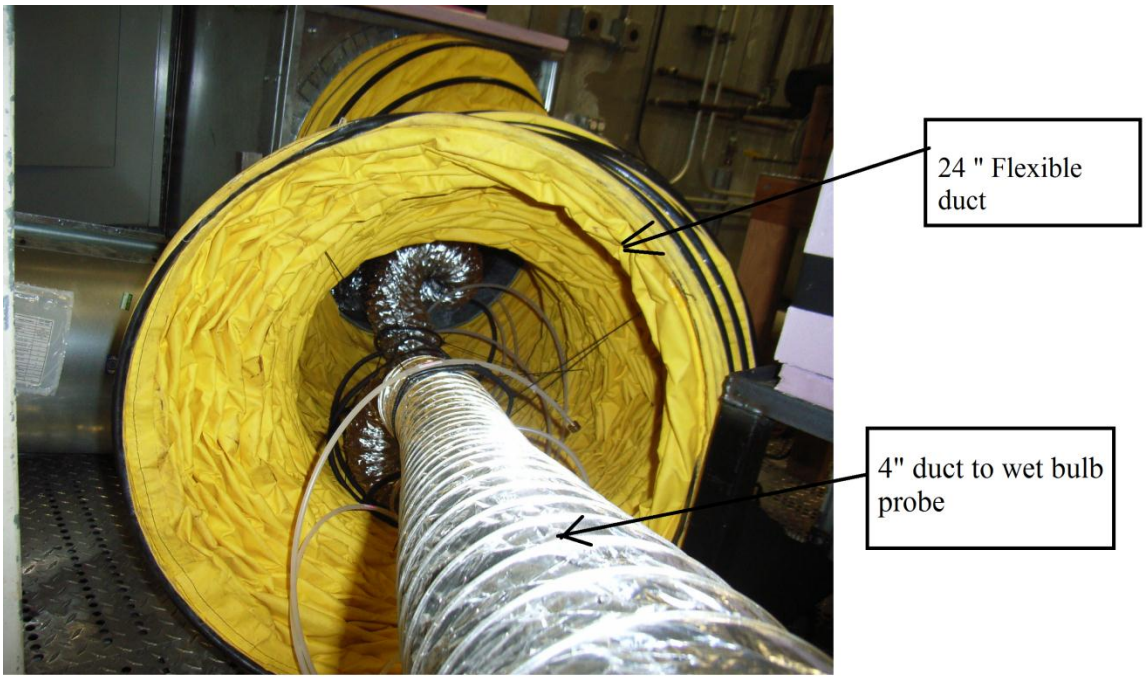

Figure 11: Flexible duct carrying conditioned air from the indoor unit

The opening at the code tester was a hole of 2 feet diameter. It was decided to connect the lower box to the code tester with a 24" diameter flexible duct shown in figure 5 and figure 11. In order to lock the flexible duct in place on the aluminum box and at the opening of the code tester 'quick connects' were used. Quick connect joint served as a lip on the metal board which enables the flexible duct to slide on. Once the duct was on the lip, it is tightened with the help of metal zip tie to avoid air leaks. The most difficult part in making the quick connect was to give the curvature to the thick sheet metal. 2 feet hole was made to a thin metal frame. 4" X 80" long aluminum strip was bent in a circle with its ends bent to make a sleeve as shown in figure 12. The sleeve was bolted to the metal frame aligning the 2 ft. holes. The flexible duct was then fastened over the

quick connect never to be removed. The metal frame served as the access point for the flexible duct.

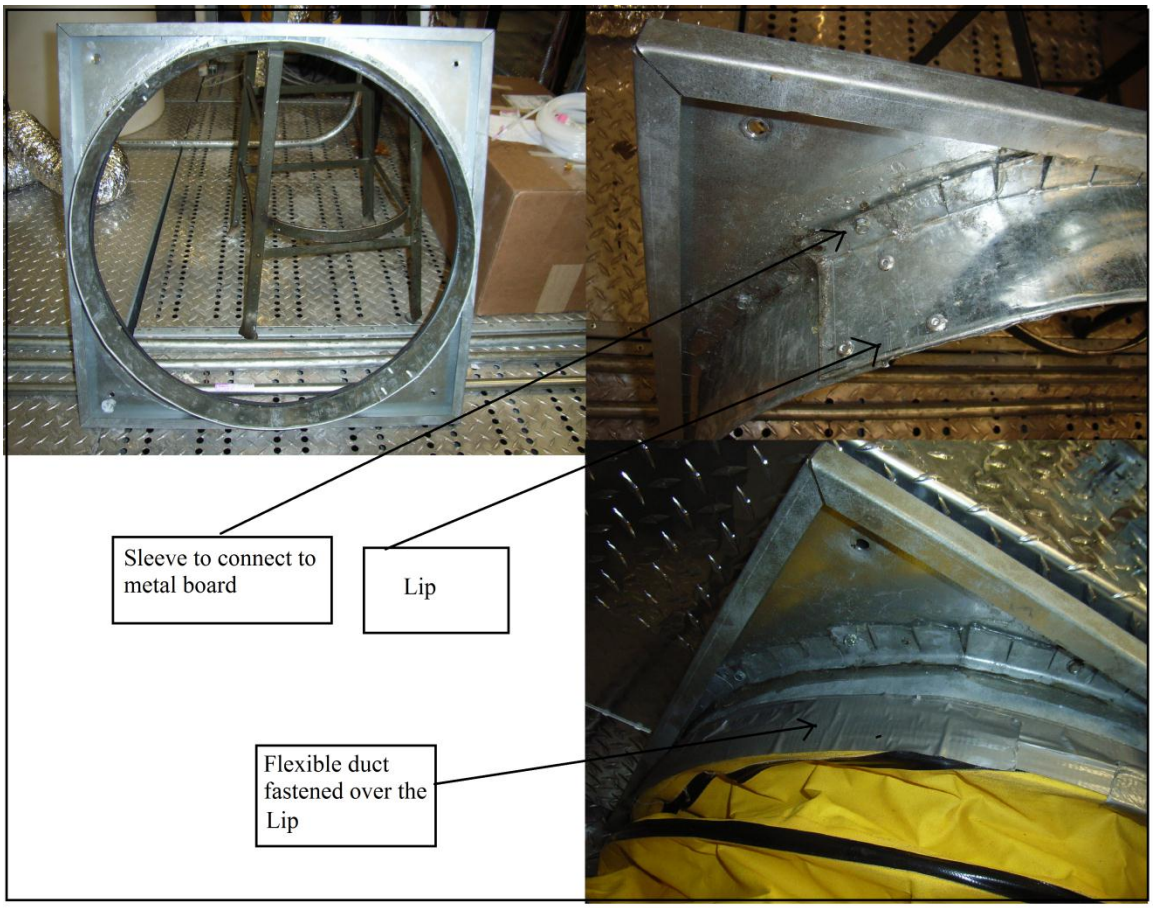

Figure 12: Quick connects to connect flexible ducts to the code tester

Refrigerant side measurement

The unit was instrumented as shown in Figure 13. Temperature and pressure sensors were installed at the inlet and outlet of each component of the refrigeration system. This enables us to know the two independent properties of temperature and pressure at every state point of the refrigerant loop. With these independent properties the secondary quantities such as enthalpy, entropy etc. can now be calculated. Special care was taken while installing the pressure

transducer as they came with a threaded fitting. Threaded fittings are more susceptible to leaks when high pressure is involved. A layer of Teflon tape was applied over the male joint followed by leak lock. Leak Lock is a high strength, pipe joint sealant consisting of chemically resistant film formers, plasticers, reinforcing fillers and solvents. Leak Lock adheres to the threads of the fitting and sets to form a chemically resistant flexible fluid-tight seal. This method was applied to seal all the threaded joints around the loop.

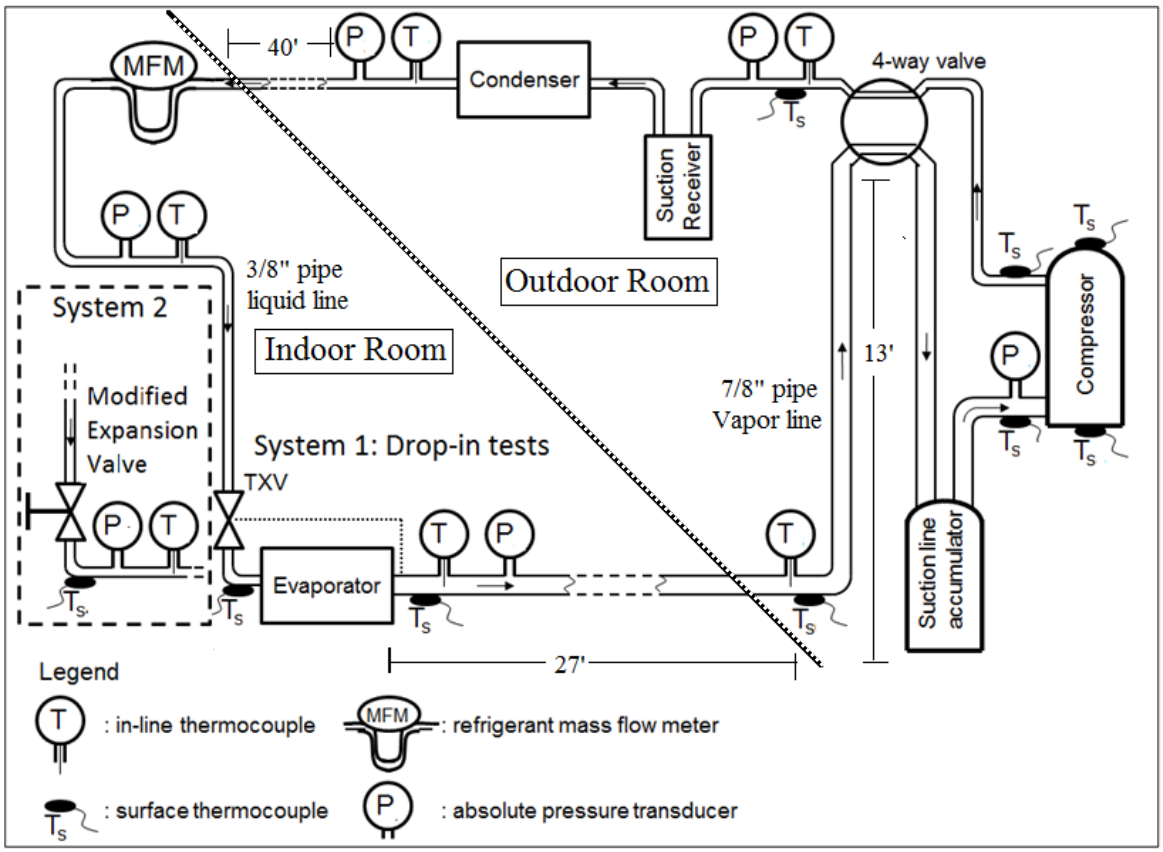

Figure 13: Schematic of heat pump system and layout of instrumentation

The discharge pressure and temperature (P_1 and T_1 in Figure 12) were located on the refrigerant discharge line after the 4-way valve. It was not feasible to dig through the discharge line right after the compressor. The distance between these sensors and the compressor discharge port was

about 2 ft. of pipeline. The 4-way valve and the refrigerant pipelines were well insulated to prevent heat losses to the ambient. However, some heat exchange was expected to occur between the hot vapor in the discharge line and the cold vapor in the suction line when the refrigerant crossed the 4-way valve. Several surface thermocouples were also installed on the compressor crankcase to monitor the compressor housing temperature.

There were some places on the loop where it was not possible to get into the original piping by the manufacturer in order to install the inline thermocouple or the pressure transducer. These places include suction and discharge port of the compressor and indoor coil inlet conditions. To solve this problem, a surface thermocouple was installed right next to the inline thermocouple and one where the accurate measurement of temperature was required. Later the temperature difference between the inline thermocouple and the surface thermocouple was recorder. This difference was later accounted for surface thermocouple at the desired position just as if the inline thermocouple existed there. For example, it can be seen that T_6 is away from the point where the reading would be desired. It would be nice to have T_6 right next to P_6.In such case, difference between T_6 and T_{s6} is recorded and this difference is either added or subtracted to T_{s7} depending upon which one tends to be higher. Similar approach was applied for discharge temperatures.

In cooling mode, the evaporator inlet will have the same enthalpy value as that of the TXV inlet condition since the process through the TXV is isenthalpic. The evaporator inlet temperature is estimated the same way as the compressor suction and discharge temperatures. The refrigerant is going to be in two phase at the evaporator inlet. Thus the evaporator inlet temperature is the saturation temperature and saturation pressure corresponding to it can be determined. With the knowledge of P_{sat} and the enthalpy, the refrigerant quality at the evaporator inlet could be accurately calculated.

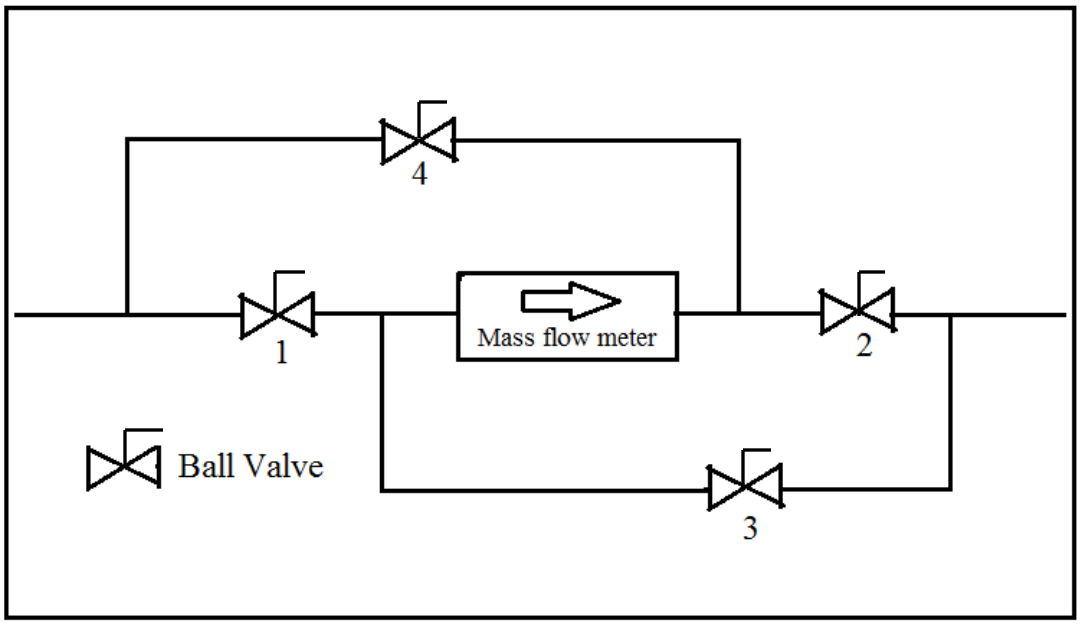

Figure 14: Flow corrector for unidirectional mass flow meter

ValvA Coriolis type flow meter was also mounted in the refrigerant liquid line. The flow meter reads accurately only if the 100% liquid passes through it. If the refrigerant enters the flow meter in two phase the flow meter displays a warning in the form of a blinking amber light on it. The flow meter could measure the flow rate for one direction. It is important to note that during heating and cooling mode the direction of the refrigerant flow along the loop is opposite. The 4-way valve reverses the direction of flow depending on the mode in which the unit is made to run. Thus the flow meter is facilitated with a direction corrector shown in figure 14 so that irrespective of the mode of operation, the flow meter sees the refrigerant flowing in one direction. For example, by closing valve 3 and 4 indicated in figure 14, flow from left to right is possible. On the other hand by closing valves 1 and 2 flow from right to left can be measured. It is important to note that the flow meter can read the flow only in one direction. Before the start of every test it was ensured that the valves on the flow corrector were in place for the particular mode. A

wattmeter was used to measure the electric power of the unit and the unit capacity was measured from the air side (primary method) and from the refrigerant side (secondary method).

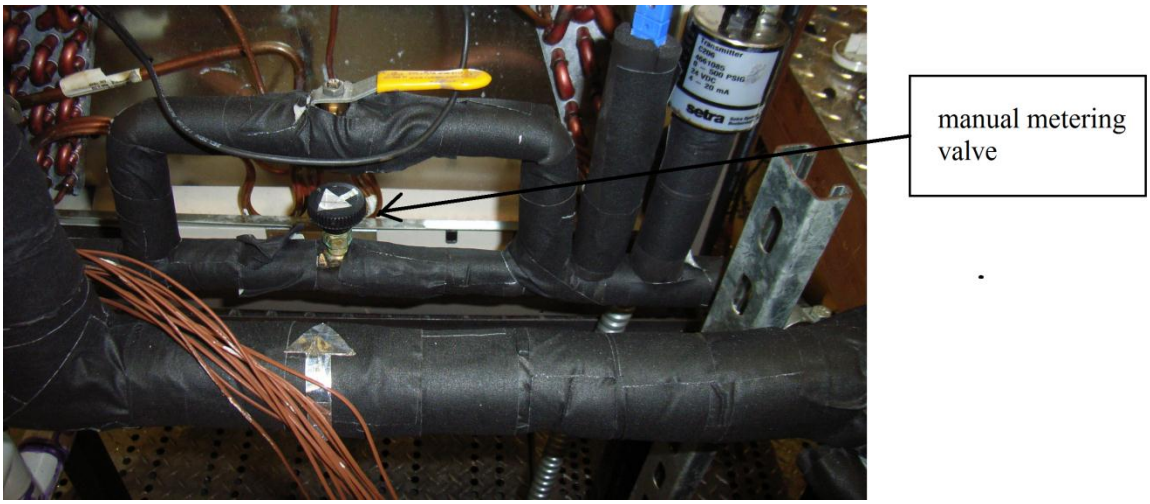

Figure 15: Manual metering valve at the indoor coil inlet

During the TXV soft optimization tests, the TXV provided by the manufacturer was replaced by a manual metering valve as suggested in figure 15 under the box labeled 'modified system option'. The valve used was a 1/8" pipe size Parker instrumentation needle valve with a compression fitting. A set of pressure transducer, inline thermocouple and a surface thermocouple was also installed after the valve and before the distributor. Now the exact pressure drop across the expansion process could be measured and even controlled. Thus the needle valve also referred as metering valve will play the role of TXV with adjustment made manually in order to achieve the required degree of superheat.

Data Acquisition (DAQ) system

This paragraph deals with the procedures for reading the data and recording it. The data such as temperatures, absolute pressures, differential pressures unit power and barometric pressure are directly measured quantities. Quantities such as COP, refrigerant enthalpies, degree of superheat,

sub cooling, etc. are calculated from the direct measurements and hence are called calculated variables. The sensors and the thermocouples installed as hardware act as resistances.

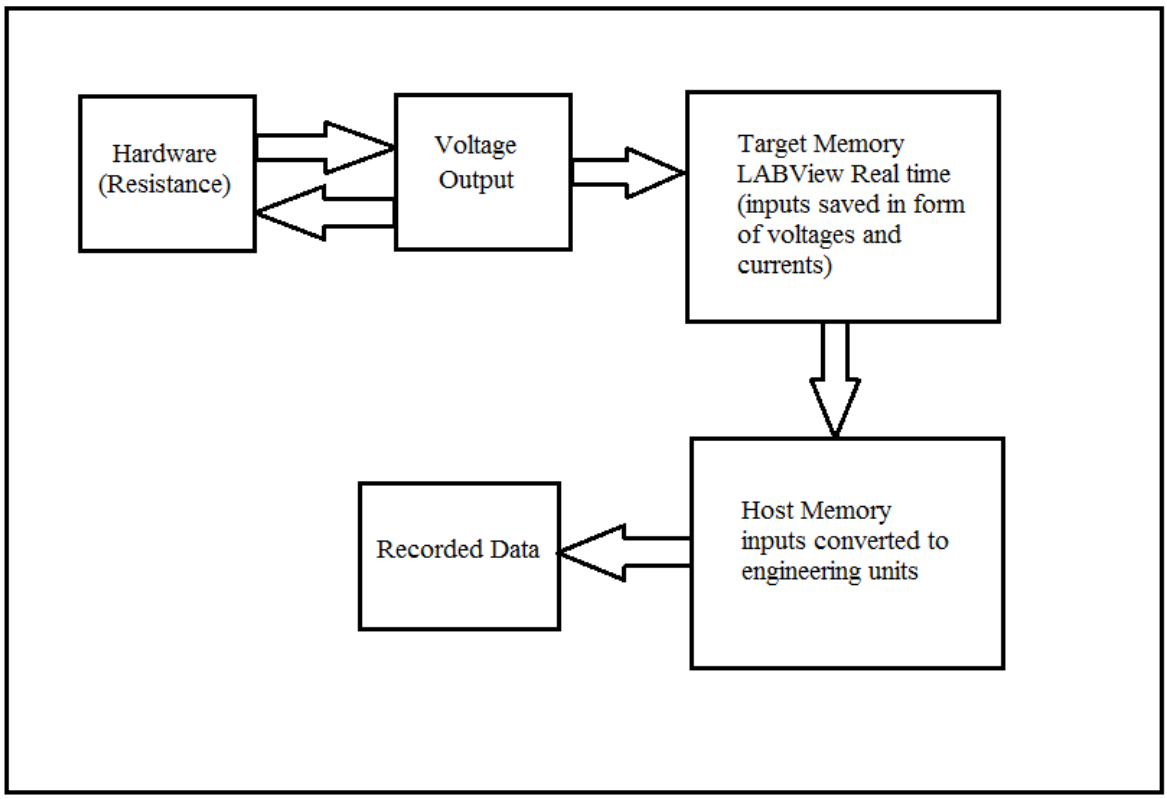

Figure 16: Primary logic of data acquisition

Voltage is applied across these hardware and they draw some amount of current. This voltage drop or current drawn is measured back in the loop. This data of voltage drops signals and current is then received at the target memory. It is stored here without any processing. It is then read onto the LabVIEW real time software also called as the host memory. Here, the raw data or voltage drops and current inputs are converted into more meaningful engineering quantities such as temperatures, absolute pressure, mass flow rate etc. secondary measurements such as COP, degree of super heat are also calculated out here by feeding in formulae. Finally the engineering

quantities are recorded to a notepad document on the host memory and also at external back up drive.

Hardware for instrumentation

The following table gives a list of the hardware used as far the data acquisition is concerned. The hardware was purchased from LabVIEW instruments and more details regarding the set up and control can be obtained from Worthington et al. (2011).

Table 12: Specification of LabVIEW instrumentation

Card	Terminal	Front-	Type of sensor	No. of channels
SCXI 1001	SCXI 1102	SCXI 1303	Thermocouple	32
	SCXI 1102	SCXI 1303	Thermocouple	32
	SCXI 1102B	SCXI 1303	Thermocouple	32
	SCXI 1102B	SCXI 1303	Thermocouple	32
	SCXI 1102B	SCXI 1303	Thermocouple	32
	SCXI 1102	SCXI 1303	Thermocouple	32
	SCXI 1102	SCXI 1303	Thermocouple	32
	SCXI 1102	SCXI 1303	Thermocouple	32
	SCXI 1102	SCXI 1303	RTD	32
	SCXI 1581	SCXI 1300	Current	32
	SCXI 1102B	SCXI 1308	Current Input	32
	SCXI 1102B	SCXI 1308	Current Input	32
SCXI 1001	SCXI 1102	SCXI 1300	Feedback	32
	SCXI 1160	SCXI 1324	SPDT Relay	16
	SCXI 1160	SCXI 1324	SPDT Relay	16
	SCXI 1160	SCXI 1324	SPDT Relay	16
	SCXI 1160	SCXI 1324	SPDT Relay	16
	SCXI 1102	SCXI 1303	Thermocouple	32
	SCXI 1102	SCXI 1303	Thermocouple	32
	SCXI 1102B	SCXI 1308	Current Input	32
	SCXI 1160	SCXI 1324	SPDT Relay	16
	SCXI 1102	SCXI 1303	Thermocouple	32
SCB 68	-	-	AO/DO	40
SCB 68	-	-	AO/DO	40

The CPU or the target memory was NI PXI 10420. This system was coupled with a normal laboratory PC termed as host memory. The LabVIEW code for controlling the parameters for the

current project was developed on this host memory. It is here that the formulation takes place and data is recorded.

The following paragraph provides a list of information regarding the connections of different sensors.

Table 13: Specification of refrigerant side thermocouples

Refrigerant side thermocouples						
INDEX NO	**NEW LABEL**	**DAQ MODULE #**	**Channel Number**	**Type of Data**	**TYPE/MODEL OF SENSOR/DEVICE**	**Location**
196	T4_11	SCXI 1-MODULE7	Ch_4	Temperature	T-TYPE TERMOCOUPLE	BOX4
197	T4_12	SCXI 1-MODULE7	Ch_5	Temperature	T-TYPE TERMOCOUPLE	BOX4
198	T4_13	SCXI 1-MODULE7	Ch_6	Temperature	T-TYPE TERMOCOUPLE	BOX4
153	T7_35	SCXI 1-MODULE5	Ch_25	Temperature	T-TYPE TERMOCOUPLE	BOX7
396	T7_41	SCXI 2-MODULE6	Ch_12	Temperature	T-TYPE TERMOCOUPLE	BOX7
397	T7_42	SCXI 2-MODULE6	Ch_13	Temperature	T-TYPE TERMOCOUPLE	BOX7

The index number is the number associated with the sensor with respect to the entire library. This library includes all the sensors used inside the psychrometric chamber. The label is the physical label on the wire mainly used for identification. DAQ module number and channel number are the source to which the sensor is connected and read from. The table also lists the location of the connector namely the DAQ box number inside the chamber.

Table 14: Specification of surface thermocouples

Surface thermocouples						
INDEX NO	**NEW LABEL**	**DAQ MODULE #**	**Channel Number**	**Type of Data**	**TYPE/MODEL OF SENSOR/DEVICE**	**Location**
199	T4_14	SCXI 1-MODULE7	Ch_7	Temperature	T-TYPE TERMOCOUPLE	BOX4
200	T4_15	SCXI 1-MODULE7	Ch_8	Temperature	T-TYPE TERMOCOUPLE	BOX4
202	T4_17	SCXI 1-MODULE7	Ch_10	Temperature	T-TYPE TERMOCOUPLE	BOX4
203	T4_18	SCXI 1-MODULE7	Ch_11	Temperature	T-TYPE TERMOCOUPLE	BOX4
204	T4_19	SCXI 1-MODULE7	Ch_12	Temperature	T-TYPE TERMOCOUPLE	BOX4
205	T4_20	SCXI 1-MODULE7	Ch_13	Temperature	T-TYPE TERMOCOUPLE	BOX4
398	T7_43	SCXI 2-MODULE6	Ch_14	Temperature	T-TYPE TERMOCOUPLE	BOX7
399	T7_44	SCXI 2-MODULE6	Ch_15	Temperature	T-TYPE TERMOCOUPLE	BOX7

Table 15: Specification of air side thermocouples

Air-side thermocouples						
INDEX NO	**NEW LABEL**	**DAQ MODULE #**	**Channel Number**	**Type of Data**	**TYPE/MODEL OF SENSOR/DEVICE**	**Location**
410	T7_55	SCXI 2-MODULE6	Ch_26	Temperature	T-TYPE TERMOCOUPLE	BOX7
411	T7_56	SCXI 2-MODULE6	Ch_27	Temperature	T-TYPE TERMOCOUPLE	BOX7
412	T7_57	SCXI 2-MODULE6	Ch_28	Temperature	T-TYPE TERMOCOUPLE	BOX7
413	T7_58	SCXI 2-MODULE6	Ch_29	Temperature	T-TYPE TERMOCOUPLE	BOX7
415	T7_60	SCXI 2-MODULE6	Ch_31	Temperature	T-TYPE TERMOCOUPLE	BOX7
400	T7_45	SCXI 2-MODULE6	Ch_16	Temperature	T-TYPE TERMOCOUPLE	BOX7
402	T7_47	SCXI 2-MODULE6	Ch_18	Temperature	T-TYPE TERMOCOUPLE	BOX7
404	T7_49	SCXI 2-MODULE6	Ch_20	Temperature	T-TYPE TERMOCOUPLE	BOX7
405	T7_50	SCXI 2-MODULE6	Ch_21	Temperature	T-TYPE TERMOCOUPLE	BOX7
406	T7_51	SCXI 2-MODULE6	Ch_22	Temperature	T-TYPE TERMOCOUPLE	BOX7
407	T7_52	SCXI 2-MODULE6	Ch_23	Temperature	T-TYPE TERMOCOUPLE	BOX7
408	T7_53	SCXI 2-MODULE6	Ch_24	Temperature	T-TYPE TERMOCOUPLE	BOX7

Table 16: Specification of input/output signals

Input/Output Signals						
INDEX NO	**NEW LABEL**	**DAQ MODULE #**	**Channel Number**	**Type of Data**	**TYPE/MODEL OF SENSOR/DEVICE**	**Location**
302	IN/OUT4_5	SCXI 1-MODULE11	Ch_14	Pressure	1000 psi PRESSURE GAUGE	BOX4
339	IN/OUT7_6	SCXI 1-MODULE12	Ch_19	Pressure	500 psi PRESSURE GAUGE	BOX7
340	IN/OUT7_7	SCXI 1-MODULE12	Ch_20	Pressure	500 psi PRESSURE GAUGE	BOX7
341	IN/OUT7_8	SCXI 1-MODULE12	Ch_21	Pressure	500 psi PRESSURE GAUGE	BOX7
326	IN/OUT6_5	SCXI 1-MODULE12	Ch_6	Pressure	500 psi PRESSURE GAUGE	BOX6
327	IN/OUT6_6	SCXI 1-MODULE12	Ch_7	Pressure	500 psi PRESSURE GAUGE	BOX6
337	IN/OUT7_4	SCXI 1-MODULE12	Ch_17	Flow Rate	Corriolis Mass Flow Meter	BOX7

LabVIEW interface

This section deals with LabVIEW program control strategies and the overall interface used for this project.

Target interface:

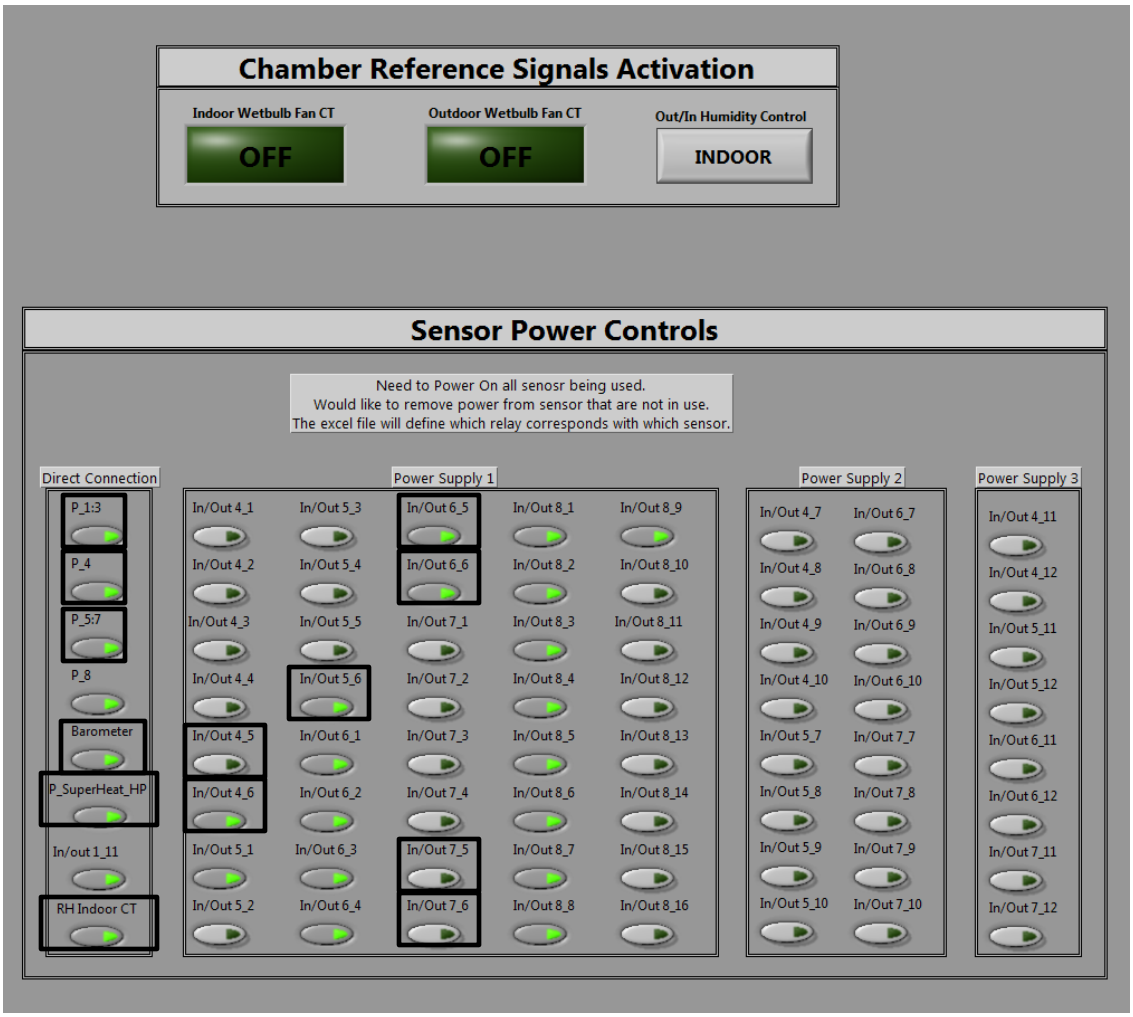

Figure 17: Sensor power control panel and sensors that must be activated in order to energize the instrumentation on the unit

Figure 17 is the power control for the sensor. Sensors such as pressure transducers barometer, code tester fans and differential pressure transducer need power. This window is mainly important since there are simultaneous projects running inside the psychrometric chamber but with the help of selective control these projects could run independent of each other. The sensors marked in the box need to be turned on for energizing the instrumentation required by this particular unit.

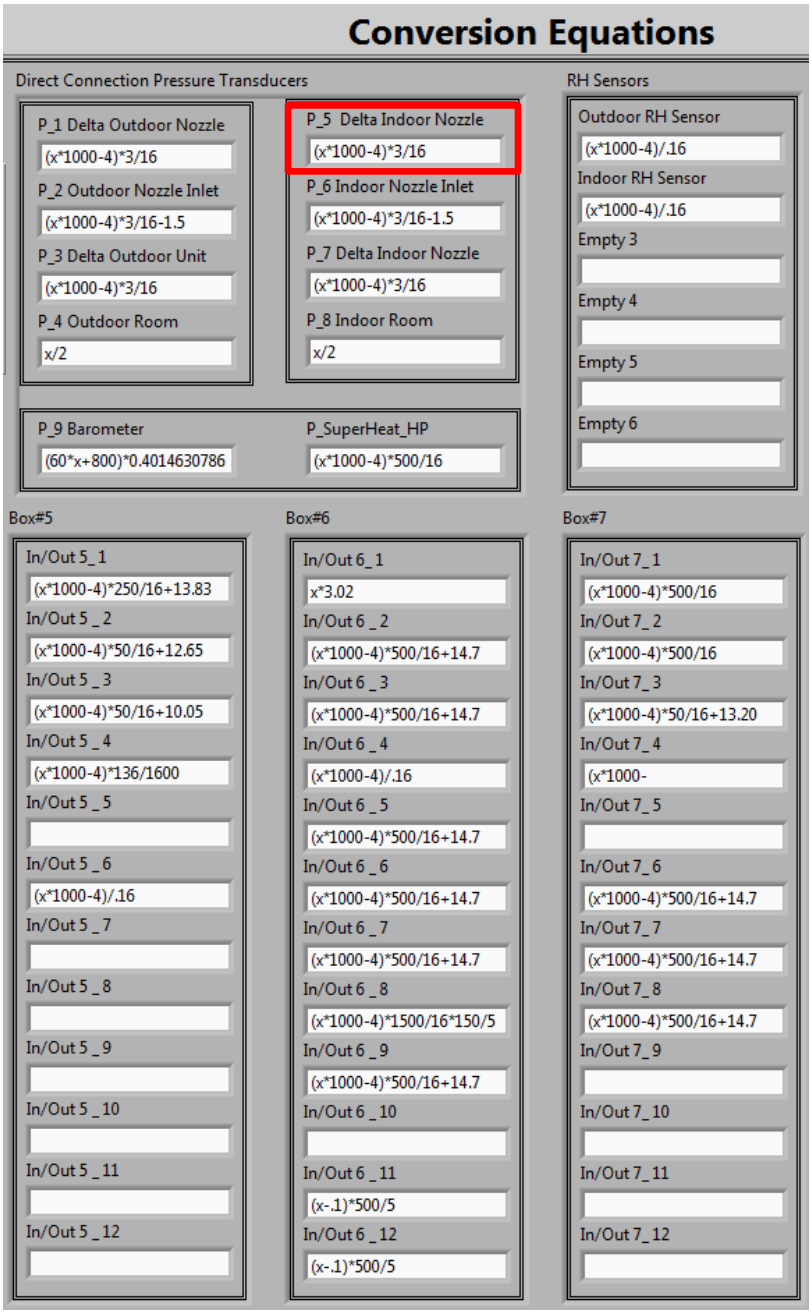

Figure 18: Equation window panel

Figure 18 is the equation conversion window. As described earlier, the target receives the data in the form of current and voltage signals. These data are converted to engineering quantity by plugging in an explicit equation for the quantity. For example, for P_5 Delta indoor nozzle

highlighted in the box is a differential pressure transducer with 4-20 mA output current. This current signal is the converted to a pressure reading using the equation provided within the dashed box which is $(x * 1000 - 40) * 3/16$

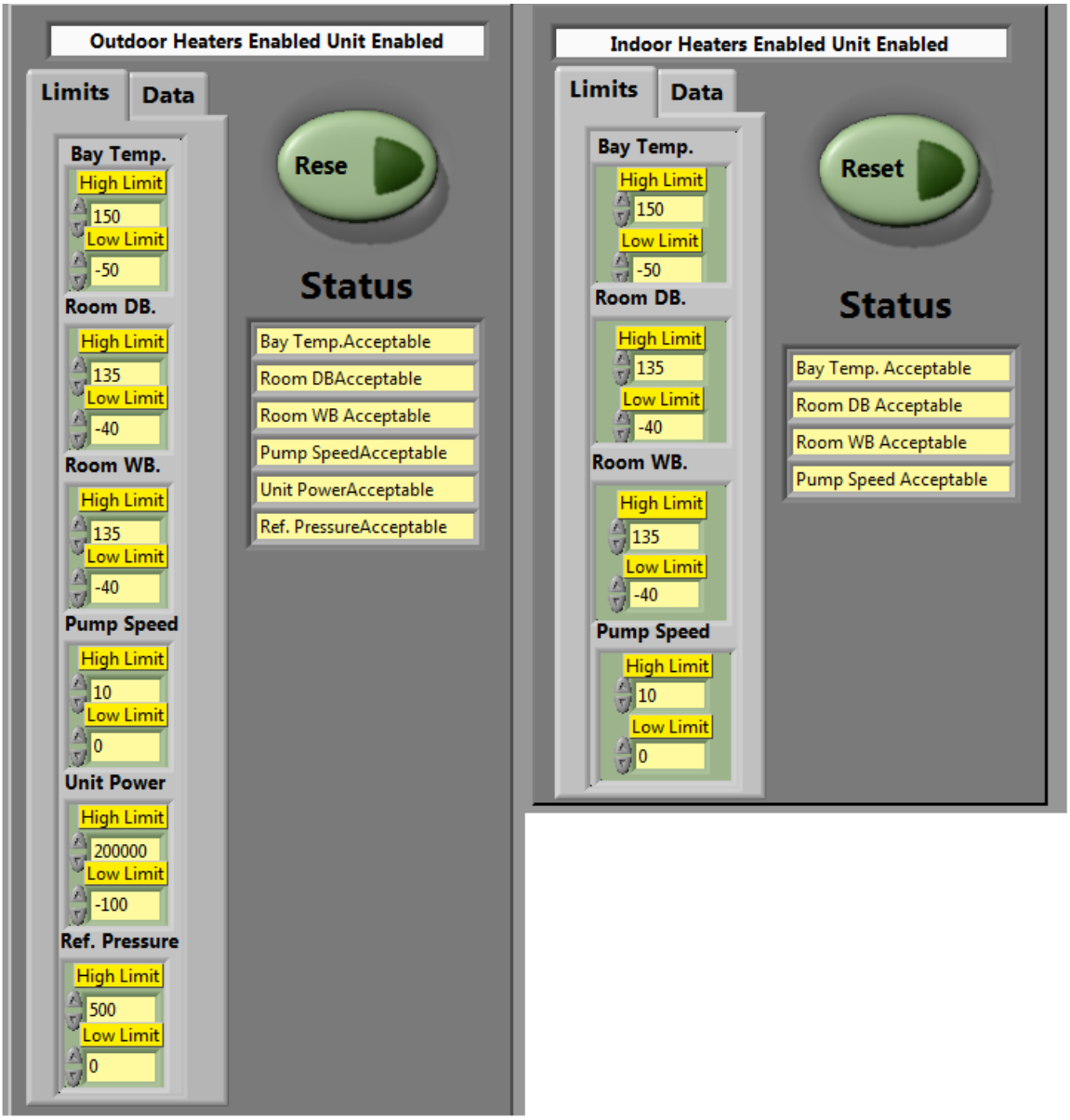

Figure 19: Shut-off limits control panel

Figure 19 is the tab for shut of limits. The shut off limits ensure the safety of the chamber as a whole as well as specific project running inside it. Lower and higher limits of specific quantities can be set in this tab. If at all either a higher or lower limit is hit the power to heaters and equipment is terminated followed by a complete automatic shutdown of the project. For example, the outdoor room dry bulb cut-of for high side is set at 135 F as indicated in figure 19. Thus if in case where the temperature inside the outdoor room reaches 135F, the power to the electric heater will be terminated and the chamber will come to a shutdown. This safeguards the heater coils from melting and also avoids chamber overheating. On the other hand if the lower limit is hit on the refrigerant side, the heat pump will be shut down as there could be a possible leakage of the refrigerant. This makes sure the compressor won't run without refrigerant. Similar cut of limits are also set for the indoor room in such a way that the two rooms are independent and in the event of emergency in one room the other room is not disturbed.

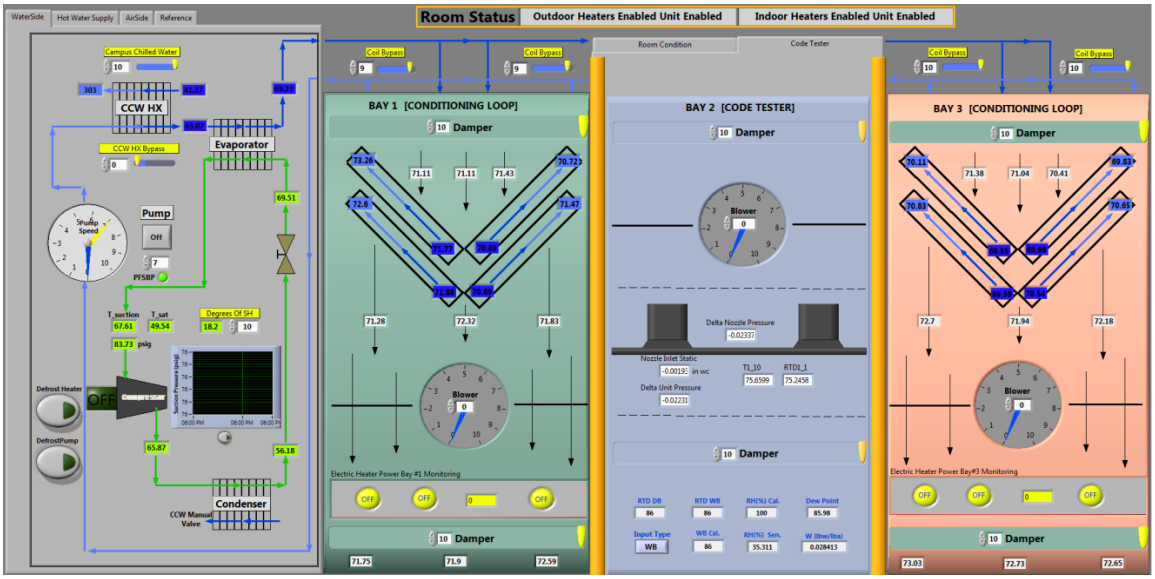

Figure 20: Layout of target control panel

Figure 20 is the host window with water-side control conditioning bay and code tester control panel. Each control panel will now be discussed briefly in following paragraph.

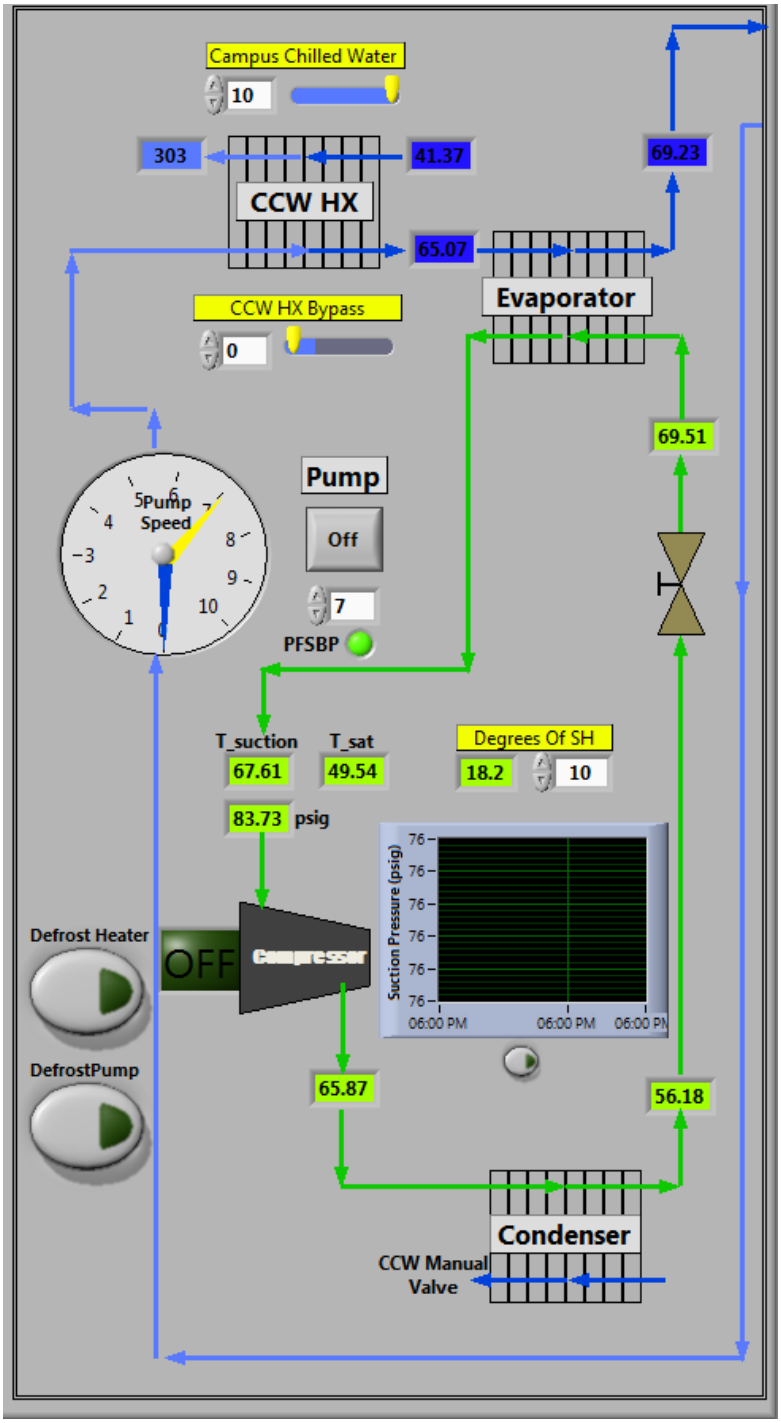

Figure 21: Chilled water control window panel

Figure 21 is the water side control panel for outdoor and indoor room. To achieve the set point temperature inside the chamber, the air is first cooled and then heated to achieve the set point.

The cold water is supplied by the campus chilled water, or for extreme low temperature the chiller provides cooling. Campus chilled water line is marked in blue while chiller circuit is marked in green. The feedback signal from the pump on the campus chilled water line enables to track the exact speed of the pump.

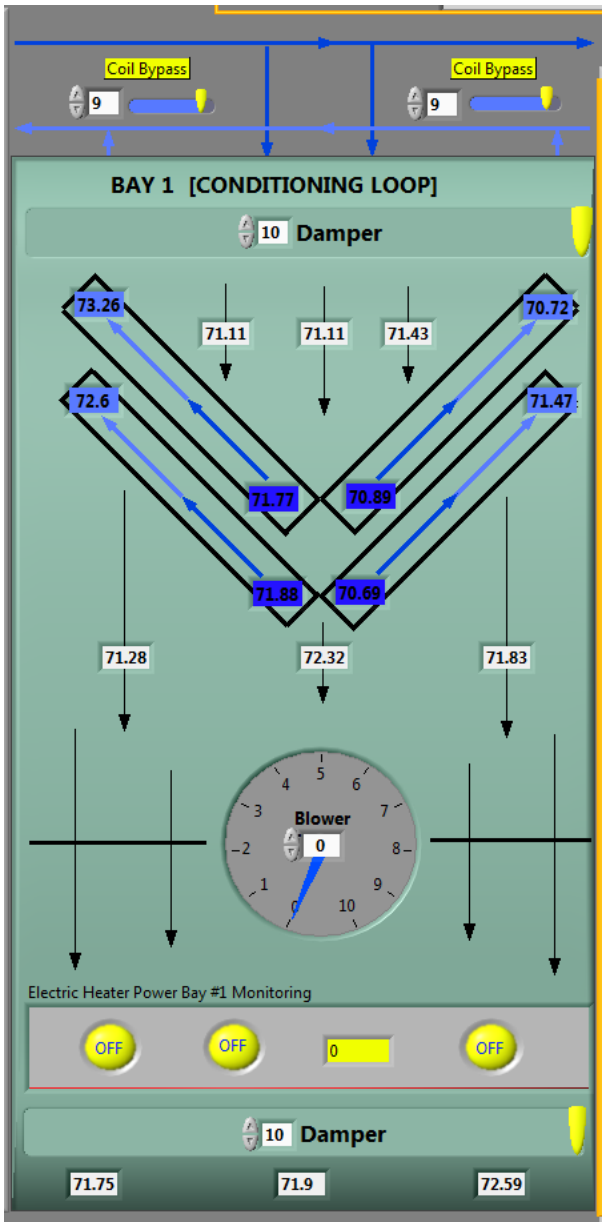

Figure 22: Air-side control panel for conditioning loop bay

Conditioning bay loop is described in figure 22. The same strategy is applied for bays loops 2, 3and 4. The cold water enters from the top and passes through big V-shaped cooling coils. Then the cold air is passes over the electric heater which heats the air to the set point temperature. The blower placed between cooling coil and the heater directs the air flow from to the bottom. The dampers located after the heater control the air flow rate along with the variable frequency drive (VFD) on the blower. Temperature of air after every process can be monitored along with the cold water temperature and heater power.

Host interface

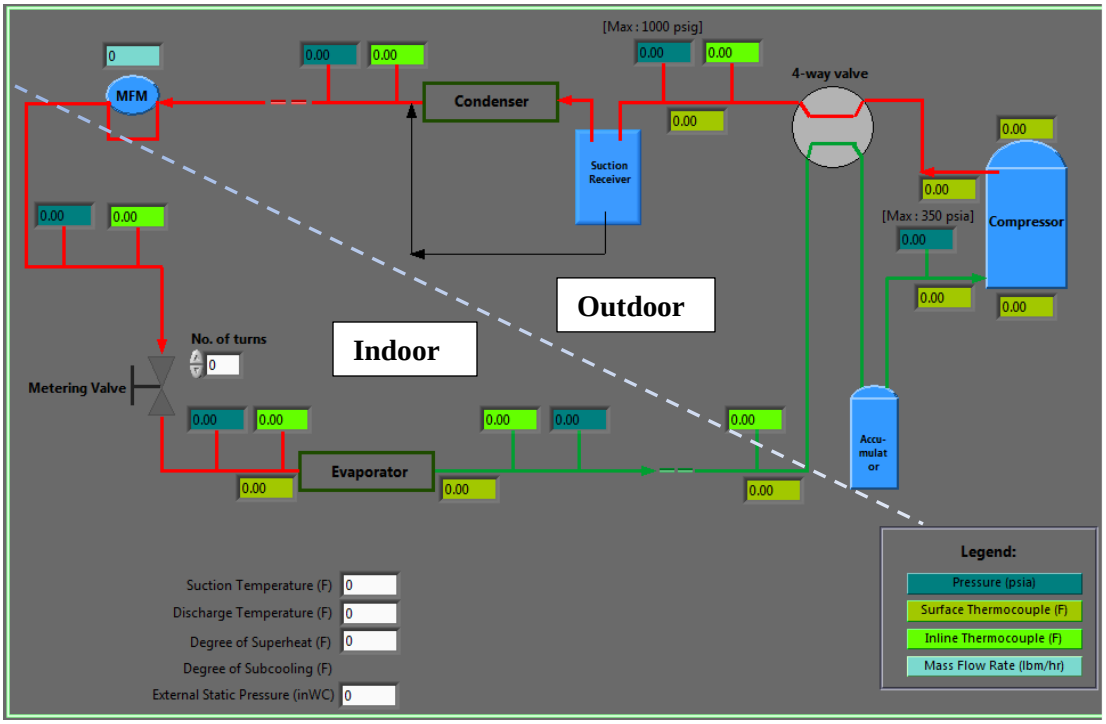

Figure 23: Layout of host control interface for cooling mode

Figure 23 is the refrigerant loop in the cooling mode with metering valve in place. The interface displays inline thermocouple, and surface thermocouple reading along with the absolute refrigerant pressure at every state point. Important quantities such as degree of superheat and sub cooling are also displayed. It required by the standards to maintain a 0.2 inwc of external static

pressure across the indoor coil. This quantity can always be scrutinized by keeping a watch in this window.

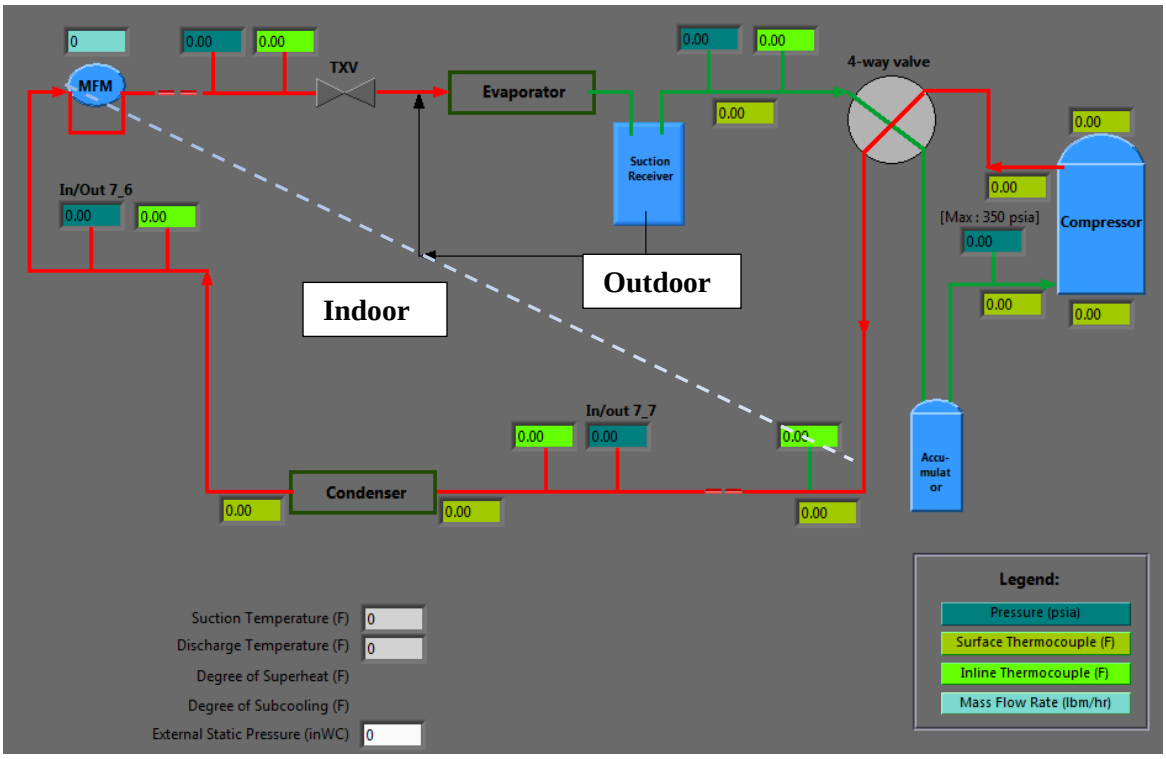

Figure 24: Layout of host control interface for heating mode

A similar refrigerant loop is provided for heating condition shown in figure 24. The difference is the pipeline across the 4-way valve and the location of the expansion valve. The refrigerant flow is reversed with respect to the cooling mode.

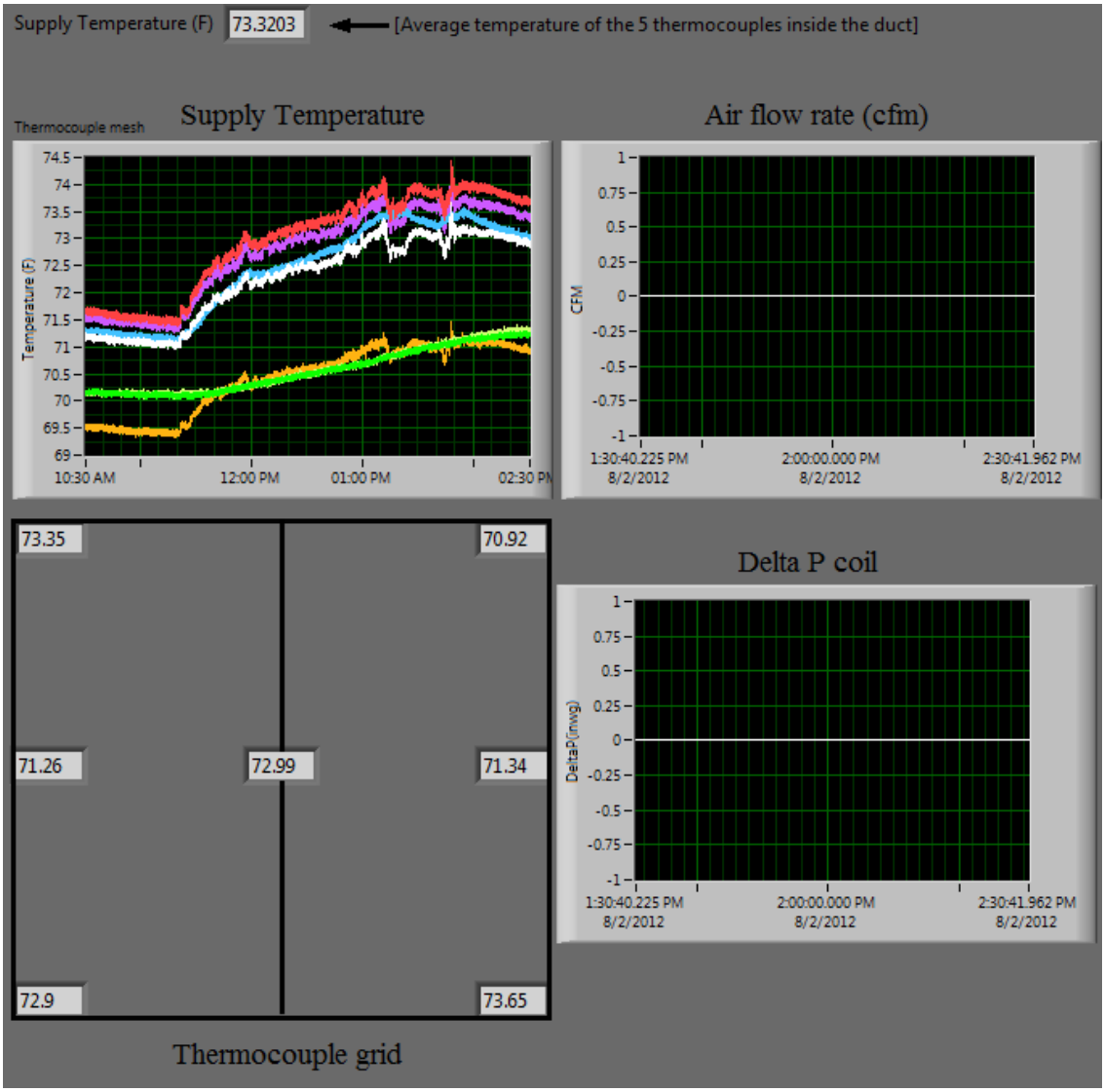

Figure 25: Supplied air properties interface

Figure 25 is the air side control panel for the heat pump. History of supply temperature air flow rate of the unit and the pressure drop across the coil can be monitored in this window. The supply temperature is the average of the 5 thermocouple attached inside the duct.

CHAPTER V

DATA REDUCTION AND UNCERTAINTY

The recorded file contains data for the entire psychrometric chamber. Thus the recorded file is very big in size and most of the readings are not pertaining to this project. In this section I will explain how the appropriate data was selected from the bank of readings. This section also deals with processing the data and translating it to calculated variables and finally gives a summary at the end of each test.

Every instrument on the test setup has a level of accuracy associated it. Deviation from the accuracy would mean error on the following calculated quantities. These errors propagate in every measurement following the other. Thus it is very important to know the goodness or the range of accuracy on the final deciding parameters such as COP and air-side capacity. The estimation of the error on the calculated quantities due to the limitation on accuracy of primary measurements is called uncertainty analysis. Uncertainty analysis for COP and air side capacity is carried out in this section.

Data Reduction

A data file is recorded for one hour at every two seconds. Thus when imported to Microsoft Excel the data matrix is 1800 rows by 650 columns. Out of this bank of numbers, useful data is referenced to a new excel sheet where the template is made with the labels so that it is easy to read the numbers. Once the measured quantities are indicated on the spreadsheet with appropriate labels, air-side capacity, refrigerant side capacity, COP, heat balance etc. are calculated as follows.

Air side capacity:

$$\dot{Q}_{air} = [\dot{m}_{air} * C_p * (T_{return} - T_{supply})] + [\dot{m}_{air} * h_{fg} * (\omega_{return} - \omega_{supply})] \quad (5.1)$$

Where

$\dot{Q}_{air}$ = air side heat transfer capacity [btu/hr]

$\dot{m}_{air}$ = mass flow rate of air [lb/hr]

C_p = Specific heat of air at constant pressure calculated at supply temperature [Btu/lb-R]

T_{return} = Temperature of return air (indoor room temperature) [°F]

ω_{return}= Humidity ratio of return air [-]

T_{supply} = Temperature of supplied conditioned air by the unit [°F]

ω_{supply} = Humidity ratio of supply air [-]

h_{fg} = Difference in enthalpy of water vapor and saturated water at supply temperature [Btu/lb]

The total air side capacity for cooling load has two parts namely sensible load and cooling load. Thus from eq. 5.1, the product of mass flow rate of air, specific heat of air at supply temperature

and the temperature difference of return and supplied air contributes to the sensible load. On the other hand product of mass flow rate of air, difference in the enthalpy of saturated vapor and water at supply temperature and humidity ratio difference of return and supplied air accounts for latent load. It is important to realize that for heating load or for unit operating in heating mode, the total capacity is the sensible capacity. There is no latent load for heating and thus the air side capacity in heating mode is first part in equation 5.1.Enthalpies and humidity ratios are calculated in Engineering Equation Solver (EES). Typical inputs to the EES are the dry bulb and wet bulb temperatures and the absolute pressure. As described in the previous section, a relative humidity sensor is located in every wet bulb probe. Thus the measure value of R.H is compared to one calculated from dry bulb and wet bulb. It is required that the calculated and the measured value have an agreement within 3% or else calibration on wet bulb and dry bulb RTD's would be conducted.

Latent heat balance:

In order to check the measurements for the air-side capacity a latent heat balance is calculated. Latent load calculated from the above equation is compared to the amount of condensate collected in the duration of the test. The latent heat balance is presented in eq. 5.2.

$$\text{Latent heat balance} = \frac{\text{Calculated latent load} - (\text{amount of condensate} * h_{fg})}{\text{Calculated latent load}} * 100 \qquad (5.2)$$

For every test the latent heat balance was within 15% owing to the error in the measurement of mass of water on the weighing scale. The least count of the weighing scale was 0.5 lb and thus it could not measure anything less than that. The accuracy on the scale was 2% contributing to the measurement error.

Refrigerant side capacity:

Refrigerant loop is independent of the air side control. The primary equation that governs the refrigeration load is given in eq. 5.3

$$\dot{Q_{ref}} = \dot{m_{ref}} * \Delta h \quad (5.3)$$

Where,

$\dot{Q_{ref}}$ = Refrigerant side heat transfer capacity [Btu/hr] , [W]

$\dot{m_{ref}}$ = mass flow rate of refrigerant [lb/hr]

Δh = Difference in the enthalpies of refrigerant at inlet and outlet of the indoor coil. [Btu/lb]

Thus the refrigeration load is the product of mass flow rate of the refrigerant and the difference in the enthalpy across the indoor coil. Refrigerant mass flow rate is a measured quantity. For cooling mode the indoor coil gains heat and thus the outlet enthalpy is greater than the inlet while for heating mode it is exactly opposite since during this mode indoor coil rejects heat. For superheated refrigerant enthalpy is a function of temperature and pressure. For cooling mode, the refrigerant enters the indoor coil in two phase and exits as superheated vapor. Temperature and pressure at the evaporator outlet are accurately measured and corresponding enthalpy can be found with these two parameters. The expansion process through the TXV is assumed to be isentropic. This means that enthalpy at TXV inlet is same as the one TVX outlet and also indoor coil inlet. The evaporator inlet temperature is the saturation temperature which is calculated as shown in previous section and saturation pressure corresponding to it can be determined. With the knowledge of P_{sat} and the enthalpy, the refrigerant quality at the evaporator inlet could be accurately calculated.

Heat balance:

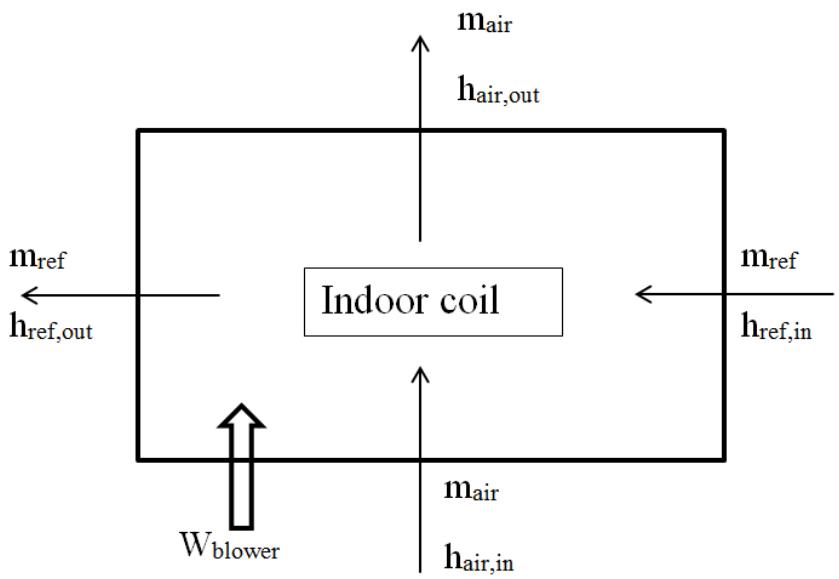

Figure 26: Control volume analysis for indoor coil

In order to validate air side and refrigerant side loads, energy balance at the indoor coil heat balance is calculated. Figure 25 is the control volume chosen as indoor coil for cooling mode where in the refrigerant enters cold and leaves hot while the air enters hot and leaves cold. The blower work is done on the indoor coil for air circulation.

Applying the first law of thermodynamics around the indoor coil control volume,

$$\frac{dE}{dt} = \dot{Q} - \dot{W} + \sum_{in} \dot{m_{in}} h_{in} - \sum_{out} \dot{m_{out}} h_{out}$$

The work is negative since it's done on the control volume and thus energy balance simplifies to

$$\dot{W_{blower}} + \dot{Q_{air}} - \dot{Q_{ref}} = 0$$

Similarly for heating mode the energy balance simplifies to,

$$\dot{Q_{air}} - \dot{W}_{blower} - \dot{Q_{ref}} = 0$$

The residual of the energy balance should ideally be zero. But due to heat losses to the ambient the residual is not zero. Thus the ratio of the energy balance residual to the air-side capacity is called as the heat balance residual. Eq. 5.4 and 5.5 are the heat balance equations for cooling and heating mode respectively.

$$Heat\ balance_{\ cooling} = \frac{(\dot{W_{blower}} + \dot{Q_{air}} - \dot{Q_{ref}})}{\dot{Q}air} * 100 \quad (5.4)$$

$$Heat\ balance_{\ heating} = \frac{(\dot{Q_{air}} - \dot{W}_{blower} - \dot{Q_{ref}})}{\dot{Q}air} * 100 \quad (5.5)$$

Work input:

It is required to have a heat balance within 3% for the test to be valid. In order to measure the blower power, the unit blower was turned on without turning on the compressor. Thus the power used by the unit which was solely to run the indoor blower was measured and recorded. The indoor coil blower power was measured to be 1194 Btu/hr.

$$\dot{W}_{Total} = \dot{W}_{compressor} + \dot{W}_{indoor\ blower} + \dot{W}_{outdoor\ fan} \quad (5.6)$$

Once the compressor is turned on the total power of the heat pump can be measured. This power includes indoor blower power, compressor power and outdoor air fan as indicated in eq. 5.6. It is not possible to isolate compressor power and outdoor fan power. Thus the compressor and outdoor fan power is the difference between the total measured power and indoor blower power.

Loop energy balance:

In order to check tightness of the refrigerant loop energy balance was also calculated for the entire refrigerant loop. This quantity suggests how good the loop is insulated. Thus applying energy balance along the refrigerant loop, we get

$$loop\ energy\ balance = \frac{\dot{Q}_{condenser} - (\dot{Q}_{evaporator} + \dot{W}_{compressor})}{\dot{Q}_{condenser}} * 100 \quad (5.7)$$

For all the tests this quantity is required to be within 2%. This would mean that there are 2% losses in the refrigerant loop due to improper insulation. One thing to notice is the condenser is the component where is rejected by the refrigerant while refrigerant gains heat at the evaporator. Thus depending upon the heating or cooling mode, proper values are to be filled in eq. 5.7.

COP/EER:

A simple definition of coefficient of performance or energy efficiency ratio will be a ratio of useful output over invested input. Thus the COP will be,

$$COP = \frac{\dot{Q}_{air}}{\dot{W}_{Total} * 3.413} \quad (5.8)$$

$$EER = \frac{\dot{Q}_{air}}{\dot{W}_{Total}} \quad (5.9)$$

Where air side capacity is measured in Btu/hr and total unit power is measured in Watts.

The difference in the COP and EER is mainly in the denominator. In case of COP the compressor power term in the denominator is in Watts while for EER it is in Btu/hr. in eq. 5.8 the power is converted from Btu/hr to Watts by the multiplier 3.413

Compressor performance:

Performance of compressor with different refrigerants is measured by comparing the discharge temperatures, refrigerant specific volume at suction and compressor thermal efficiency Discharge temperature is measured during the test and is compared as a difference with the one for R410A. Specific volume of the refrigerant at suction is a function of refrigerant pressure and temperature at compressor inlet. Compressor thermal efficiency is the ratio of isentropic enthalpy difference to actual enthalpy difference as indicated in eq. 5.10

$$\eta_{T_r} = \frac{h_{comp,out,issentropic} - h_{comp,inlet}}{h_{comp,out,actual} - h_{comp,inlet}} \quad (5.10)$$

$$\eta_{T_N} = \frac{\eta_{T_r}}{\eta_{T_{R410A}}} \quad (5.11)$$

Since the refrigerant is not in two phase, enthalpies are function of temperature and pressure. Enthalpy at compressor inlet and outlet (actual) is calculated from suction and discharge conditions respectively. Isentropic enthalpy at compressor outlet is calculated with suction entropy and discharge pressure. Thus thermal efficiency is calculated for every test condition for R410A, R32 and R1234yf. Later on thermal efficiency for each refrigerant is normalized with respect to R410A. It was not possible to insulate the compressor. As a result of this the heat losses from the compressor to the surroundings are neglected. .

Indoor coil performance:

For the assessment of indoor coil performance pressure drop across the coil normalized with respect to R410A is calculated along with the comparison of mass flow rate. The pressure drop

across the coil for a particular refrigerant is difference is absolute pressure at outlet and inlet as suggested in eq. 5.12.

$$\Delta P_r = P_{indoor\ coil,out} - P_{indoor\ coil,in} \tag{5.12}$$

$$\Delta P_N = \frac{\Delta P_r}{\Delta P_{R410A}} \tag{5.13}$$

The pressure drop across the indoor coil is then normalized with R410A in order to compare the coil performance as indicated in eq. 5.13.

Uncertainty Analysis

An uncertainty analysis on the coefficient of performance and the air side capacity of the unit was carried out in order to understand the goodness of the data and contribution of each quantity towards error propagation. A model for the COP and air-side capacity was developed in Engineering Equation Solver (EES). The parameters measured during the experiment were set as inputs to the model and COP and capacity were the outputs. Air side enthalpy method described by ASHRAE standard 37 (2009) is used in the model. The primary equations given by the standard are

$$\text{Air side capacity } = \dot{m}\,(\,h_{return} - h_{supply})$$

$$\text{COP} = \frac{\dot{Q}_{Air}}{\dot{W}_{compressor} * 3.41}$$

EES uses Taylor's expansion series method to perform uncertainty analysis. Accuracy on the measured quantities during the experiment is set in EES as inputs. Accuracy of the sensors is often given by the manufacturer or depends on the in-house and in-situ calibration.

Table 17: Accuracy of instrumentation used in the test apparatus

Sensor	Type	Range	Accuracy
Absolute refrigerant pressure transducer	Piezoelectric	0 – 500 psig	±0.25% F.S.
Differential air pressure transducer (for air flow rate measurments)	Piezoelectric	0 – 3 in wc.	±0.14% F.S.
Mass flow meter	Coriolis	100 – 1000 lb_m/hr	±0.1% F.S
Thermocouple	T-type	17 to 115 °F	±0.5°F
RDTs	100 Ohm DIN Platinum RTDs with 1/3 DIN Accuracy	17 to 115 °F	±0.2°F*
Unit power	Watt transducer with current transformer	0- 50amps 0-230 VAC, 3 phase	±0.2%
Refrigerant charge	Electronic Scale	About 65 lb_m	±0.5 lb_m

*in-house and in-situ calibration with high precision temperature bath

Results show that the uncertainty on capacity measurement was about 3.2% and that on COP measurement was 3.4%. Tables 18 and 19 illustrate the sensitivity of respective measured quantity towards the error propagation on capacity and COP respectively. It can be seen that the pressure measurement is the most sensitive to error propagation. Other factors such as air flow measurement and room wet bulb temperatures are also fairly sensitive towards the uncertainty.

Table 18: Sensitivity of measure quantities towards error propagation on air side capacity

Measured Quantity	**% of uncertainty**
Air flow rate	11.36
P_{return}	27.5
P_{supply}	35.1
Unit Power	0
Mesh temperature	1.26
T_{db} return	0
T_{db} supply	1.35
T_{wb} return	13.96
T_{wb} supply	9.46

Table 19: Sensitivity of measure quantities towards error propagation on COP

Measured Quantity	% of uncertainty
Air flow rate	10.3
P_{return}	24.94
P_{supply}	31.84
Unit Power	9.32
Mesh temperature	1.14
T_{db} return	0
T_{db} supply	1.22
T_{wb} return	12.66
T_{wb} supply	8.58

Test Procedure

Drop-in tests

Improper refrigerant charge can reduce the efficiency of the system by 10 to 20 percent in the field applications (Downey and Proctor, 2002). Both undercharge and overcharge of refrigerant in the system could affect the lifespan of the equipment, capacity and efficiency. Undercharge decreases the capacity and COP because of the drop in the refrigerant mass flow rate. The flow rate decreases mainly because of a decrease in the evaporating pressure and an increase in suction superheat. Overcharge tends to increase the capacity but the energy efficiency of the system decreases (Kim and Braun, 2010). In this work, first the unit was tested with R410A and the refrigerant charge was optimized for maximum COP at AHRI 210 A rating test conditions (AHRI, 2010). In each test, once the control tolerances were satisfied and steady state conditions were achieved, data were recorded for 1 hour with a sample rate of 2 seconds and the average COPs and cooling capacities were calculated. Then the refrigerant charge was increased in steps of 0.5 lbm at a time. Each test was conducted multiple times before moving to the next one to guarantee that the measurements were repeatable. The refrigerant charge that provided the maximum COP was selected as to the optimum charge in the system. During the charge optimization process the degree of vapor superheat at the compressor suction was above of at

least 4°F. This limit guaranteed safe operation of the compressor. Once the optimum refrigerant charge in the system was determined, the unit was run for a broad range of temperatures from -17°F to 95°F and in both heating and cooling modes at full load conditions. Additional tests were conducted at extreme high temperature conditions of 110° and 115°F to investigate the differences and similarities (if any) of the refrigerant condensation pressures and compressor discharge temperatures of R32 and R1234yf with respect to those of R410A. These ambient conditions were extreme but often occur during the summer months in the South and Midwest regions of the United States, as well as in the Middle East areas and Southeast Asia.

Table 20: Test conditions for heat pump unit having single-speed compressor and a fixed speed indoor fan, a constant air volume rate indoor fan as per standard AHRI 210

	Description	**Indoor conditions**				**Outdoor conditions**			
		Dry bulb		Wet bulb		Dry bulb		Wet bulb	
		^{0}F	^{0}C	^{0}F	^{0}C	^{0}F	^{0}C	^{0}F	^{0}C
Cooling Tests	A -Test	80.0	26.7	67.0	19.4	95.0	35.0	75.0	23.9
	B - Test	80.0	26.7	67.0	19.4	82.0	27.8	65.0	18.3
Heating Tests	H1 Test	70.0	21.2	60.0	15.6	47.0	8.3	43.0	6.1
	H2 Test	70.0	21.2	60.0	15.6	35.0	1.6	33.0	0.5
	H3 Test	70.0	21.2	60.0	15.6	17.0	-8.3	15.0	-9.4
Off-design conditions	HT 1 - test	80.0	26.7	67.0	19.4	110.0	43.3	-	-
	HT 2 - test	80.0	26.7	67.0	19.4	120.0	46.1	-	-

Once the tests of R410A were completed, this refrigerant was slowly recovered in 2 to 3 hours. Then the system was vacuumed for about 30 to 40 minutes and R32 was charged into the system. R32 charge optimization was conducted first at A test cooling conditions until the optimum charge of R32 was identified. Then the system with optimum charge was run at other outdoor temperatures and in both cooling and heating modes. A similar procedure was adopted for R1234yf; once the optimum charge for R1234yf was determined at AHRI A test cooling conditions it was modified during the remaining tests at higher and lower temperatures only if the degree of superheat became lower than 4°F. At the end of the experiments with R1234yf, R410A

was recharged into the system and the performance tests were repeated. These tests served to verify the hypothesis that any potential removals of compressor lubricant from the system during the recovery of the previous refrigerant did not produce any measurable effects on the COPs and capacities of the system. In other words, since the first and last series of tests with R410A showed similar data and R32 and R1234yf were tested in between those two series, the results presented in the next sections were considered independent from the chronological order on which the refrigerants were charged and tested in the system.

TXV soft optimization test

The unit TXV controls the degree of superheat at the evaporator outlet based on R410A cycle characteristics. Once the straight drop-in tests with R32 and R1234yf were completed, the original TXV of the unit was replaced with a manual expansion valve in order to set different degree of superheat and pressure ratios for R32 and R1234yf. For each refrigerant, an initial mass was charged into the system similar to the one of the straight drop-in tests. Then the opening of the expansion valve was varied in search of further improvements of the COP. If similar COPs were measured, the expansion valve opening was optimized for augmenting the capacity of the system. These tests were carried out with the unit in cooling mode only. The refrigerant charge was kept constant as of the optimum charge obtained in drop-in tests. The optimization procedure of the expansion valve opening and refrigerant charge continued until either a maximum COP was identified or the degree of superheat at the compressor suction became lower than 4°F.

Calibration and verification of data

In order to demonstrate the accuracy of the COP and capacity measurements, two types of experimental validation of the test apparatus were carried out. The unit cooling performances with R410A were compared with the unit cooling rating performance data provided by the manufacturer. The measured energy efficiency ratios (EER) were within 10% of the manufacturer

data. Good confidence for the accuracy and repeatability of the measurements for air side capacity was established by comparing measured air flow rates, supply dry bulb and wet bulb temperatures, and external static pressure across the indoor coil with the corresponding data provided by the manufacturer.

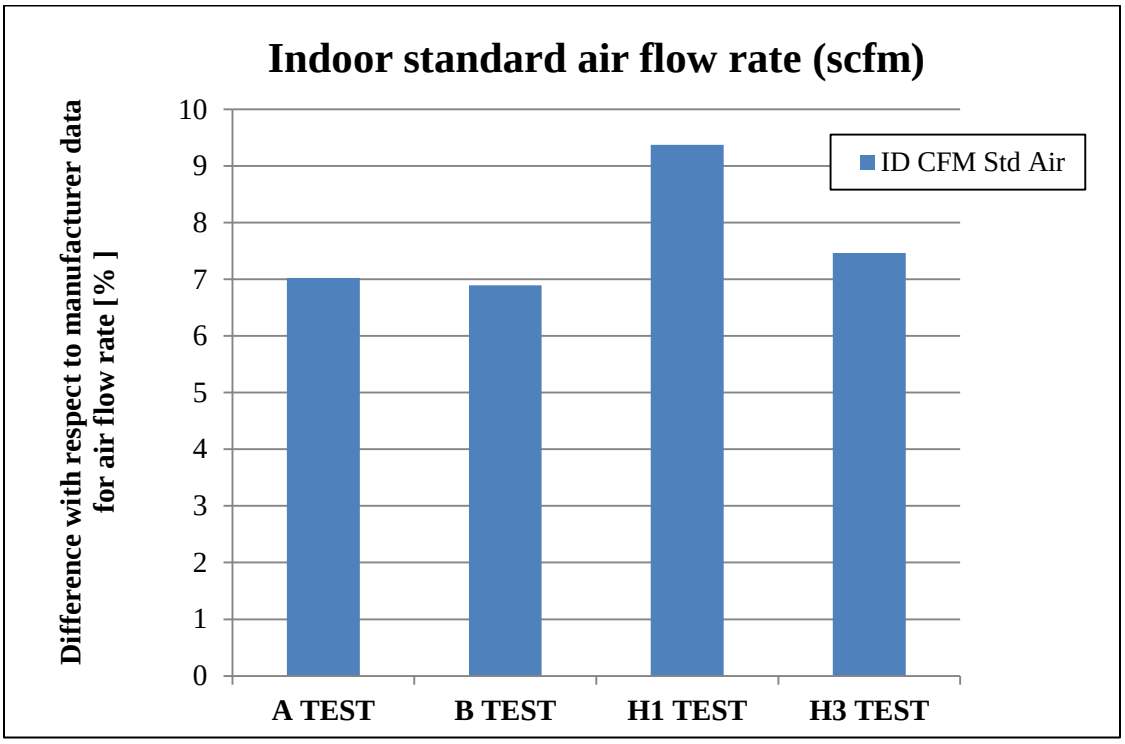

Figure 27: Validation of air flow measurements

Figure 27 compares the standard air flow rate supplied by the unit used for testing with the data provided by the manufacturer. Standard flow rate of SCFM is standardized at 14.7 psia of atmospheric pressure, 68 °F and 36% relative humidity. This converts to a density of 0.075 lb./cu.ft. for air. Thus scfm is calculated by converting actual mass flow rate of air to a standardized volumetric flow rate using the air density of 0.075 lb./cu.ft. Figure 27 presents the percentage difference of measured air flow rate with the manufacturer's data. It can be seen that the measured flow rate is within 9.5% of the rated flow at a given test condition. This comparison

is typically important to validate the air flow measurements used in the test apparatus. The actual mass flow rate of air depends of density of supplied air which is very sensitive to the measure wet bulb temperature. When the data for an hour is averaged the average wet bulb temperature during the tenure of the test is not a good representation for the density calculation. Instantaneous density calculated over for every data point will yield an air flow rate which will be in better agreement with the rated flow rate.

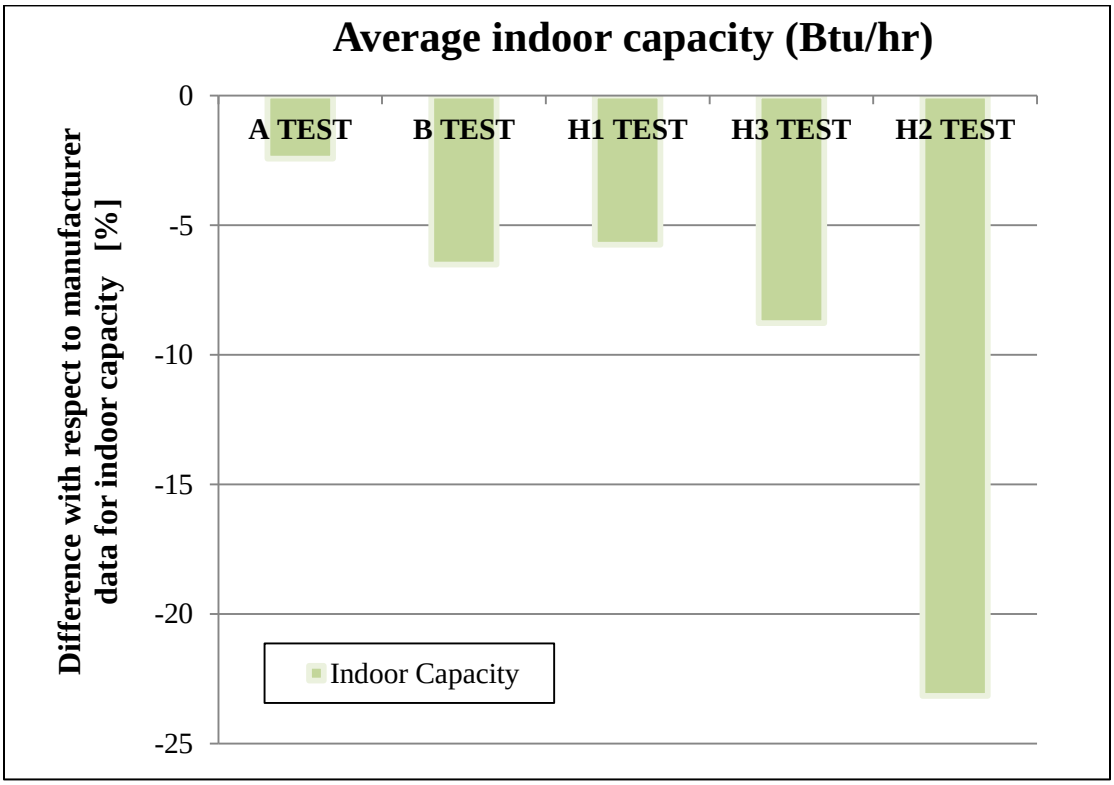

Figure 28: Validation of indoor coil air side capacity

Figure 28 is the validation of indoor coil air side capacity. It can be seen from the figure that the capacity is within 8 % for cooling tests, H1 and H3 tests. This number is comparable to the rated value since the measurements involve humidity ratio calculations for the latent part of the total capacity. The humidity ratio is not captured completely if the data is averages over the period of

an hour. Humidity ratio tends to fluctuates about the set point conditions but when averaged does not give a good representation of instantaneous value.

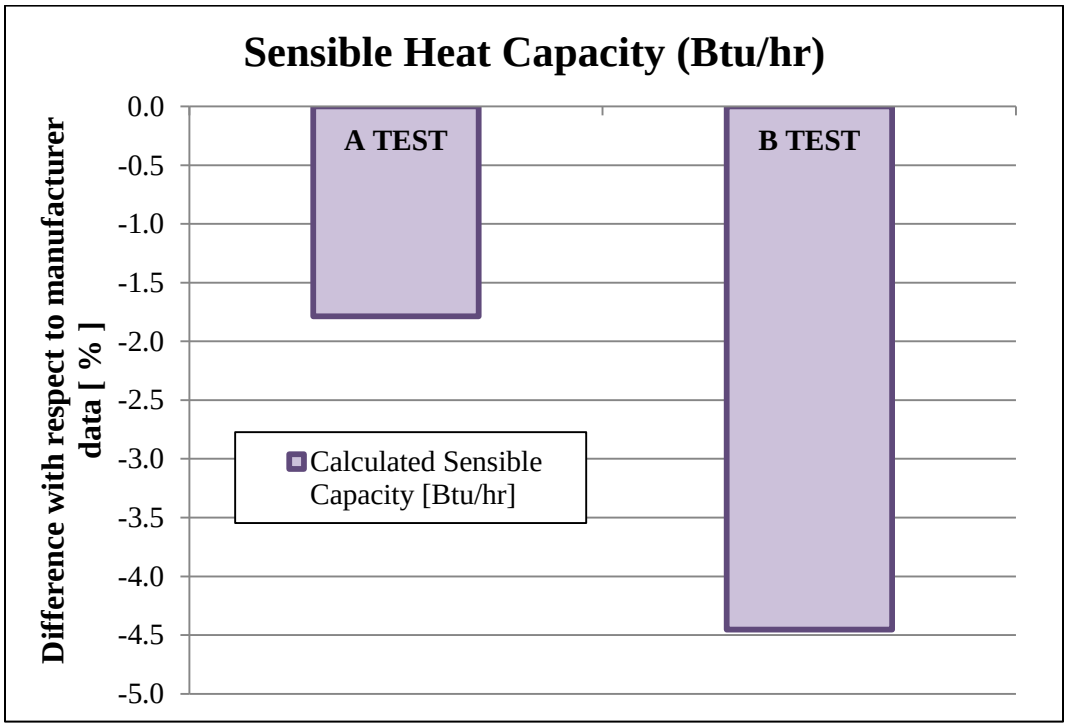

Figure 29: Comparison of sensible heat capacity with the data provided by the manufacturer

The fact that sensible heat capacity in figure 29 agrees within 4.5% of the rated capacity assures that the error must be in latent capacity. In the case of H2 test the difference is 22% which is on the higher side. This is due to the fact that H2 test is a transient frosting test. If a proper unbiased comparison is to be achieved it is important that the data is recorded at the same defrost cycle and the data should capture same conditions. This means if we compare second defrost cycle to the sixth cycle the conditions especially the latent load is going to be different. Sixth cycle is going to be more stable than the second. Moreover, if one file captures a defrost cycle and the other doesn't then it is not a good notion to compare the two files. The data recorded during the comparison test was at initial stages of defrost cycles .The exact details of the data recording from

the manufacturer were unknown. Thus there might be a higher difference between the rated capacity and the measured capacity for frost-defrost H2 test.

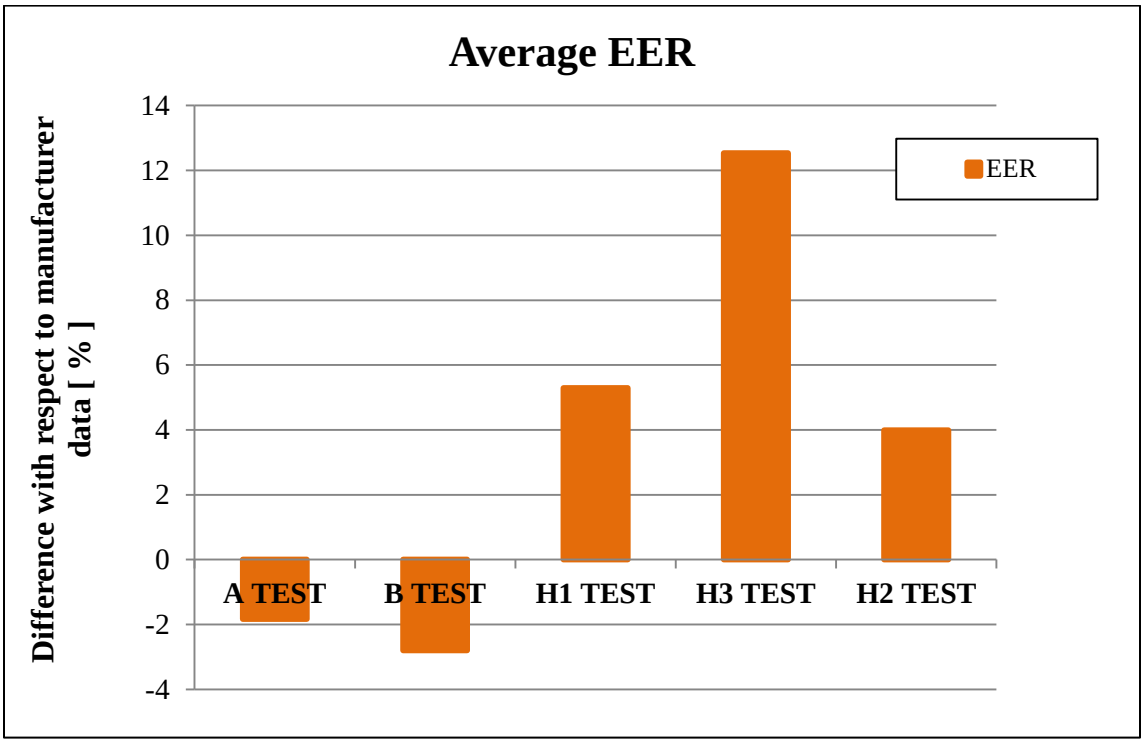

Figure 30: Comparison of measured EER with rated EER for the test heat pump

Lastly the most important quantity to compare is the average EER presented in figure 30. A good agreement with the rated EER would validate the air side and the refrigerant side measurements on the test apparatus. For all the tests except for extreme low temperature test H3 the measured EER is within 5% of the rated EER provided by the manufacturer.

It is important to note that the difference in the measured quantities and the readings from manufacturer data could also be possible because of the uncertainty on the particular quantity. The uncertainty on air side capacity was within 3 % and on the COP/EER was within 4 %. Secondly, the lengths of refrigerant piping also matter while striking a comparison. There was about 40 ft. of suction line for this project while the length of the suction line for the

manufacturers test is unknown. The refrigerant charge also influences the EER. For the A test conditions, the compressor pressure ratio (P_r) for manufacturers test was 2.62 and for current project was 2.85. The discharge and suction pressures for my test was higher than those for the manufacturers test. Thus the refrigerant charge on my project was higher. Higher refrigerant charge will yield higher refrigerant capacity and thus higher EER. Another reason which could have contributed towards higher difference in the data comparison is the TXV. The manufacturer shipped the unit without the TXV. The TXV was shipped separately and not assembled in the unit. It could be possible that the specifications for the TXV in the unit shipped to me and the one in the manufacturer test setup were different. Since I installed the TXV, there are chances that TXV was not installed in the same way as it would at the assembly plant of the manufacturer.

Heat Balance results

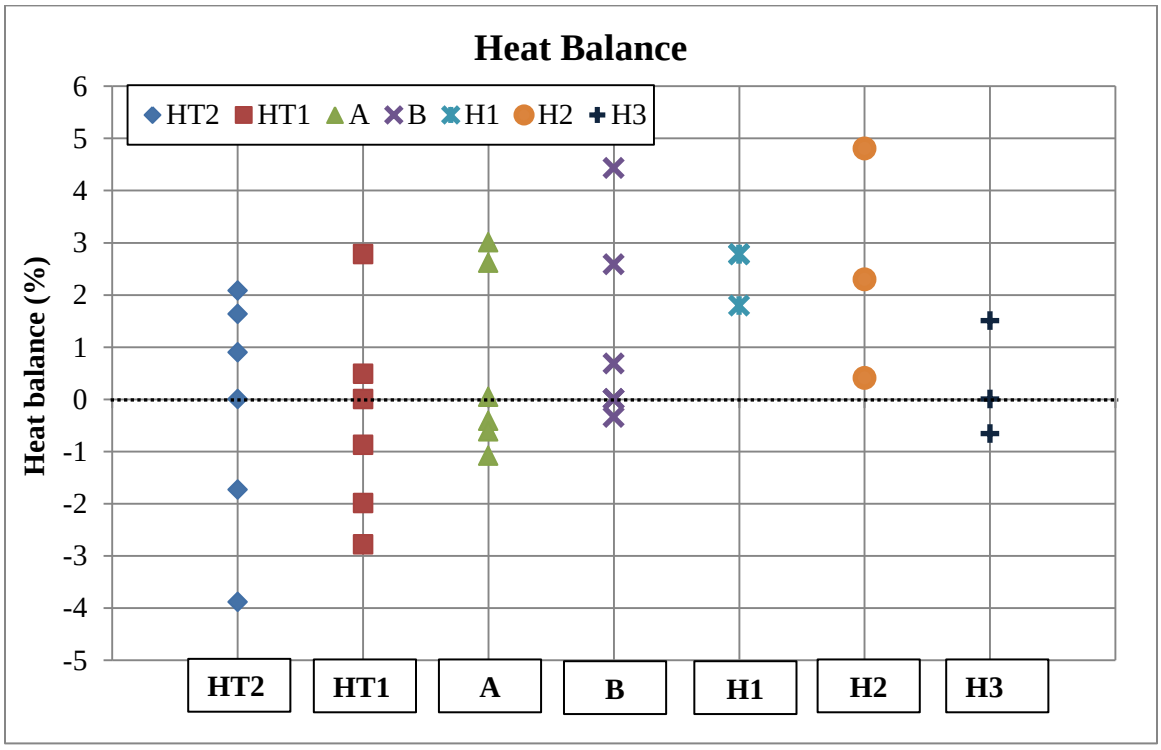

Figure 31: Heat balance for all the tests for drop-in performance and TXV optimization test

Heat balance is not only a way to validate the test facility but also can proof of correct data point. Having a heat balance within 3% is very important for the data point to be accurate. Figure 31 shows heat balance of all the tests undertake. X-axis in the figure 31 represents different test conditions while heat balance is plotted on the Y-axis. Tests data for both drop-in and TXV soft optimization tests are included in this graph. Thus there are three points pertaining to three candidates of refrigerants. For cooling mode (HT2, HT1, A and B tests) there are a total of 6 points from drop-in and soft optimization tests. It can be seen that for all the tests conducted the heat balance was well within ±3 % and only two tests were higher than 3%. One was the H2 test which was transient and the other was a B steady state test.

CHAPTER VI

RESULTS AND DISCUSSION

Charge Optimization Results

Figure 32 and 33 shows the data for the charge optimization tests for refrigerant R32. The COPs and capacities were normalized with respect to that for optimum charge of R410A. The compressor pressure ratios, P_r, are shown on the x-axis and they were also normalized with respect to R410A.

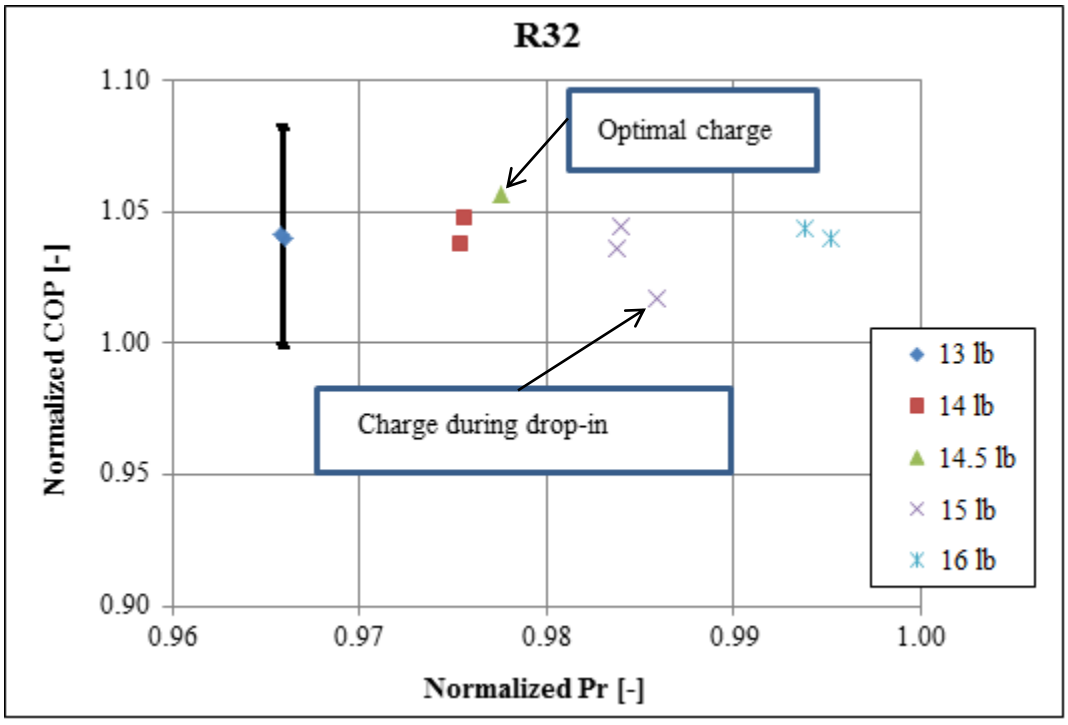

Figure 32: COP analysis for R32 charge optimization

The normalized compressor pressure ratio is defined as follows,

$$P_r = \frac{\gamma_{R32\ or\ R1234yf}}{\gamma_{R410A}} \tag{6.1}$$

Where γ is the compressor pressure ratio

$$\gamma = \frac{Discharge\ pressure}{Suction\ pressure} \tag{6.2}$$

In this figure the normalized COP is defined as,

$$Normalized\ COP = \frac{COP_{R32}}{COP_{R410A}}\Big]_{At\ A\ test\ condition} \tag{6.3}$$

For 14 lb. of R32 charged in the unit there are two solid square data points in Figure 32 that corresponds to two positions of the expansion valve. The COPs of the unit with this charge of R32 were about 4% higher than that for R410A and the corresponding cooling capacities were about 8% higher than R410A. The pressure ratios with R32 were lower than that for R410A. When the refrigerant charge was increased to 14.5 lb. and the expansion valve was properly adjusted, the COP for R32 was 5.5% higher than that for R410A. A further increase in charge slightly decreased the COP until the compressor superheat reached the lower limit. The data of Figure 32 indicate that when the unit was retrofitted with R32 and the expansion valve was properly adjusted, the COP was up to 5.5% higher, cooling capacity was up to 10% higher, and the cycle pressure ratio was about 0.98 times lower than that for R410A. For figures 32 and 33 the P_r is the fraction between $\gamma_{R1234yf}$ and γ_{R410A}.

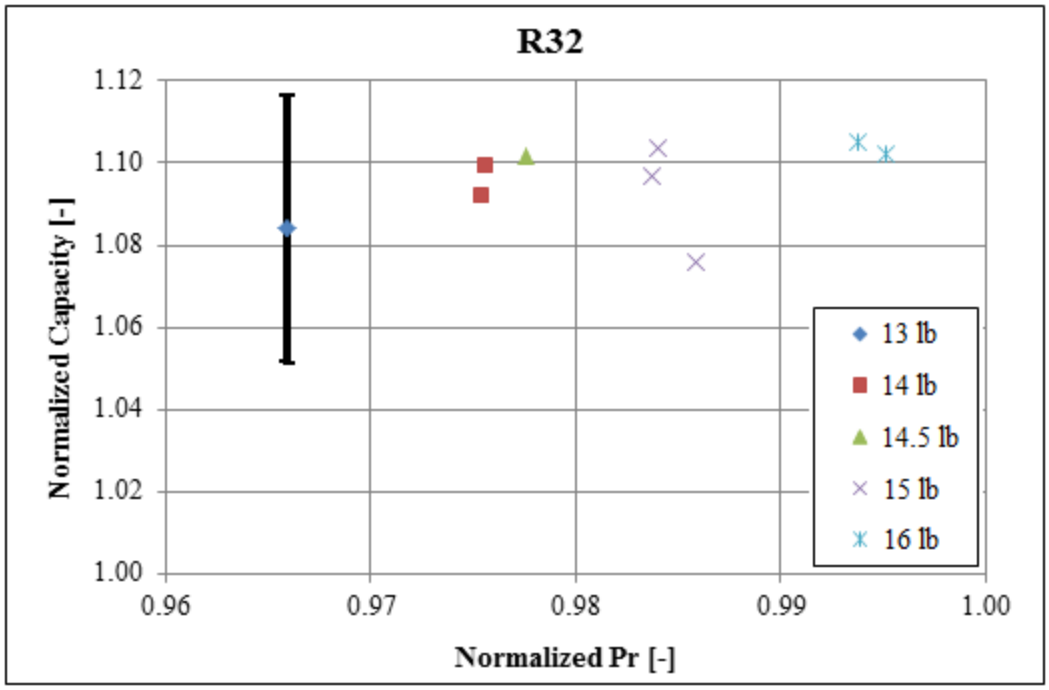

Figure 33: Capacity analysis for R32 charge optimization

In this figure the normalized capacity id defined as,

$$Normalized\ capacity = \frac{\dot{Q}_{R32\ or\ R1234yf}}{\dot{Q}_{R410A}}\Big]_{At\ A\ test\ condition} \tag{6.4}$$

Figure 34 shows the charge optimization for R1234yf. In this case, the optimal charge of R1234yf was 21 lb. and the COP was 1% higher than that for R410A. The corresponding capacity of the unit with R1234yf was 46% lower than that for R410A and the R1234yf pressure ratio was 0.8 times lower than that for R410A.

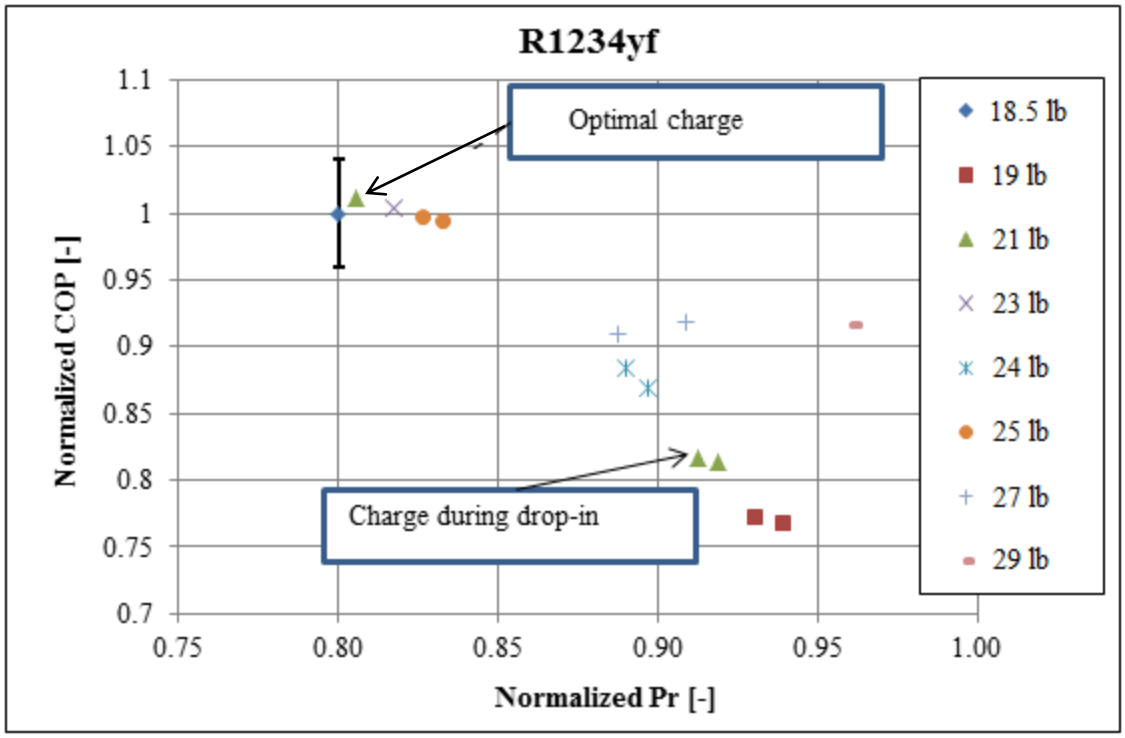

Figure 34: COP analysis for charge optimization for R1234yf

From the data of Figure 34 and 35 it was evident that even when R1234yf provided similar COPs, the unit cooling capacity was significantly reduced and a soft optimization of the expansion valve was not sufficient for augmenting the cooling capacity of the unit when R1234yf was used. From this perspective I conclude that R1234yf was not a suitable direct drop-in replacement for R410A and some other modifications of the system would be required.

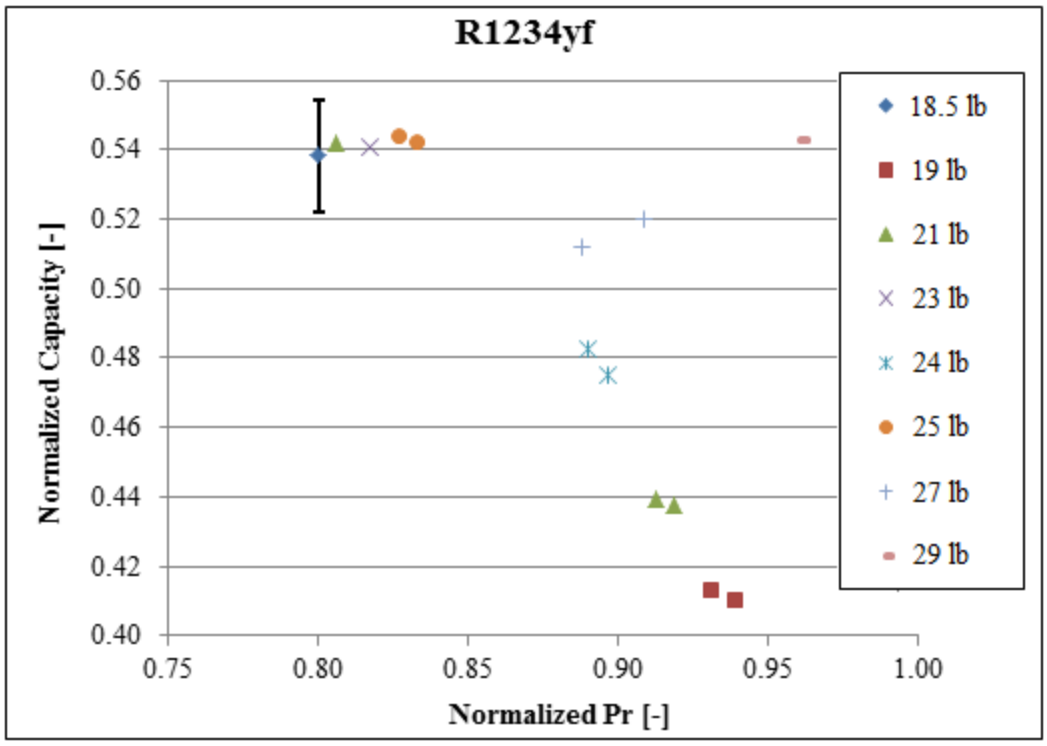

Figure 35: Capacity analysis for charge optimization of R1234yf

Drop-in Performance Tests

The drop-in performances of the heat pump with R32 and R1234yf are shown in figure 36 and 37 for both cooling and heating modes. The COPs are normalized with respect to that for R410A at similar outdoor temperatures operating conditions. In other words, the normalized COP is defined as,

$$Normalized\ COP = \frac{COP_{R32\ or\ R1234yf}}{COP_{R410A}}\Big]_{Same\ boundary\ ambient\ conditions} \quad (6.5)$$

In figures 36 and 37, the X-axis is the outdoor ambient temperature and Y-axis is the normalized COP with respect to R410A. The error bar shown on one point is applicable to all the points. The

uncertainty on COP value is within 3.5 %. In order to maintain the esthetics of the graphs, the error bar is marked on only one point. The dotted line indicates unity which would mean similar value as R410A. In all the future graphs in this section R410A data point will be represented by a diamond, R32 with a square and R1234yf with a triangle.

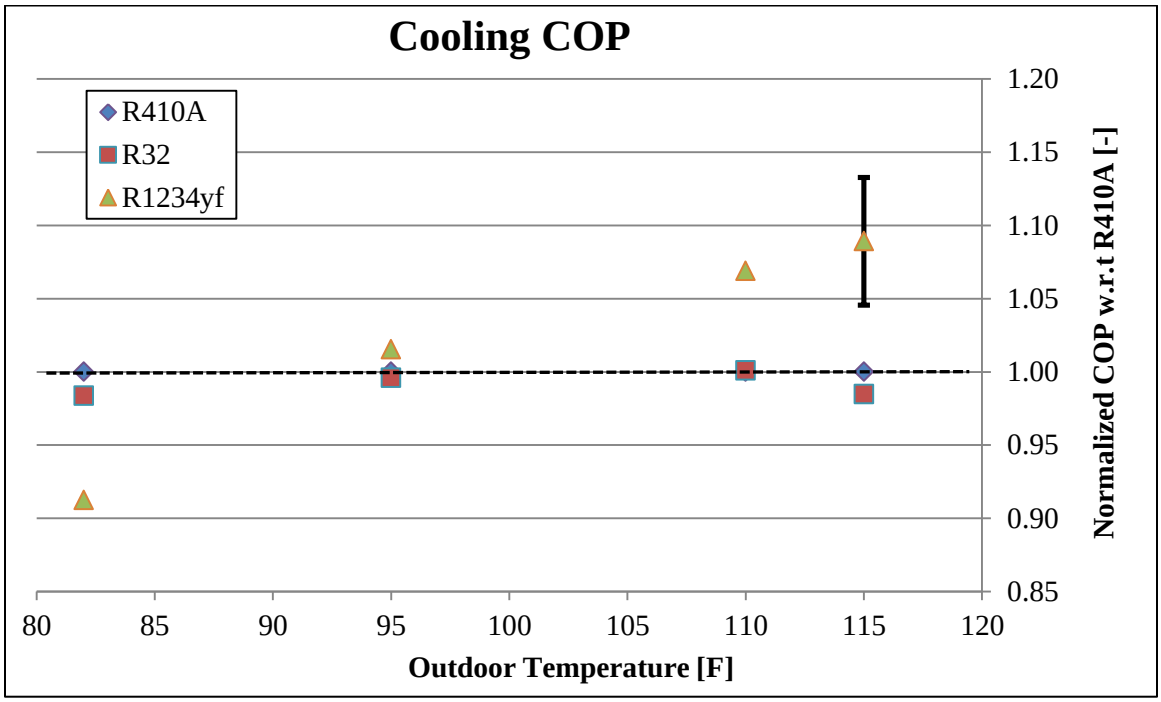

Figure 36: Normalized COP with respect to R410A for R32 and R1234yf in cooling mode

In cooling mode R32 had similar COPs as R410A with two data points almost coinciding with each other with a difference within 1.5%. A significant increase of COP was observed in heating mode from 10 and 17%. The COP for R1234yf was higher in both cooling and heating modes with an exception at B-test where the COP of R1234yf was 10% lower than that of R410A. This was due to the fact that the TXV used for drop-in tests was originally designed for R410A and it was operating at off-design conditions for R1234yf at B conditions. It was also noted that the degree superheat for the B test was quite high, almost 19.3°F. This higher degree of superheat

penalized the compressor performance and thus decreased the system COP for R1234yf in the case of AHRI B-test cooling conditions.

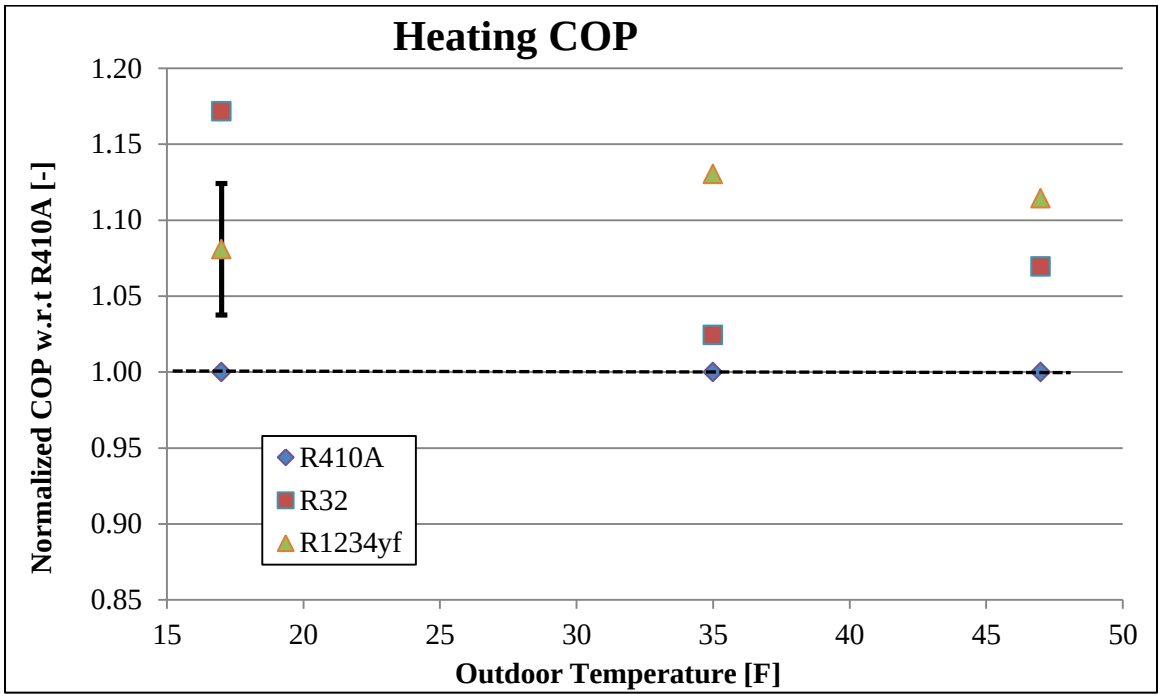

Figure 37: Normalized COP with respect to R410A for R32 and R1234yf for heating mode

For cooling tests it can be observed that with an increase in the ambient temperature, the COP for R1234yf tends to increase. In case of R1234yf managing a charge was a big issue. Optimized charge for A test conditions proved to be overcharge for B test condition. Thus there was more super heat at the compressor suction resulting is a lower COP. On the other hand as the ambient temperature was increased to HT1 and HT2 testing condition, the optimized charge failed to provide the required degree of superheat. Almost 2.5 lb. of charge had to be taken out for extreme design conditions in order to achieve the 5 °F of superheat at compressor suction. Similar trend continued for the heating tests. In order to run the heating test, 8 lb. of refrigerant charge had to be removed. In heating performance, the COP of R1234yf was5% more for H2 test and 2.5% more for H1 test than R32. Conversely, for low temperature H3 test R32 performed 4% more than

R1234yf. This discontinuous behavior might be because the charge for R32 was the same but the charge for R1234yf had to be reduced for every heating test. Optimized charge for R32 was able to run at all the heating and cooling tests. The issue of charge management will be discussed in more details in following section.

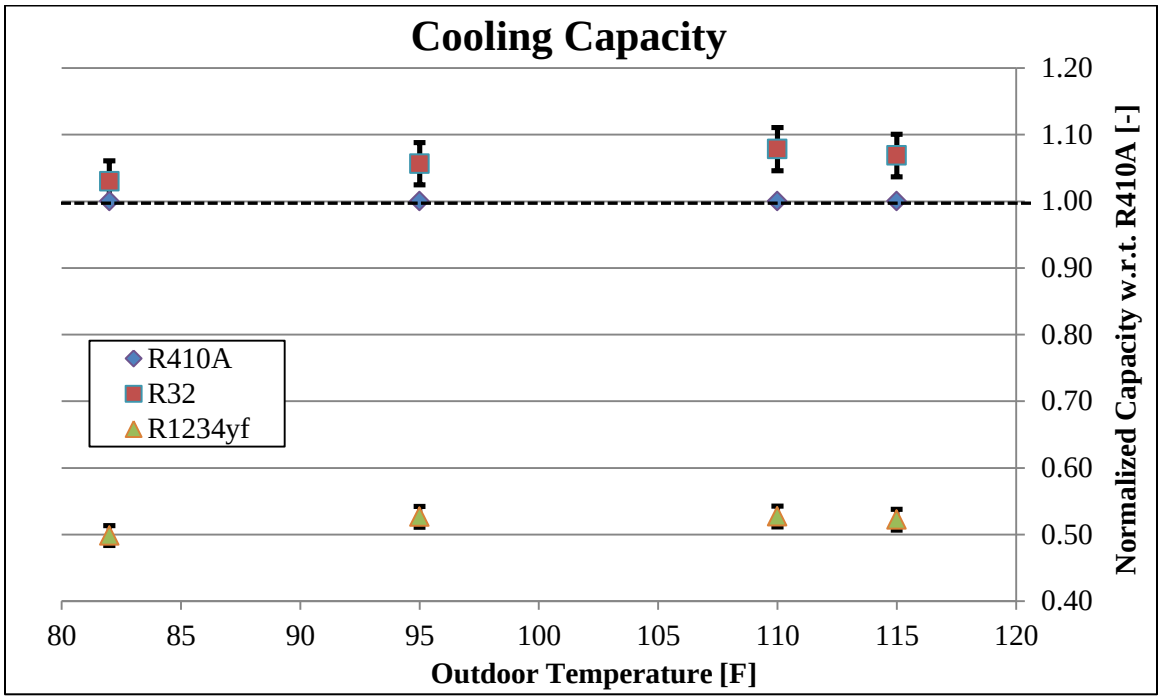

Figure 38: Normalized capacity with respect to R410A for cooling mode

The normalized capacity is defined as the ratio of capacity for R32 of R1234yf over the capacity of R410A at similar boundary conditions.

$$Normalized\ capacity = \frac{\dot{Q}_{R32\ or\ R1234yf}}{\dot{Q}_{R410A}} \tag{6.6}$$

The uncertainty on the capacity measurement was 3.2% of the measured. In figure 38 and 39, the X-axis represents the outdoor ambient temperature and the Y-axis is the cooling and heating capacity of the refrigerant candidates normalized with respect to R410A. The capacity for R32 in

cooling mode was 10% higher than R410A, especially at extreme high temperatures as shown in Figure 38. R1234yf on the other hand delivered a capacity which is about 50% lower than that of R410A baseline. Thus along with the charge management issue R1234yf has another trait of having capacity which is almost half as that of R410A.

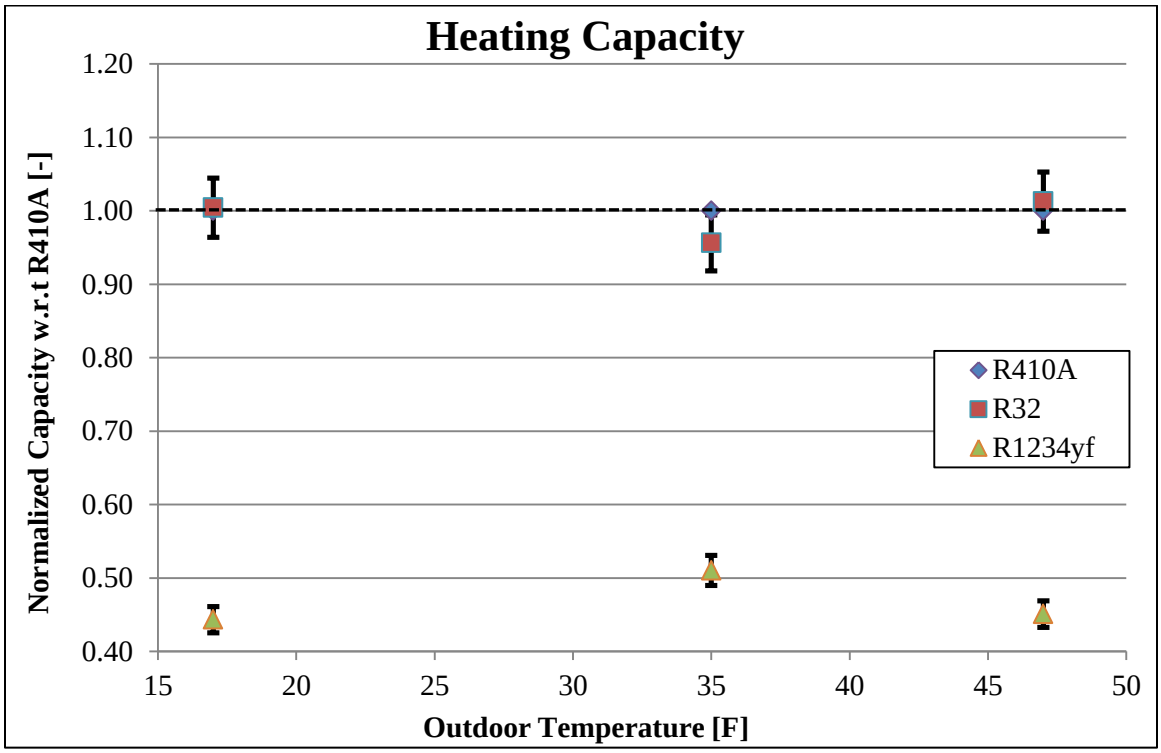

Figure 39: Normalized capacity with respect to R410A for heating mode

In heating mode, the capacity for R32 was comparable to R410A indicated in figure 39. The capacity of R1234yf was about 50% lower even for the heating mode. Thus, the charge management of R1234yf might be a challenge if R1234yf is retrofitted in R410A heat pump units for residential applications without any modification of the system refrigerant receiver.

TXV soft optimization tests

The results from TXV soft optimization tests are compared to the drop in tests in figures 40 and 41. The data in solid bars represent the straight drop-in test results. All data were normalized with respect to that of R410A at similar operating conditions. The data in solid bar represents drop-in test performance while the one with black border represents TXV optimization data. With the soft optimization of TXV, the COPs were further increased, as shown by the extended bars in figure 40. For example, at B-test condition, R32 had a normalized COP of 0.98 with respect to R410A for drop-in tests. After optimization of the TXV the COP augmented by as much as 10%, reaching 1.08 of normalized COP. R1234yf had similar COPs during both drop-in test and soft-optimization test at the A-test condition. However, the COP for the B-test condition increased by as much as 5% thanks to the TXV optimization. The high temperature tests for R1234yf were not conducted because during those extreme conditions it was not possible to control the refrigerant vapor suction superheat to above 4 ºF. This was due to the large size of the TXV used during the experiments.

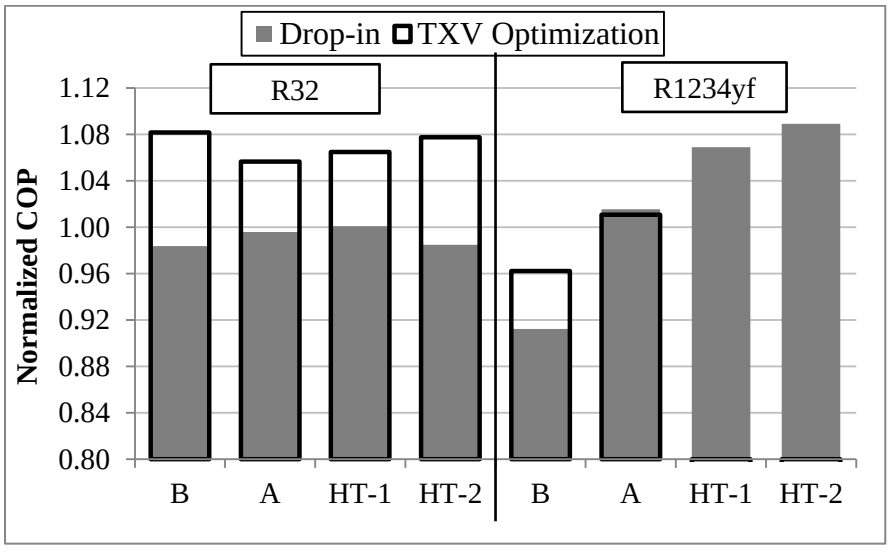

Figure 40: Normalized COP in cooling mode for drop in and TXV optimization tests

Figure 41 shows the system cooling capacities for drop-in tests and the increase in capacity for the TXV soft optimization tests. For R32 the capacity was 3 to 8% higher than that of R410A and had a further increase of 2 to 9% if the TXV was optimized. The capacity for R1234yf was about 50% lower with respect to R410A and the optimization of the TXV increased the capacity by only 2 to 4%.

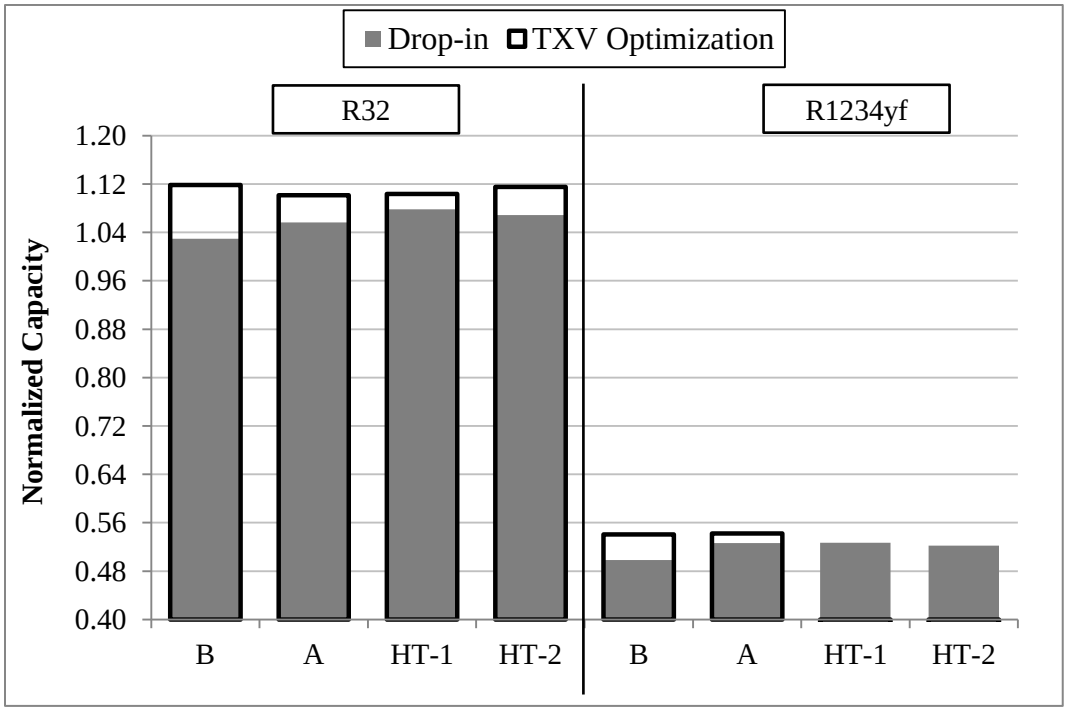

Figure 41: Normalized capacity in cooling mode for drop in and TXV optimization tests at various ambient conditions (refer to ambient conditions indicated in table 20)

Thus we can comment that the process of TXV soft optimization improved the performance of the heat pump for R32 as a working fluid. In case of R1234yf the TXV optimization process failed to deliver high temperature tests.

Compressor performance

The power consumed by the compressor for R1234yf was about 48 to 60% lower than that for R410A. This was due to lower refrigerant flow rates and lower pressure ratios of R1234yf. With R32 the compressor power was 7 to 9 % higher than the baseline with R410A. The compressor performances are discussed by analyzing the difference of suction vapor specific volume of the refrigerants and the thermal efficiencies of the compression process during the actual experiments. These data are shown in Figures 42 and 43 for various outdoor temperatures.

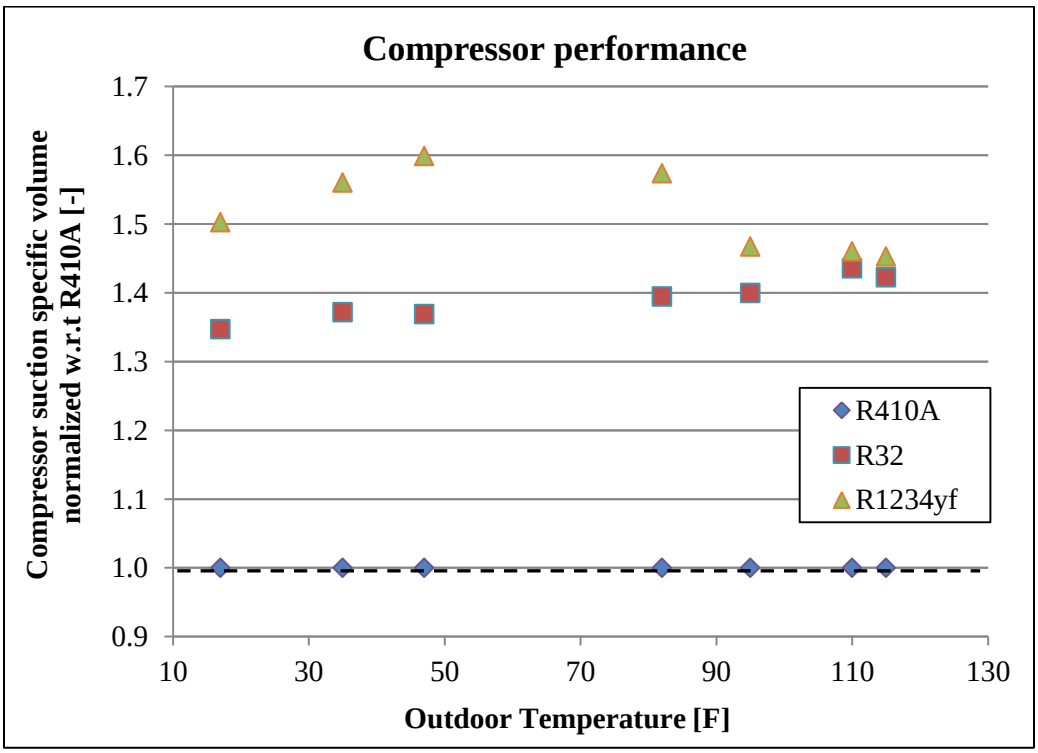

Figure 42: Compressor suction specific volume for R410A (baseline), R32 and R1234yf

During the unit run with the original TXV, the suction specific volumes for R1234yf measured from the pressure and temperature data taken at the compressor suction port, were about 45 to 60% higher than R410A. R32 specific volumes were about 35 to 40% higher than R410A. The reason behind such high specific volume of refrigerant at compressor suction is due to the low

side operating pressure. As discussed in the refrigerant characteristics section, the operating refrigeration cycle for R32 is comparable to R410A but on higher side. On the other hand if we compare the low side pressure of the system for R1234yf and R410A it is evident that the suction pressure for R1234yf is almost half of R410A. As the suction pressure decreases, the specific volume of the refrigerant at compressor inlet increases. Higher specific volume of refrigerant would mean that the compressor would displace less amount of refrigerant in one stroke or rotation. This will decrease the mass flow rate of the refrigerant. Hence the capacity will also be lower. This justifies the behavior of having low capacity and higher suction specific volume for R1234yf.

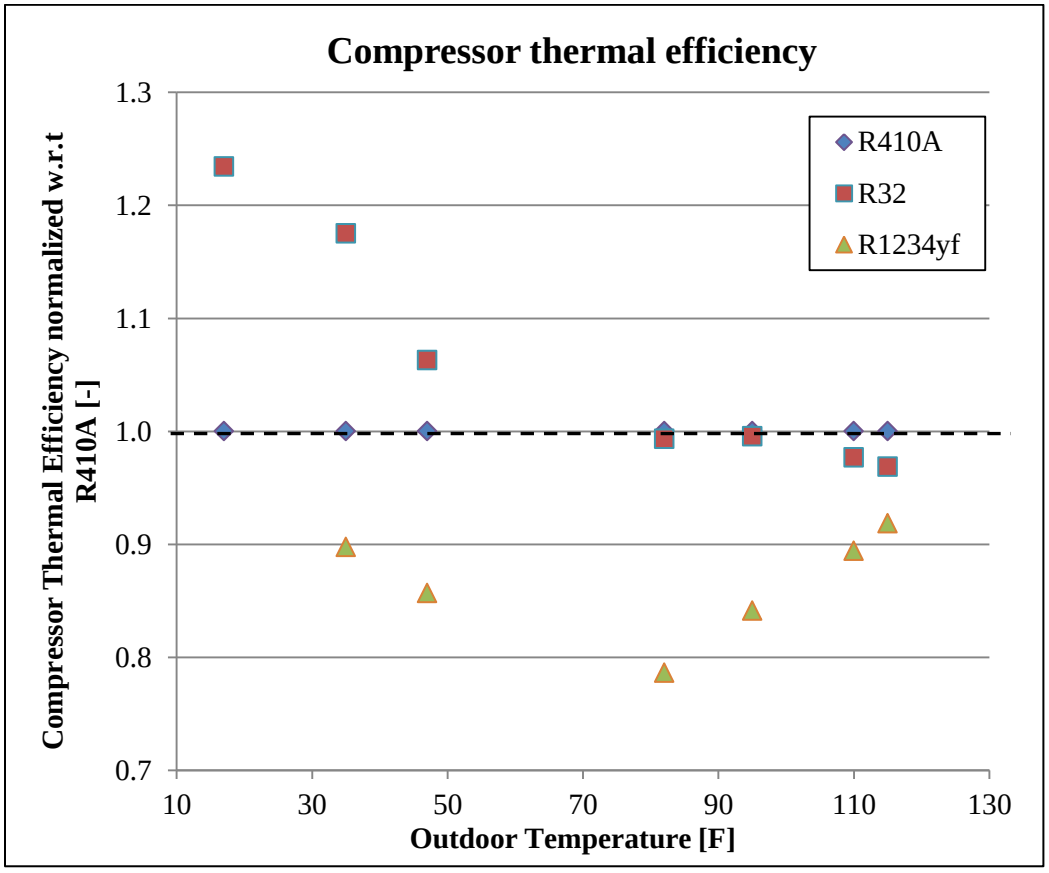

Figure 43: Compressor thermal efficiency for R410A (baseline), R32 and R1234yf

Figure 43 is the compressor thermal efficiency for different refrigerant candidates. This is not isentropic efficiency since the heat losses from the surface of the compressor were difficult to compute. Casing of the compressor becomes hot and heat is dissipated to the ambient. These heat losses have to be incorporated in the isentropic efficiency calculations. It was not possible to insulate the compressor to protect the compressor from heat losses. Thus the thermal efficiency was computed which is the ratio of isentropic compressor work over the actual work. Later on the values are normalized with respect to R410A and plotted against ambient temperature. The thermal efficiency of the compressor, normalized with respect to R410A, was generally higher for R32 and lower for R1234yf. For low temperature tests R32 fared about 8-25 % better than R410A while for heating tests R32 thermal efficiency was very comparable to R410A. Compressor thermal efficiency for R1234yf was 10 to 20% less for all the tests as compared to R410A.

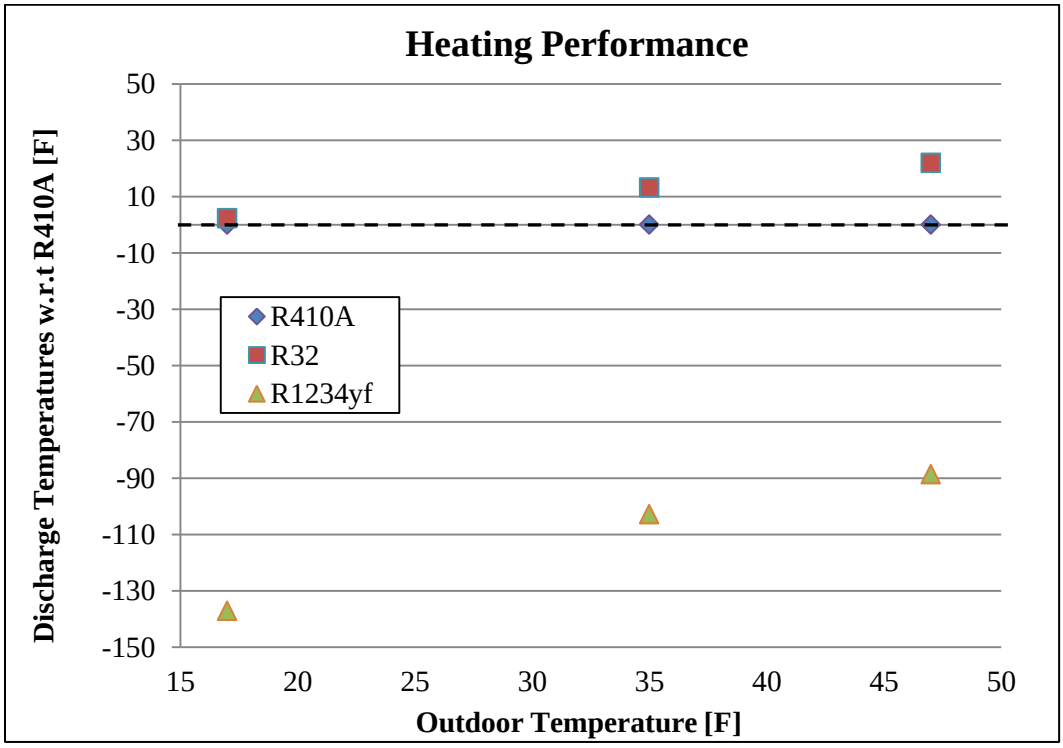

Figure 44: Compressor discharge temperatures for heating tests

Figure 44 and 45 show the compressor discharge temperatures for heating and cooling tests. Horizontal is the ambient temperature while vertical axis is the difference of discharge temperature of R32 and R1234yf with R410A. Thus for outdoor temperature of 35 °F, R32 has a discharge temperature 10 °F higher and R1234yf has 100 °F lower than R410A. It was observed that the discharge temperature for R32 was higher than for R410A, especially for the extreme high temperature tests as shown in Figure 45.

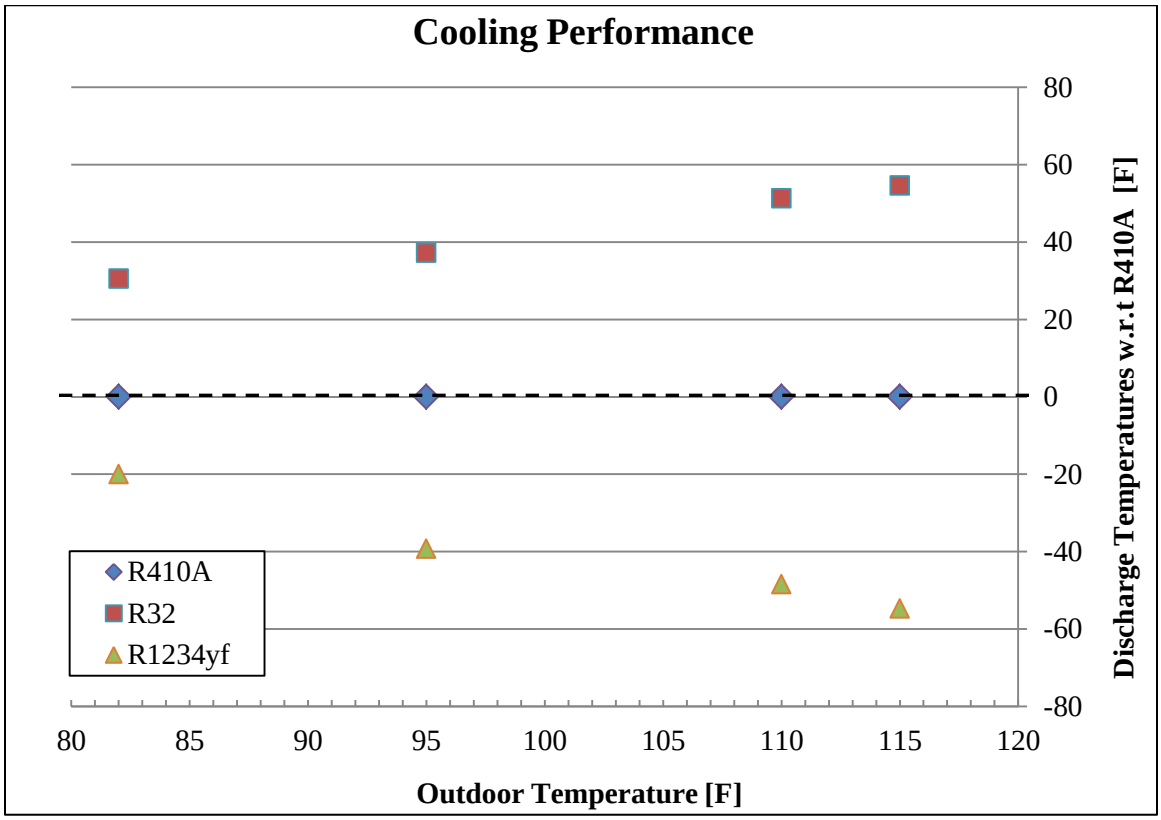

Figure 45: Compressor discharge temperature for cooling tests

The discharge temperature of the compressor with R32 was about 40 °F higher that R410A at AHRI A cooling conditions and up 54.6°F at extreme high temperatures. For R1234yf the discharge temperature was always lower than R410A and the data in Figures 44 and 45 show the

difference in discharge temperature of R1234yf and R32 with respect to R410A for a broad range of outdoor temperatures. Higher discharge temperatures would mean that compressor will have to undergo higher fatigue stress. This will affect the life of the compressor over the long run.

Coil performance

A preliminary analysis of the refrigerants characteristics inside the dx-evaporator was conducted in this work.

Table 21: Specifications of indoor and outdoor coils

	Indoor Coil	**Outdoor coil**
Type/Configuration	A-shape	Serpentine
No. of circuiting	8	6
Pipe nominal size	9.5 mm (3/8 inch)	12.2 mm (½ inch)
Fin density	13 per inch	23 per inch
Dimensions	17.5″ x 27.5″ x 2	33″ x 32″ x 2 + 33″ x 26″

* The measurements in this table were made at Oklahoma State University on off-the-shelf coils. They represent a small number of physical measurements and they were not given by the manufacturer

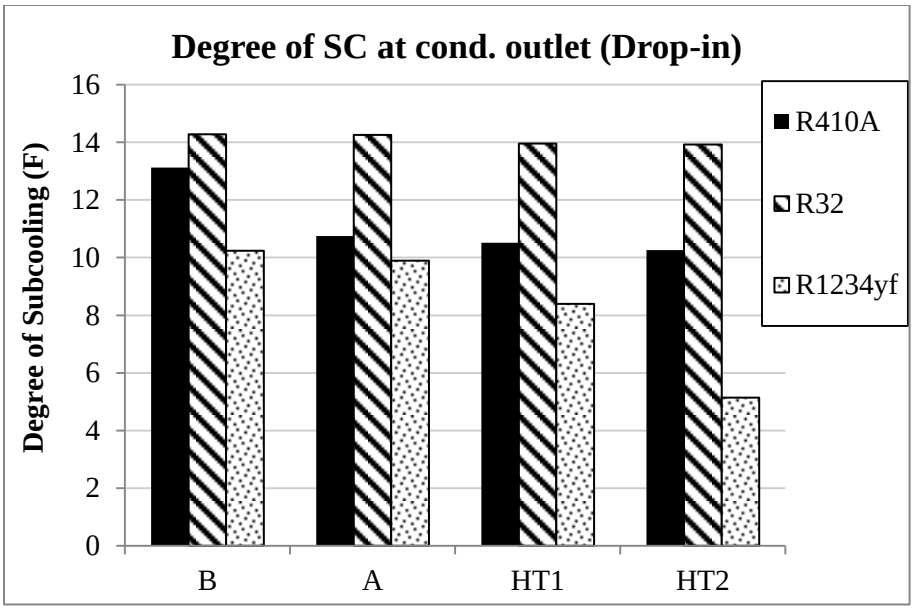

Figure 46: Degree of sub cooling at condenser outlet during drop-in tests

The degree of sub-cooling at condenser outlet for drop-in tests and TXV-optimization tests are shown in figures 46 and 47. Figure 46 indicates that R410A had a condenser sub-cooling of about 10 to 13 ºF. The degree of sub-cooling was about 14 ºF for R32. For R1234yf the degree of sub-cooling decreased from 10.2 ºF to 5ºF at extreme high temperatures, because some of the R1234yf refrigerant charge had to be taken out of the system.

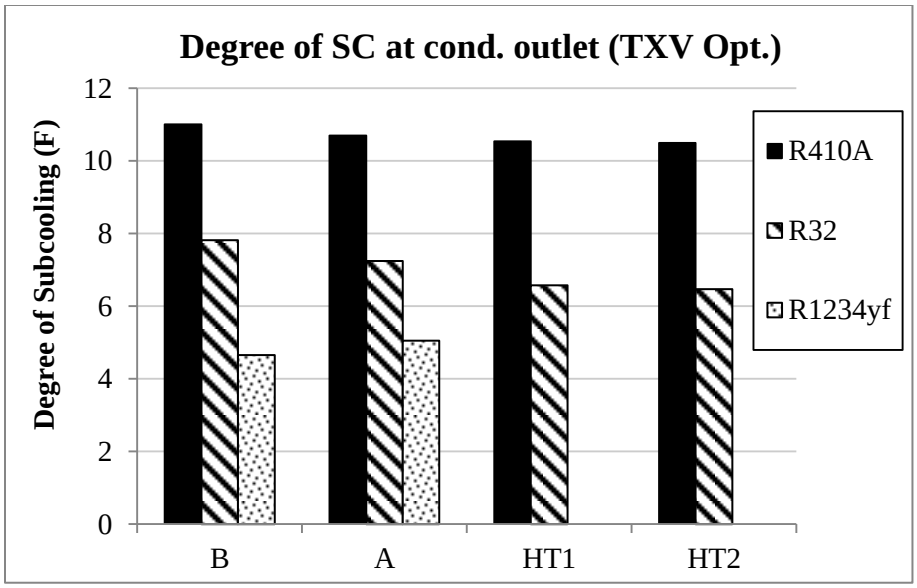

Figure 47: Degree of sub-cooling at condenser outlet during TXV optimization test

When retrofitting R410A with R32 and R1234yf at A-test cooling condition, the flow rates and corresponding pressure drops across the evaporator (including the pressure drop across the inlet distributor) shown in figure 48 were measured. Data were normalized with respect to flow rates and pressure drops for R410A, that is, the point of coordinates (1, 1) is the operating point of the system at the A-test condition by using optimum charge of R410A

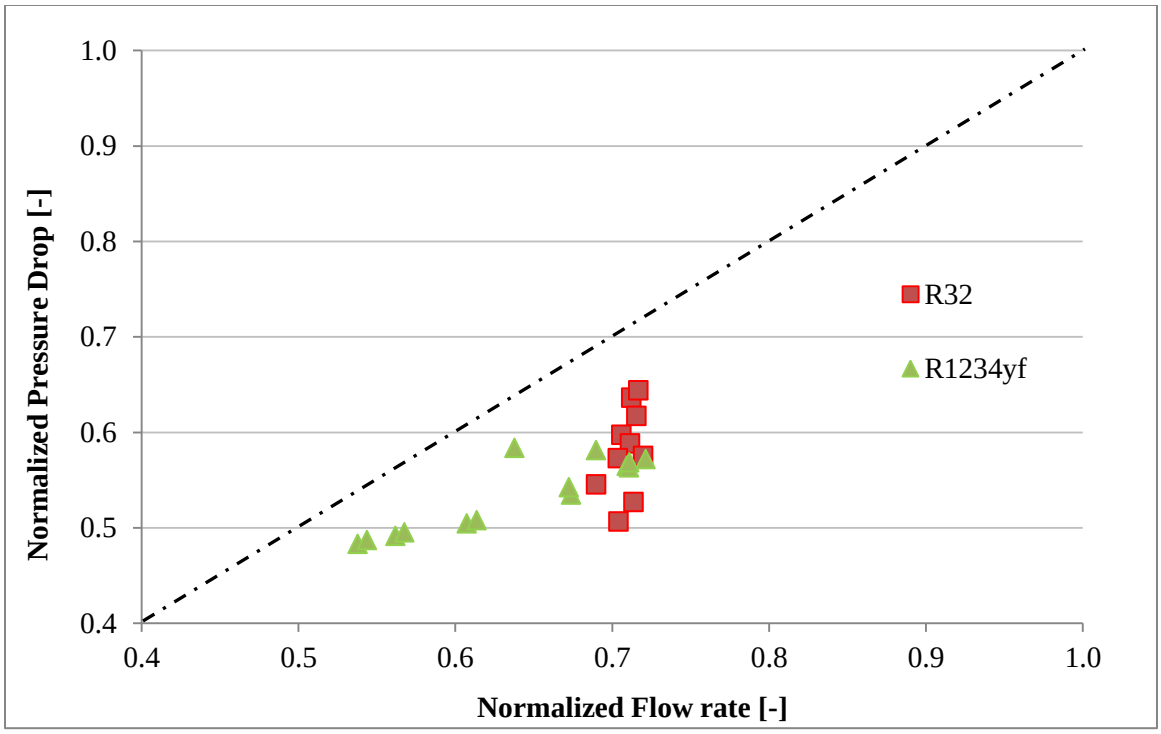

Figure 48: Normalized pressure drop versus normalized flow rate at A test condition (during TXV soft optimization test)

R32 had flow rates of 0.69 to 0.71 times lower than that of R410A and the pressure drops across the evaporator were also 0.51 to 0.64 times lower. The data of R32 were measured for various refrigerant charges and various openings of the expansion valve in the system. Similarly, R1234yf had flow rates of 0.54 to 0.72 and evaporator pressure drops of 0.48 to 0.58. The region above the diagonal line would indicate that the flow regimes, refrigerant densities and viscosities of the two phase mixture circulating in the evaporator yielded higher flow losses with respect to R410A. It should be emphasized that because of physical constraints in the distributor and indoor coil assembly, the refrigerant pressure tap at the inlet of the evaporator was installed at the inlet of the indoor coil refrigerant distributor. Thus, the pressure drops reported in figure 48 are actually the pressure drops across the coil plus the pressure drop across the refrigerant inlet distributor.

The original TXV of the R410A unit was designed to adjust the load of the evaporator for a broad range of outdoor temperatures. For all the refrigerants, the superheat at compressor suction was controlled to at least 4 ºF for the purpose of safe operation of compressor.

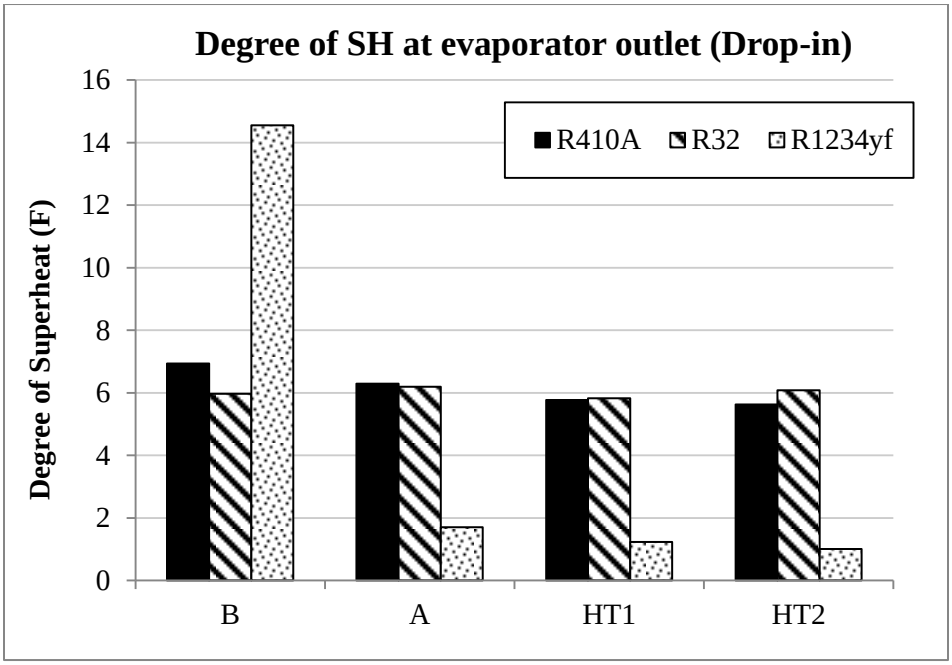

Figure 49: Degree of superheat at evaporator outlet for drop-in tests

The superheat at the evaporator outlet is shown in figures 49 and 50 for the drop-in tests and TXV soft optimization tests. During drop-in tests, R410A had a degree of superheat at the evaporator outlet from 5.6 to 7 ºF, which yielded to a degree of superheat at the compressor suction of about 10ºF. For R32, the TXV worked well, that is, it controlled the evaporator loading and provided similar degree of superheat at the outlet of the evaporator. For R1234yf at extreme high temperatures, controlling the superheat to above 1ºF to 1.7 ºF if the system charge was constant was a major challenge. The charge that yielded to optimum COP at A-test conditions also produced very low degree of superheat at extreme high temperature conditions and very high degree of superheat at B-test conditions. Figure 50 shows that it was possible to decrease the

degree of superheat by adjusting the TXV, which also resulted in higher capacities and COPs of the system with the LGWP refrigerants.

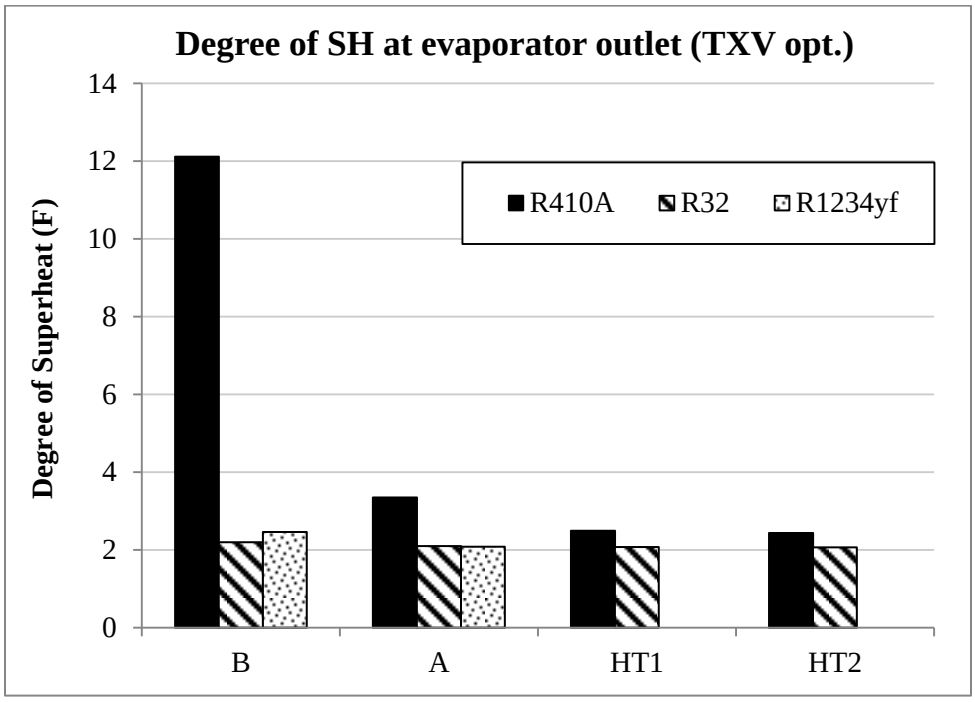

Figure 50: Degree of superheat at evaporator outlet for TXV optimization tests

Charge Management

In this test campaign for the first part the refrigerant charge was varied with the same TVX. In the later part, TXV optimization process, the refrigerant charge was kept constant and the system pressure was optimized for improvements. During the analysis it was observed that the charge plays a very important role in system performance and for protection of components. Undercharge and overcharge of refrigerant worsens the system performance and deteriorate reliability. Degree of sub-cooling at the condenser outlet strongly affects the cooling capacity and refrigerant flow rate. Undercharge decreases the condenser sub-cooling leading to loss of capacity (Choi & Kim, 2002).

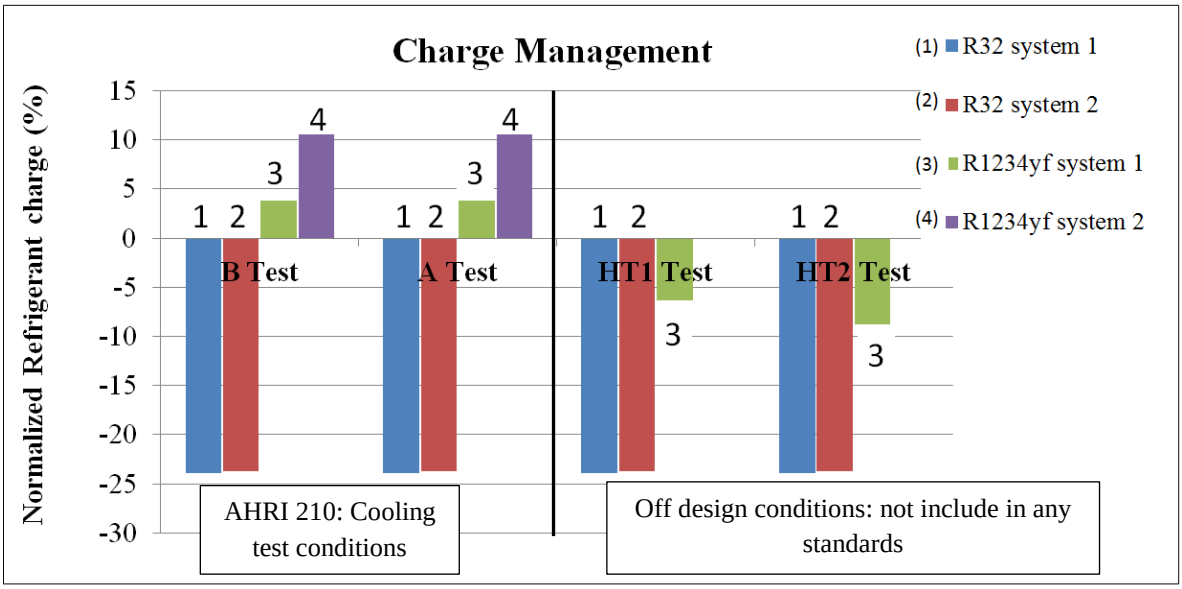

Figure 51: Comparison of refrigerant charge for drop-in and TXV soft optimization tests

Figure 51 demonstrates the comparison of charge of R32 and R1234yf for drop-in and TXV optimization tests. The X-axis represents different tests conditions for cooling mode. The refrigerant charge for R32 and R1234yf is normalized and a percent value is plotted on the Y-axis. In the plot, system 1 refers to drop-in tests and system 2 refers to TXV soft optimization tests. The numbers 1 through 4 represent specific refrigerant in a particular system presented in the legend and is shown next to the data column. Thus series number 1 would represent R32 refrigerant for drop-in tests and so on. A point to remember is AHRI standard 210 prescribes B and A tests, while extreme temperature or off design condition tests HT1 and HT2 were not included in the standards.

It can be seen that for R32 drop-in tests (series 1) the charge required was about 23 % less than that for R410A. Less charge would mean less cost for the consumers. On the other hand series 3 which is the R1234yf drop in test, about 4 % more charge is required for A and B test condition. For off design condition the charge requirement by the system reduces with 6 % less for HT1 and

9 % less for HT2. Apart from the amount of charge required to run the system another important result is the consistency. Series 1 appears very consistent for all the test conditions, while series 3 the amount of charge is different for various test condition. What this means is, the heat pump system with R32 as refrigerant would work with the same amount of charge for an ambient temperature ranging from 85 ºF to 115 ºF. But for R1234yf one charge will not run for the same range of outdoor temperature. In the event of such high ambient temperatures the refrigerant charge for R1234yf system will have to be reduced or it will lose superheat and thus endanger the life of compressor. It must be noted that, if the testing would have been limited to test conditions suggested by AHRI standard 210, this problem would have never been detected. It is at the off design conditions that charge management issues with R1234yf come up. It can be concluded from this discussion that R32 is a drop-in replacement for 5 ton R410A heat pump system. R1234yf is not a suitable drop-in replacement for 5 ton R410A heat pump system not only because it delivers only half the capacity but also owing to the issue of charge management.

Similar analysis is done for TXV optimization tests. Series 2 suggests that the amount of charge of R32 in soft optimization tests is constant. No doubt constant charge is the objective of TXV optimization tests, but the fact that the heat pump system was able to run with R32 and optimization of cycle pressure was possible is a very important result. The optimal charge for R1234yf from drop-in tests was not able to perform for optimization of cycle pressure. As we can see, series 4 is discontinuous and off design tests were not possible for R1234yf. Again, the testing conditions suggested by AHRI 210 alone would not have captured these results. Thus while analyzing the performance of alternative LGWP refrigerants, off design conditions are important considerations.

It is evident from the charge management analysis that, R32 is a suitable drop-in replacement for R410A and an optimization process over the cycle pressure is also possible. In case of R1234yf, the refrigerant charge has to me managed in such a way that less charge is made available for low

temperature cooling and surplus charge is supplied for extreme cooling conditions. Heat pump unit is usually fitted with refrigerant receivers. Refrigerant receivers are containers which store excess refrigerant circulated in the system. The receiver is designed to provide storage capacity in the event of overcharge or when the system is shut down for repairs. Receiver also accommodates fluctuating charge when the condenser is subjected to different load conditions or varying ambient temperatures. Thus in order to run R1234yf in R410A system, suction receiver must be selection is very important. If the suction receiver is designed in such a way that adequate charge is supplied for medium ambient conditions and proper amount is stored in during high ambient temperatures, the heat pump can run without endangering the compressor. Design of receiver for R1234yf system can be part of future work for this project.

Summary of the experimental findings from present work

The following section provides a summary of the new findings from this experimental campaign of the present thesis.

GWP: The GWP values for R410A, R32 and R1234yf are 2088, 675 and 4 respectively.

Toxicity and Flammability: R410A is a non-flammable and low toxic refrigerant which is listed in A1 category by ASHRAE ratings (Zheng et al, 1998). R32 belongs to a low flammable refrigerant class 2L but has a potential fire hazard as a result of its faster flame propagation speed. R32 is also a low toxic refrigerant. R1234yf is a low flammable and low toxic refrigerant which is classified as 2L in refrigerant category.

COP: The cooling COP for R32 is similar to that of R410A. R32 yielded in a cooling COP in the range of 3% of R410A while for heating COP, R32 showed a 17% increase for extreme low conditions and 7% increase for medium low ambient temperatures. On the other hand, R1234yf showed a 5-10% increase for cooling and heating COP.

Capacity: Heating and cooling capacity for R32 increased by 10% in comparison to R410A. R1234yf yielded in heating and cooling capacity which was about 50% less or half as that of R410A.

Refrigerant charge: Managing the charge of R410A and R32 on the unit was not an issue. Once the unit was charged with the optimal refrigerant charge the unit was able to run over the wide range of ambient temperatures including extreme hot and cold temperatures. The charge of R1234yf had to be altered for varying ambient temperature in order to maintain enough degree of superheat at the compressor.

Ease of operation: In the case of R410A and R32 the transition from cooling to heating mode was hassle free. The optimal charge for cooling mode yielded adequate compressor superheat and indoor capacity for heating tests as well. For R1234yf however, the transition from cooling to heating mode and vice versa was not smooth. Charge manipulation and close monitor of the compressor superheat was required during the experiments. This was due to the design of the TXV, which was suitable for R410A and R32 but not for R1234yf.

Behavior at off design conditions: For extreme high ambient temperatures of 110 °F and 115 °F, R32 performed quite equivalent to R410A. The cooling capacity was 5% higher while COP was within 2 % than R410A performance. No charge management issues were observed for extreme ambient temperatures. R1234yf, yielded 7 % higher COP than R410A but the capacity was again, 50% less than R410A. Managing the refrigerant charge for R1234yf for off design conditions was a challenge.

CHAPTER VII

CONCLUSION

This work presents data of drop-in energy performance and capacities of two low GWP refrigerants in a R410A heat pump split system for ducted HVAC residential applications. The experiments were conducted for cooling and heating mode of the unit and the outdoor temperature was varied from 17°F to 115°F. Cooling tests at AHRI standard rating conditions were performed and the refrigerant charge was optimized. Two additional off-design conditions were considered with outdoor temperatures of 110°F and 115°F to analyze the behavior of the refrigerant at extreme high temperature ambient. Each specific objectives of this thesis are repeated below followed by the associated outcomes of this study.

To study of thermodynamic cycle characteristics of R32 and R1234yf when they are used in heat pump split systems.

The study shows the operating refrigeration cycle for R32 is equivalent to R410A. R1234yf operates at 50% reduced pressure than that of R410A. R32 has physical and heat transfer characteristics which are very close to R410A. R1234yf is not comparable to R410A as far as physical properties are concerned, in fact R1234yf resembles R134a.

To assess the energy performance and capacity for R32 and R1234yf with respect to R410A for 5 ton residential heat pump units commercially available in the US.

R32 has comparable heating and cooling capacities as R410A and similar COPs. On the other hand, R1234yf has similar COPs as R410A but yields capacity which about 50 % less than R410A.

To investigate minor adjustments on the system that can yield equal or comparable performance as R410A.

TXV soft optimization improves the capacity for both the refrigerant by at least 7 % as compared to the drop-in performance. . The soft optimization tests improved the capacity of R1234yf by 8%, but still was 45% lower than R410A.

To identify the potentials and shortcomings of these two low GWP refrigerants.

For R32 the discharge pressures and discharge temperatures were higher than those for R410A, especially for moderate to extreme high temperature conditions. R1234yf was not a straight drop-in replacement for refrigerant R410A because charge had to be significantly decreased at off-design conditions

Table 22: Summary of experimental findings

Description	R410A	R32	R1234yf
COP	1	1	1
Capacity	1	1	0.5
Refrigerant charge	1	0.75	1.1
Easy of operation	1	1	0.7
behaviour at off design condition	1	1	0.6
Charge levels in transition between A/C and heat pump mode	1	1	0.8
Cost	$	$	$$$
Flamability	Low	Slightly flamable	Slightly flamable
Toxicity	Low	Low	Mildly
Compressor discharge temperatures	1	1.3	0.4

Too high discharge temperature and pressure of R32 in extreme high temperature conditions was a concern for the safe operation of the unit and might be a concern for the compressor lifetime cycle. Refrigerant R1234yf provided similar COPs as R410A but this refrigerant had rather low capacities with respect to those for R410A. Optimizing the expansion valve improved the R1234yf capacity by up to 10% with respect to drop-in capacities but it was still 46% lower than that for R410A at similar operating conditions. From this point of view R1234yf was not a drop-in replacement for refrigerant R410A when considering a 5 ton commercially available heat pump split system for ducted HVAC residential applications. A tabulated summary for the evaluation parameters for the refrigerant candidates is provided in Table 22.

REFERENCES

ANSI/AHRI Standard 210/240, 2010, Standard for Performance Rating of Unitary Air-Conditioning & Air-Source Heat Pump Equipment, Arlington, VA.

ANSI/ASHRAE Standard 37, 2009, Methods of Testing for Rating Electrically Driven Unitary Air-Conditioning and Heat Pump Equipment, GA.

ANSI/ASHRAE Standard 41.2, 1987, Standard Method for Laboratory Airflow Measurement, Atlanta, GA.

ANSI/ASHRAE Standard 116, 1995, Methods of Testing for Rating Seasonal Efficiency of Unitary Air Conditioners and Heat Pumps, Atlanta, GA.

Biswas, A., Barve, A., and Cremaschi, L. (2013). An experimental study of the performance of new Low Global Warming Potential (LGWP) Refrigerants at extreme high temperature ambient conditions in residential AC ducted split systems. *ASHRAE Winter Conference*, Dallas, TX, Jan 26-30, 2013.

Calm, J. M. (2008). The next generation of refrigerants – Historical review, considerations, and outlook. *International Journal of Refrigeration, 31(7),* 1123-1133. doi: 10.1016/j.ijrefrig.2008.01.013

Calm, J. M., & Didion, D. A. (1998). Trade-offs in refrigerant selections: past, present, and future. International Journal of Refrigeration, 21(4), 308-321. doi: 10.1016/s0140-7007(97)00089-3

Choi, J. M., & Kim, Y. C. (2002). The effects of improper refrigerant charge on the performance of a heat pump with an electronic expansion valve and capillary tube. Energy, 27(4), 391-404. doi: 10.1016/s0360-5442(01)00093-7

.

Cremaschi, L., Lee, E., 2008, Design and heat transfer analysis of a new psychrometric environmental chamber for heat pump and refrigeration systems testing, *ASHRAE Transactions*, P.114

Downey, T., Proctor, J., 2002, "What Can 13,000 Air Conditioners Tell Us?" In Proceedings of the ACEEE 2002 Summer Study on Energy Efficiency in Buildings, 1:53-68. Washington D.C.: American Council for an Energy-Efficient Economy.

Eckaus, R. S., & Massachusetts Institute of Technology. (1990). *Comparing the effects of greenhouse gas emissions on global warming*. Cambridge, Mass: Center for Energy Policy Research, Massachusetts Institute of Technology.

Endoh, K., Matsushima, H., Takaku, S., 2010, Evaluation of Cycle Performance of Room Air Conditioner Using HFO1234yf as refrigerant, *International Refrigeration and Air Conditioning Conference at Purdue*, West Lafayette, IN, Paper No. 2208

Forster, P., V. Ramaswamy, P. Artaxo, T. Berntsen, R. Betts, D.W. Fahey, J. Haywood, J. Lean, D.C. Lowe, G. Myhre, J. Nganga, R. Prinn, G. Raga, M. Schulz and R. Van Dorland, 2007: Changes in Atmospheric Constituents and in Radiative Forcing. In: Climate Change 2007: The Physical Science Basis. Contribution of Working Group I to the Fourth Assessment Report of the Intergovernmental Panel on Climate Change [Solomon, S., D. Qin, M. Manning, Z. Chen, M. Marquis, K.B. Averyt, M.Tignor and H.L. Miller (eds.)]. Cambridge University Press, Cambridge, United Kingdom and New York, NY, USA.

IPCC, 1990: *Climate Change: The Intergovernmental Panel on Climate Change Scientific Assessment* [Houghton, J.T., G.J. Jenkins, and J.J. Ephraums (eds.)]. Cambridge University Press, Cambridge, United Kingdom and New York, NY, USA, 364 pp.

Karber, K., Abdelaziz, O., Vineyard, E., 2012, Experimental Performance of R-1234yf and R-1234ze as Drop-in Replacements for R-134a in Domestic Refrigerators, *International Refrigeration and Air Conditioning Conference at Purdue*, West Lafayette, IN, Paper No. 2241

Kim, W., Braun. J., 2010, Impacts of Refrigerant Charge on Air Conditioner and Heat Pump Performance, *International Refrigeration and Air Conditioning Conference at Purdue*, West Lafayette, IN, Paper No. 2433

Kruse, H. (1998). Is the TEWI Number Suitable for Evaluating the Combined Global Warming Effect of Refrigeration and Heat Pump Systems? *HVAC&R Research, 4(3)*, 203-204. doi: 10.1080/10789669.1998.10391400

Leck, T. J., 2010, New High Performance, Low GWP Refrigerants for Stationary AC and Refrigeration, *International Refrigeration and Air Conditioning Conference at Purdue*, West Lafayette, IN, Paper No. 2160

Minor, B., Spatz, M., 2008, HFO-1234yf low GWP refrigerant update, *International Refrigeration and Air Conditioning Conference at Purdue*, West Lafayette, IN, Paper No. 2349

Papasavva, S., Hill, W. R., & Andersen, S. O. (2010). GREEN-MAC-LCCP: A tool for assessing the life cycle climate performance of MAC Systems. *Environmental Science and Technology, 44*(19), 7666-7672. doi: 10.1021/es100849g

Pham, H., Rajendran, R., 2012, R32 And HFOs As Low-GWP Refrigerants For Air Conditioning, *International Refrigeration and Air Conditioning Conference at Purdue*, West Lafayette, IN, Paper No. 2262

Reasor, P., Radermacher, R., Aute, V., 2010, Refrigerant R1234yf Performance Comparison Investigation, *International Refrigeration and Air Conditioning Conference at Purdue*, West Lafayette, IN, Paper No.2300

Taira, S., Yamakawa, T., Nakai, A., Yajima, R., 2011, Analysis of LGWP Alternatives for Small Refrigeration (Plugin) Applications, *IEH Heat Pump Conference*, Tokyo, Japan, vol. 29, P. 22-29

United Nations Environmental Programme (UNEP), 1987, Montreal Protocol on Substances That Deplete the Ozone Layer Final Act, New York; United Nations.

Wang, X., Amrane, K., Johnson, P., 2012, Low Global Warming Potential (GWP) Alternative Refrigerants Evaluation Program (Low-GWP AREP), *International Refrigeration and Air Conditioning Conference at Purdue*, West Lafayette, IN, Paper No.2233

Worthington, K., Cremaschi., L., Aslan, O., 2011, A new experimental low temperature facility to measure comprehensive performance rating of unitary equipment and systems operating at design and off-design conditions, *Proceedings of the International Conference on Air-Conditioning and Refrigeration ICACR 2011, July 6-8, 2011*, Yongpyong Resort, Gangwon-Do, KOREA, paper no 147, P. 81

Yana Motta, S., Vera Becerra, E. D., Spatz, M., 2010, Analysis of LGWP Alternatives for Small Refrigeration (Plugin) Applications, *International Refrigeration and Air Conditioning Conference at Purdue*, West Lafayette, IN, Paper No. 2499

Yana Motta, S., Vera Becerra, E. D., Spatz, M., 2010, Low Global Warming Alternative Refrigerants For Stationary AC&R Applications, *International Refrigeration and Air Conditioning Conference at Purdue*, West Lafayette, IN, Paper No. 2500

Zheng, J., Hughes, H. M., Spatz, M., Zyhowski, G. J., 1998, Optimization Strategies for Unitary Air Conditioners Using R-410A, *International Refrigeration and Air Conditioning Conference at Purdue*, West Lafayette, IN, Paper 390.

NOMENCLATURE

$\dot{Q}_{air}$ = Air side heat transfer capacity [btu/hr]

$\dot{m}_{air}$ = Mass flow rate of air [lb/hr]

C_p = Specific heat of air at constant pressure calculated at supply temperature [Btu/lb-R]

T_{return} = Temperature of return air (indoor room temperature) [°F]

ω_{return}= Humidity ratio of return air [-]

T_{supply} = Temperature of supplied conditioned air by the unit [°F]

ω_{supply} = Humidity ratio of supply air [-]

h_{fg} = Difference in enthalpy of water vapor and saturated water at supply temperature [Btu/lb]

$\dot{Q_{ref}}$ = Refrigerant side heat transfer capacity [Btu/hr]

$\dot{m_{ref}}$ = Mass flow rate of refrigerant [lb/hr]

Δh = Difference in the enthalpies of refrigerant at inlet and outlet of the indoor coil. [Btu/lb]

$h_{air,\ out}$ = Enthalpy of air at outle [Btu/lb] t

$h_{air,\ in}$ = Enthalpy of air at inlet [Btu/lb]

$h_{ref,\ out}$ = Enthalpy of refrigerant at outlet [Btu/lb]

$h_{ref,\ in}$ = Enthalpy of refrigerant at inlet [Btu/lb]

$\dot{W}_{blower}$ = Indoor unit blower power [Btu/hr]

$\dot{W}_{Total}$ = Total work or power input to the unit as whole. [Btu/hr]

$\dot{W}_{compressor}$ = Compressor work [Btu/hr]

$\dot{W}_{indoor\ blower}$ = Indoor unit blower power [Btu/hr]

$\dot{W}_{outdoor\ fan}$ = Outdoor unit fan power [Btu/hr]

$\dot{Q}_{condenser}$ = Refrigerant capacity at the condenser (heat rejection coil) [Btu/hr]

$\dot{Q}_{evaporator}$ = Refrigerant capacity at the evaporator (heat gaining coil) [Btu/hr]

η_{T_r} = Compressor thermal efficiency of particular refrigerant [-]

$\eta_{T_{R410A}}$ = Compressor thermal efficiency of R410A [-]

η_{T_N} = Compressor thermal efficiency of a refrigerant normalized with respect to R410A. [-]

$h_{comp,out,issentropic}$ = Issentropic enthalpy at compressor outlet [Btu/lb]

$h_{comp,inlet}$ = Enthalpy at compressor inlet [Btu/lb]

$h_{comp,out,actual}$ = Actual enthalpy at compressor outlet [Btu/lb]

ΔP_r = Pressure drop across the indoor coil for a particular refrigerant [psi]

ΔP_{R410A} = Pressure drop across the indoor coil for R410A [psi]

ΔP_N = Pressure drop across the indoor coil for normalized with respect to R410A [psi]

$P_{indoor\ coil,out}$ = Absolute pressure at indoor coil outlet [psia]

$P_{indoor\ coil,in}$ = Absolute pressure at indoor coil inlet [psia]

P_r = Compressor pressure ratio [-]

γ = Compressor pressure ratio [-]

VITA

Atharva A. Barve

Candidate for the Degree of

Master of Science

Thesis: STUDY OF LOW GLOBAL WARMING POTENTIAL REFRIGERANTS IN HEAT PUMP SYSTEMS FOR STATIONARY APPLICATIONS

Major Field: Mechanical Engineering

Biographical: From Mumbai, India. I am the proud son of Mr. Abhay Barve and Mrs. Arti Barve.

Education: Bachelor of Science in Mechanical Engineering (Oklahoma State University)

Completed the requirements for the Bachelor of Science in Mechanical Engineering at Oklahoma State University, Stillwater, Oklahoma in July, 2010.

Professional Memberships: American Society of Heating, Refrigerating and Air Conditioning Engineers (ASHRAE) student member.

Name: Atharva Barve Date of Degree: December, 2012

Institution: Oklahoma State University Location: Stillwater, Oklahoma

Title of Study: STUDY OF LOW GLOBAL WARMING POTENTIAL REFRIGERANTS IN HEAT PUMP SYSTEMS FOR STATIONARY APPLICATIONS

Pages in Study: 108 Candidate for the Degree of Master of Science

Major Field: Mechanical Engineering

Scope and Method of Study: Completed the construction of test facility for testing the performance of Low GWP refrigerants for a split system heat pump. Tests divided in two stages namely drop-in performance and TXV soft optimization tests. Conducted tests according to AHRI standard 210. Analyzed data and summarized the results.

Findings and Conclusions: This work presents data of drop-in energy performance and capacities of two low GWP refrigerantsR32 and R1234yf in a R410A heat pump split system for ducted HVAC residential applications. The experiments were conducted for cooling and heating mode of the unit and the outdoor temperature was varied from 17°F to 115°F. Cooling tests at AHRI standard rating conditions were performed and the refrigerant charge was optimized. Two additional off-design conditions were considered with outdoor temperatures of 110°F and 115°F to analyze the behavior of the refrigerant at extreme high temperature ambient. Each specific objectives of this thesis are repeated below followed by the associated outcomes of this study. The study shows the operating refrigeration cycle for R32 is equivalent to R410A. R1234yf operates at 50% reduced pressure than that of R410A. R32 has comparable heating and cooling capacities as R410A and similar COPs. On the other hand, R1234yf has similar COPs as R410A but yields capacity which about 50 % less than R410A. TXV soft optimization improves the capacity for both the refrigerant by at least 7 % as compared to the drop-in performance. . The soft optimization tests improved the capacity of R1234yf by 8%, but still was 45% lower than R410A.

ADVISER'S APPROVAL: Dr. Lorenzo Cremaschi